NAVAL POSTGRADUATE SCHOOL
Monterey , California

DTIC FILE COPY

SELECTED **D** THESIS

MAY 0 6 1988

UNITED STATES NAVY · NAVAL POSTGRADUATE SCHOOL ·

ELECTRODYNAMIC DRIVER FOR THE
SPACE THERMOACOUSTIC REFRIGERATOR (STAR)

by

Michele Fitzpatrick

March 1988

Thesis Co-advisor: S. L. Garrett
Thesis Co-advisor: T. Hofler

---

88   5 02   18 8

A192337

REPORT DOCUMENTATION PAGE

1a. REPORT SECURITY CLASSIFICATION Unclassified	1b. RESTRICTIVE MARKINGS
2a. SECURITY CLASSIFICATION AUTHORITY	3. DISTRIBUTION / AVAILABILITY OF REPORT Approved for public release;
2b. DECLASSIFICATION / DOWNGRADING SCHEDULE	distribution is unlimited.

4. PERFORMING ORGANIZATION REPORT NUMBER(S)	5. MONITORING ORGANIZATION REPORT NUMBER(S)

6a. NAME OF PERFORMING ORGANIZATION Naval Postgraduate School	6b. OFFICE SYMBOL (If applicable) 61Gx	7a. NAME OF MONITORING ORGANIZATION Naval Postgraduate School
6c. ADDRESS (City, State, and ZIP Code) Monterey, CA 93943-5000		7b. ADDRESS (City, State, and ZIP Code) Monterey, CA 93943-5000

8a. NAME OF FUNDING / SPONSORING ORGANIZATION Office of Naval Research	8b. OFFICE SYMBOL (If applicable) Code 1112	9. PROCUREMENT INSTRUMENT IDENTIFICATION NUMBER

8c. ADDRESS (City, State, and ZIP Code) 800 N. Quincy St. Arlington, VA 22217	10. SOURCE OF FUNDING NUMBERS

PROGRAM ELEMENT NO.	PROJECT NO.	TASK NO	WORK UNIT ACCESSION NO.

11. TITLE (Include Security Classification)
ELECTRODYNAMIC DRIVER FOR THE SPACE THERMOACOUSTIC REFRIGERATOR (STAR)

12. PERSONAL AUTHOR(S)
Fitzpatrick, Michele

13a. TYPE OF REPORT Master's Thesis	13b. TIME COVERED FROM Jan 87 TO Mar 88	14. DATE OF REPORT (Year, Month, Day) 1988 March	15. PAGE COUNT 187

16. SUPPLEMENTARY NOTATION

17.	COSATI CODES		18. SUBJECT TERMS (Continue on reverse if necessary and identify by block number)
FIELD	GROUP	SUB-GROUP	Electrodynamic loudspeaker, Thermoacoustic refrigerator

19. ABSTRACT (Continue on reverse if necessary and identify by block number) The objective of the STAR project is to test and space qualify a new continuous cycle cryogenic refrigeration system for cooling of sensors and electronics which is based upon the newly discovered thermoacoustic heat pumping effect. The new refrigerator has no sliding seals, a cycle frequency of about 300 Hz, and uses acoustic resonance to enhance the overall power density and efficiency. This thesis is concerned specifically with the design and testing of the electrodynamic transducer which is responsible for the electro-acoustic power conversion. A computer model of the driver/resonator system is presented along with the techniques for measurement of the electrical and mechanical parameters used as input for the model.

A final driver design (including dimensional drawings) utilizing a modified JBL 2450J neodymium-iron-boron compression driver and associated leak-tight electrical feed-throughs, microphone, accelerometer, pressure gage, pressure housing, and resonator interface is provided. (Keywords)

20. DISTRIBUTION / AVAILABILITY OF ABSTRACT ☒ UNCLASSIFIED/UNLIMITED ☐ SAME AS RPT. ☐ DTIC USERS	21. ABSTRACT SECURITY CLASSIFICATION Unclassified
22a. NAME OF RESPONSIBLE INDIVIDUAL Steven Garrett	22b. TELEPHONE (Include Area Code) 408-646-2540	22c. OFFICE SYMBOL 61Gx

DD FORM 1473, 84 MAR 83 APR edition may be used until exhausted. SECURITY CLASSIFICATION OF THIS PAGE
All other editions are obsolete.

☆ U.S. Government Printing Office: 1986—606-2

i

**Electrodynamic Driver for the
Space Thermoacoustic Refrigerator (STAR)**

by

Michele Fitzpatrick
Lieutenant, United States Coast Guard
B.S., United States Coast Guard Academy, 1980

Submitted in partial fulfillment of the
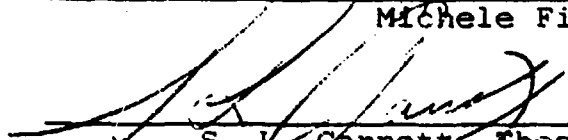requirements for the degree of

MASTER OF SCIENCE IN PHYSICS
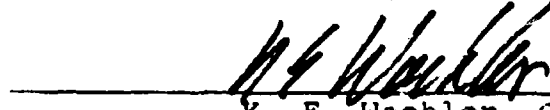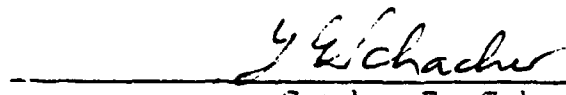
from the

NAVAL POSTGRADUATE SCHOOL
March 1988

Author: _____
Michele Fitzpatrick

Approved by: _____
S. L. Garrett, Thesis Co-Advisor

_____
T. Höfler, Thesis Co-advisor

_____
K. E. Woehler, Chairman
Department of Physics

_____
Gordon E. Schacher
Dean of Science and Engineering

ABSTRACT

The objective of the STAR project is to test and space qualify a new continuous cycle cryogenic refrigeration system for cooling of sensors and electronics which is based upon the newly discovered thermoacoustic heat pumping effect. The new refrigerator has no sliding seals, a cycle frequency of about 300 Hz, and uses acoustic resonance to enhance the overall power density and efficiency. This thesis is concerned specifically with the design and testing of the electrodynamic transducer which is responsible for the electro-acoustic power conversion. A computer model of the driver/resonator system is presented along with the techniques for measurement of the electrical and mechanical parameters used as input for the model.

A final driver design (including dimensional drawings) utilizing a modified JBL 2450J neodymium-iron-boron compression driver and associated leak-tight electrical feed-throughs, microphone, accelerometer, pressure gage, pressure housing, and resonator interface is provided.

iii

Accesion For	
NTIS CRA&I	☑
DTIC TAB	☐
Unannounced	☐
Justification	
By	
Dist.ibution /	
Availability Codes	
Dist	Avail and / or Special
A-1	

TABLE OF CONTENTS

LIST OF TABLES

LIST OF FIGURES

ACKNOWLEDGEMENT

I. INTRODUCTION

A. BACKGROUND

1. History

Thermoacoustics can generally be described as the study of the interaction between heat and sound. Scientific interest in this interaction is not new. Lord Rayleigh (1878 and 1945) discussed various qualitative examples of the production of sound by heat. In one of these examples he describes investigations by Sondhauss (1850) of an effect observed by glassblowers: heating a bulb of glass at the end of a hollow rod occasionally led to the generation of sound. Faraday (1818) demonstrated that this effect occurred with gases other than air. Sondhauss proved that the vibration of the glass itself did not generate the sound, but he offered no explanation as to what did. In his description of Sonhauss' work, Rayleigh stressed the importance of the phase difference between temperature and particle motion. Rijke (1859) built an open tube with a wire mesh inside. When the mesh was heated, the tube produced a sound of impressive intensity. The functioning of this oscillator is slightly different since it requires steady gas flow for its operation. A similar sound production effect was observed by Taconis, et al. (1949) in hollow tubes immersed in liquid helium (4.2°K). The Taconis oscillations were addressed

1

quantitatively by Yazaki, et al. (1980). The work described above deals primarily with prime movers--devices that convert a temperature gradient to sound energy. We call this the classical era of thermoacoustics.

Interest in thermoacoustics was renewed when the idea of the use of acoustical devices as refrigerators appeared. Gifford and Longsworth (1966) described the pumping of heat along a surface caused by a periodic change in the pressure of the adjoining gas. Such a change can be produced by the oscillations of a sound wave. In their experiments Merkli and Thomann (1974) explored the heating and cooling effects on the wall of a gas-filled resonant tube. They found that heat was transported from a region near the velocity antinode (or maximum value) of the sound's standing wave to regions near the adjacent pressure antinodes. Thermoacoustic prime movers have also received recent attention. Kempton (1976) investigated the excess noise of aeroengines above that predicted by theory. He determined that the sound was produced by unsteady heat transfer. Each of these latter three groups of exprimenters used some theory for comparison, but it was mostly qualitative. None provided the complete quantitative theory that would explain their experimental observations.

The theoretical breakthrough in thermoacoustics field was made by Nicklaus Rott (1969, 1974, 1975, and 1980). His theory combined basic principles from physics,

thermodynamics, and acoustics to quantitatively describe the effects found in both types of thermoacoustic devices: prime movers and heat pumps. Prime movers use a temperature gradient to create sound, as in the effects discussed by Sondhauss, Rayleigh, Taconis, and Kempton. Heat pumps, or refrigerators, use the oscillating pressure of a sound wave to produce a temperature difference, as described by Gifford and Longsworth and Merkli and Thomann. Rott described the effect found by Merkli and Thomann as thermoacoustic streaming. It is this effect that makes thermoacoustic refrigeration possible.

Inspired by Ceperley's (1979) traveling wave Sterling Cycle heat engine and Rott's quantitative theory, the team of Wheatley, Hofler, Swift, Migliori, and Garrett (1982, 1983a, 1983b, 1985, and 1986) developed a series of thermoacoustic experiments at Los Alamos National Laboratory in New Mexico. They investigated the basic thermoacoustic effects in both prime movers and refrigerators and compared their experimental results to Rott's theory.

2. Thermodynamics

We'll digress from history here to explain the thermodynamic distinction between prime movers and refrigerators. This discussion follows Sears and Salinger (1975). A prime mover receives heat at a high temperature, T_H (the hot reservoir), does work on its surroundings, and rejects heat at a lower temperature, T_C (the cold reservoir), as shown in

Figure I-1.a. The first law of thermodynamics tells us that the heat flow (Q_H) from the hot reservoir must equal the work done on the surroundings (W) plus the heat flow (Q_C) to the cold reservoir:

$$Q_H = W + Q_C. \qquad (I-1)$$

The second law of thermodynamics states that in every process the entropy of the universe must either remain constant or increase. The entropy change for the isothermal heat transport to/from the reservoirs is defined as the heat flow divided by the reservoir temperature. For a prime mover the second law can be written:

$$\Delta S_H \leqq \Delta S_C \quad \text{or} \quad Q_H/T_H \leqq Q_C/T_C. \qquad (I-2)$$

The thermal efficiency of the prime mover is defined as the ratio of the work output to the heat input:

$$\eta = W/Q_H = (Q_H - Q_C)/Q_H = 1 - Q_C/Q_H. \qquad (I-3)$$

Comparing equations I-2 and I-3 gives us a limit on the efficiency based on the temperatures of the reservoirs:

$$\eta \leqq 1 - T_C/T_H. \qquad (I-4)$$

This limit is known as the Carnot efficiency.

In a refrigerator the process is basically reversed (see Figure I-1.b). Heat (Q_C) is removed from the low temperature reservoir, work (W) is received from the surroundings, and heat (Q_H) is delivered to the higher temperature reservoir. The expression for the first law is the same as for the prime mover, Equation I-1. For the refrigerator it means that the heat flow into the hot reservoir must equal

4
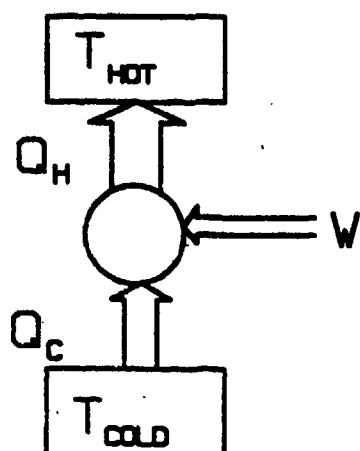
FIRST LAW: $Q_H = W + Q_C$

SECOND LAW: $\dfrac{Q_H}{T_H} \geq \dfrac{Q_C}{T_C}$

COEFFICIENT OF PERFORMANCE:

$$COP = \frac{Q_C}{W} \leq \frac{T_C}{T_H - T_C}$$

(a)
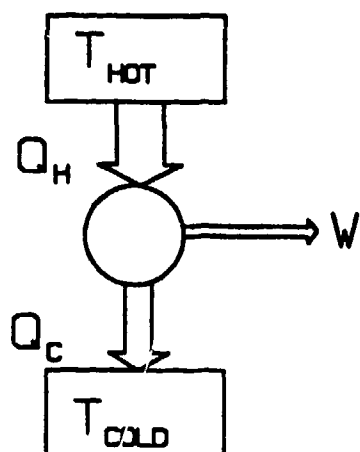
FIRST LAW: $Q_H = W + Q_C$

SECOND LAW: $\dfrac{Q_H}{T_H} \leq \dfrac{Q_C}{T_C}$

EFFICIENCY:

$$n = \frac{W}{Q_H} \leq 1 - \frac{T_C}{T_H}$$

(b)

Figure I-1. The Thermodynamics of (a) Prime Movers
and (b) Refrigerators.

5

the heat flow from the cold reservoir plus the work done to the system. The second law for this case is:

$$\Delta S_H \geq \Delta S_C \quad \text{or} \quad Q_H/T_H \geq Q_C/T_C. \tag{I-5}$$

The efficiency parameter for the refrigerator is called the coefficient of performance (COP). It is defined as the ratio of the heat flow from the cold reservoir to the work input to the refrigerator, or:

$$COP = Q_C/W = Q_C/(Q_H-Q_C) \leq T_C/(T_H-T_C). \tag{I-6}$$

The limit is known as the Carnot coefficient of performance.

The work in this thesis deals solely with refrigerators. Even though prime movers are mentioned from time to time, the primary focus of the rest of our discussion will be refrigerators.

3. Overall Efficiency

According to Hofler (1986), the early thermoacoustic work at Los Alamos focused on experimental refrigerating engines. The performance of these engines fell short of expectations, leading to simple experiments on basic thermoacoustic effects and a proof-of-principle experiment on thermoacoustic refrigeration. Hofler then applied the Rott theory to the experimental systems and solved the resulting equations numerically. For his doctoral dissertation from the University of California, San Diego, Hofler designed and constructed a completely functional thermoacoustic refrigerator. He also made accurate measurements of its thermodynamic efficiency, and used this efficiency to make compari-

6

sons to the Rott theory. After receiving his doctorate, Hofler came to the Naval Postgraduate School (NPS) as a post-doctoral fellow, and brought his prototype refrigerator with him.

The purpose of this thesis, in conjunction with the work of several other students, is to modify Hofler's refrigerator design in order to improve its overall efficiency and make it suitable for space cryocooler applications. The basic design of the thermoacoustic refrigerator is shown schematically in Figure I-2. The driver (A), which produces the sound waves, is coupled via bolts to the resonator (D) via a reducer cone (B) and bellows (C) Inside the resonator is a stack of plastic plates (E) and their heat exchangers (F) which allow the heat to be removed from the hot end and absorbed by the cold end. It is the interaction between the sound waves and the plastic plates that produces a temperature difference across the plates and/or pumps heat from the cold heat exchanger to the hot heat exchanger. A brief description of efficiency would be useful here. Figure I-3 shows a diagram of the chain of energy transformations which occurs in a thermoacoustic refrigerator. There are three conjugate variable pairs (V and I; P and U; and ΔT and $\dot{Q}_c$), and two transformations (electrical-to-acoustical and acoustical-to-thermal).

We start with electrical input power to the driver, which can be calculated (using r.m.s. values) with:
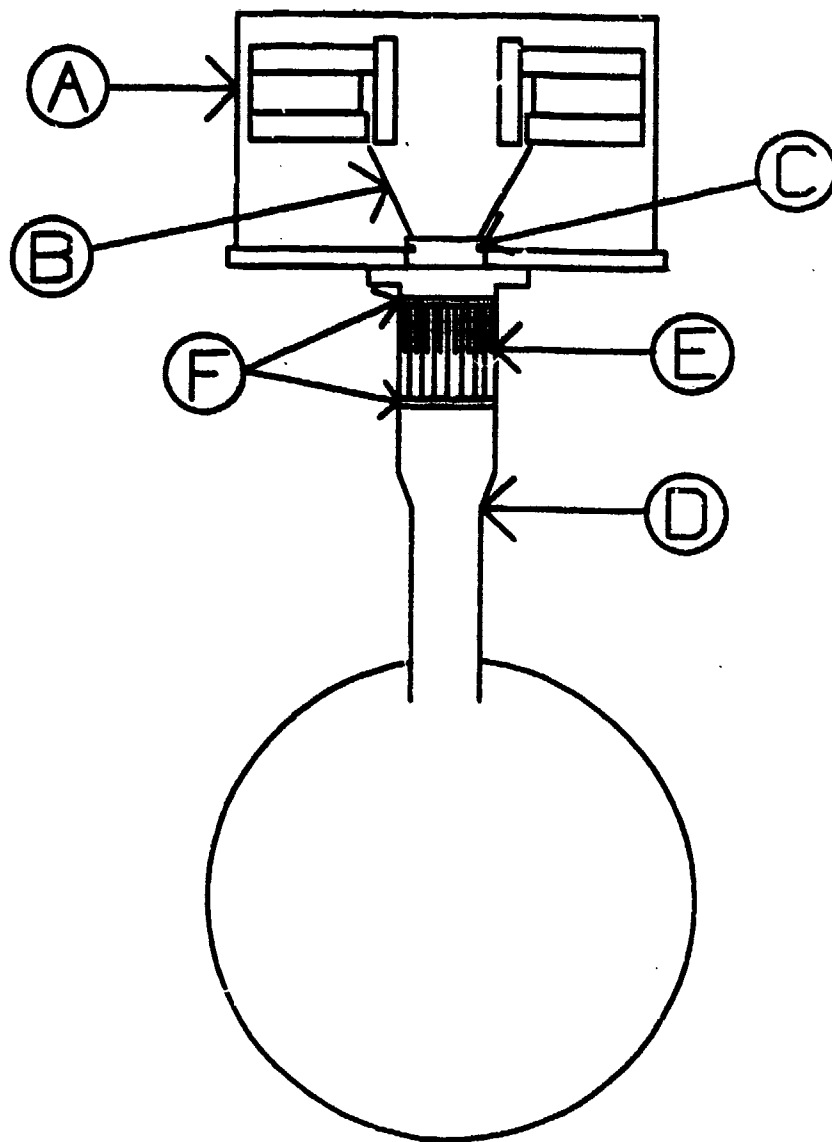
Figure I-2.   Basic Thermoacoustic Refrigerator Showing
              (A) Driver, (B) Reducer Cone, (C) Bellows,
              (D) Resonator, (E) Stack, and (F) Heat
              Exchangers.

DRIVER · · · · · · REFRIGERATOR

ELECTRIC

V, I

$P_{elec} =$

$VI\cos\theta$

ELECTRIC TO ACOUSTIC

ACOUSTIC

P, U

$\dot{W} =$

$PU\cos\phi$

ACOUSTIC TO THERMAL

THERMAL

$\Delta T, Q_c$
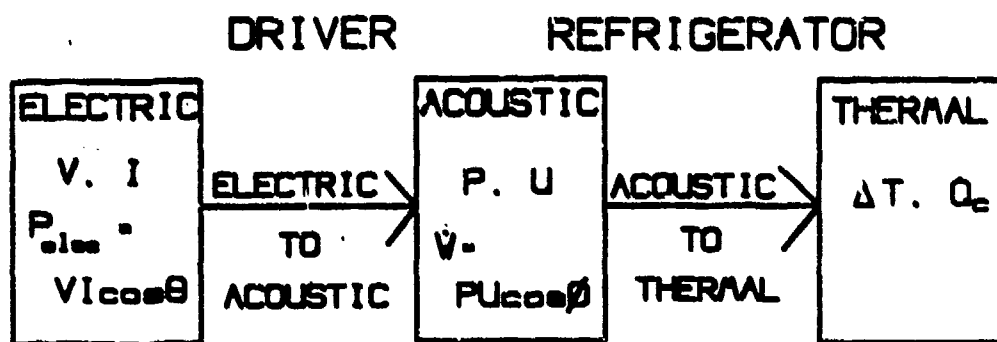
ELECTROACOUSTIC EFFICIENCY

$$n_{EA} = \frac{\dot{W}}{P_{elec}}$$

REFRIGERATOR COEFFICIENT OF PERFORMANCE

$$COP = \frac{Q_c}{\dot{W}}$$

OVERALL THERMOACOUSTIC EFFICIENCY

$$n_{TA} = \frac{Q_c}{P_{elec}} = n_{EA} \cdot COP$$

Figure I-3.   Chain of Energy Transformations in a
Thermoacoustic Refrigerator.

$$P_{elec} = I\ V \cos \theta, \qquad (I-7)$$

where I is the current into the electroacoustic driver, V is the voltage across the driver terminals, θ is the phase angle between I and V, and $\cos \theta$ is known as the "power factor." An electrodynamic driver converts the electrical power to acoustic power (the first transformation). Analogous with the previous definition of the electrical input power, the acoustic power is given by:

$$\hat{W} = P\ U \cos \phi, \qquad (I-8)$$

where P is the acoustic pressure, U is the volumetric velocity which equals the product of particle velocity and resonator cross-sectional area, and ϕ is the phase angle between them. The efficiency of this electroacoustic transformation is given by:

$$\eta_{EA} = \hat{W}/P_{elec}. \qquad (I-9)$$

In the second transformation, the refrigerator converts the acoustic power to a temperature gradient (∇T) and heat flow ($\dot{Q}$). As discussed previously, the efficiency for this transition is given as the coefficient of performance:

$$COP = \dot{Q}_C/\hat{W}. \qquad (I-10)$$

The overall thermoacoustic efficiency is therefore the product of the efficiencies for the two transformations:

$$\eta_{TA} = \eta_{EA} \cdot COP = \dot{Q}_C/P_{elec}. \qquad (I-11)$$

Improvements in the overall refrigerator efficiency can thus be divided into two distinct, though interrelated, efforts. The first is the subject of this thesis: modifica-

tions to the driver to optimize the electroacoustic efficiency. The second effort involves the optimization of the coefficient of performance and is addressed by LT Michael P. Susalla, USN, in his master's thesis.

B. SPACE THERMOACOUSTIC REFRIGERATOR (STAR)

1. Motivation

In addition to improving overall efficiency, our experimental refrigerator will be designed and built with the intention of flying it on the Space Shuttle as part of the National Aeronautics and Space Administration's (NASA) Get Away Special (GAS) program. As of 3 February 1988, there is a Memorandum of Agreement between the Naval Postgraduate School (NPS) and the Air Force which provides funding for the space flight and which assigns the NASA payload number G-337 to this project. The reason for testing the thermoacoustic refrigerator in space is that the immediate applications of the STAR are expected to be the cooling of electronics, high T_c superconductors, and infrared detectors in space.

There are currently two primary methods for cooling satellite systems in space: (1) evaporation of expendable cryogens (liquid helium, nitrogen, ammonia-methane, and solid hydrogen, etc.), and (2) closed cycle refrigerators (Stirling cycle, Vuilleumier cycle, etc.), which involve large reciprocating piston masses operating at low

11

frequency. [Walker (1983) and Smith, et al. (1984)] The disadvantages of these current cooling methods are their short lifetimes (expendable cryogens) and high vibration levels and low reliability (closed cycle refrigerators). The advantages of the thermoacoustic refrigerator over these and other systems lies in its simplicity and reliability. The STAR has no sliding seals, efficient performance, low vibration levels, and (hopefully) a longer life span.

The thermoacoustic refrigerator needs to be surrounded by a vacuum and insulation material to minimize heat loss due to thermal conduction and radiation. The vacuum of space will provide the best insulation to determine the refrigerator's ultimate efficiency. The absence of gravity removes the possibility of thermal convection as an additional nuisance heat transport mechanism.

2. Get Away Special (GAS) Program

NASA's GAS program allows small, self-contained payloads to fly on the Space Shuttle in GAS canisters for relatively low cost ($10,000) (Get Away Special Team, 1984). The GAS can is five cubic feet in volume and can house a payload of up to 200 pounds. Each payload must contain its own electrical power, control, data acquisition and storage facilities, etc. The Shuttle's astronauts will turn a switch on or off at designated times during the flight, but are otherwise not involved with the experiment.

12

3. Shared Subsystems from NASA G-313

Another group of NPS students and faculty (Boyd, et al., 1987) have taken advantage of the GAS program to measure the resonant acoustic modes of the shuttle payload bay and the ambient acoustic environment produced as a result of main engine and booster operation during launch. This experiment is titled "The Space Shuttle Cargo Bay Vibroacoustics Experiment" and is designated by NASA as payload G-313. Several subsystems that were developed for NASA G-313 will be used by NASA G-337 (STAR). A schematic of the STAR in its GAS can is shown in Figure I-4. One of the systems borrowed from NASA G-313 is the electronics system used to run the experiment and record the data. The recorder system consists of the INTEL model BPK 5V75 magnetic bubble memory module and an NSC 800 microprocessor-based controller. Two other NPS students, LT Charles B. Cameron, USN and CPT Ronald Byrnes, USA, will be designing the analog electronics and software to integrate these systems into the STAR experiment for their master's thesis. A block diagram of the electronics is shown in Figure I-5.

Another borrowed system is the power supply, which consists of Gates brand lead acid battery cells (five ampere-hour, two volts each). These gelled electrolyte batteries are ideal for the STAR due to their high power density, low cost, and the absence of outgassing during discharge cycles. NASA G-313 used a one layer battery of 68
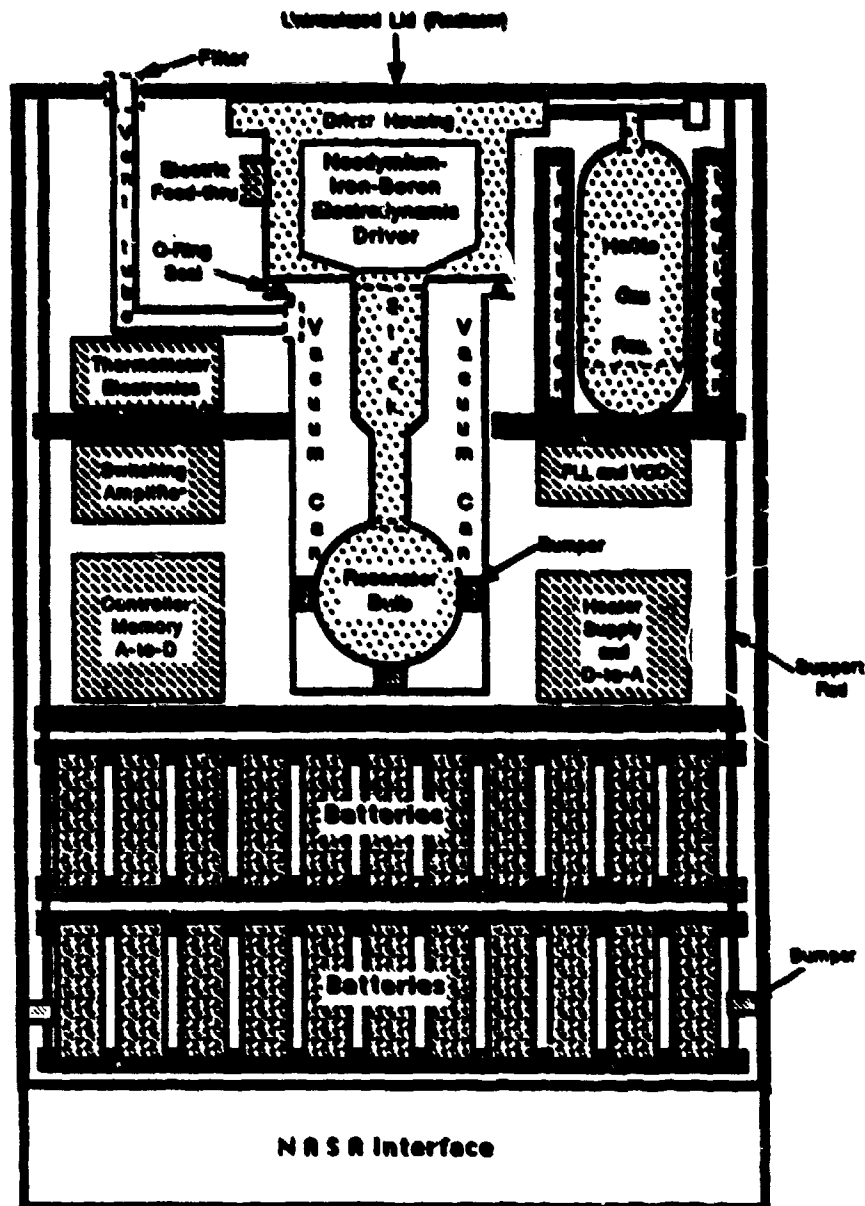
Figure I-4.   Schematic of the Space Thermoacoustic
             Refrigerator in its Get Away Special
             Cannister.

14

Acoustic Refrigerator Control and Thermometry

Computer/Controller

DC Power

[A] Accelerometer

[Pm] Microphone

[Pg] Pressure Gage

(VCO) Voltage Controlled Oscillator

[TC4] Thermocouple
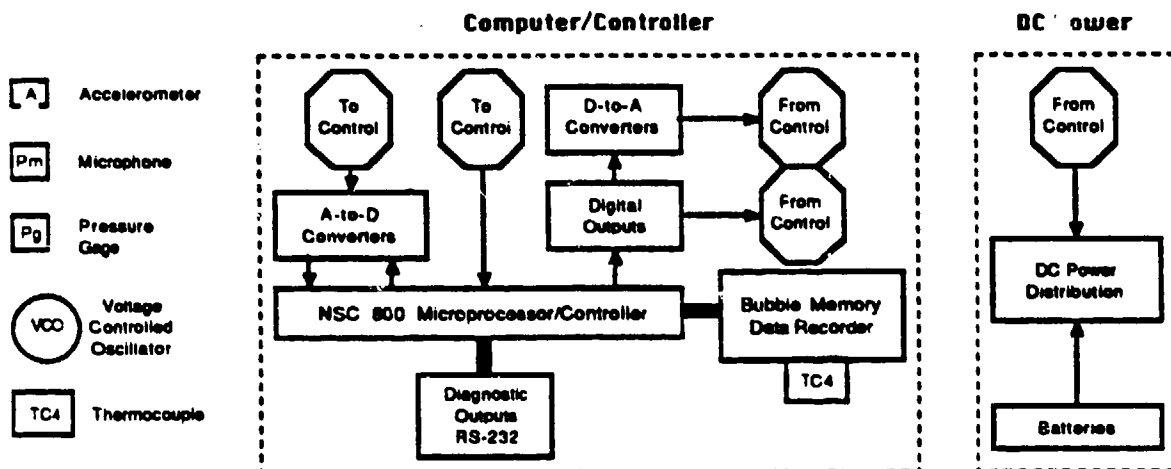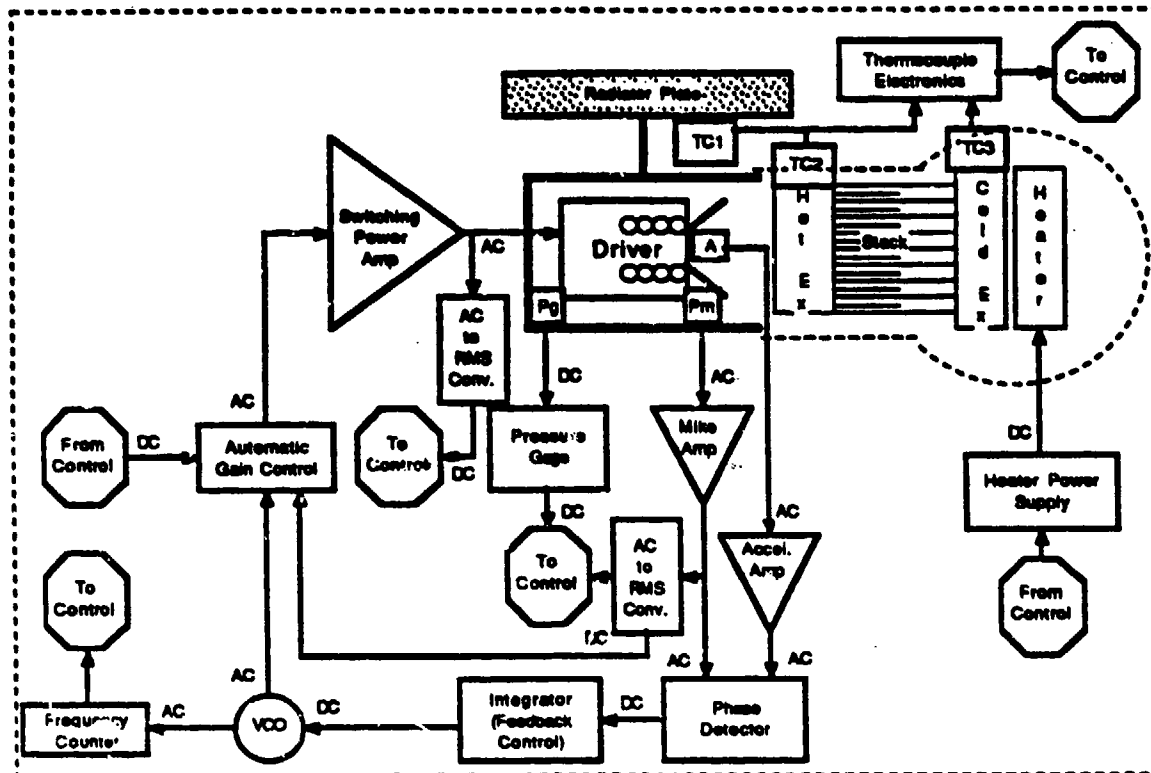
Figure I-5. Block Diagram of the Electronics for the Space Thermoacoustic Refrigerator.

cells providing 680 watt-hours of energy and weighing about 80 pounds (including the cells' support structure). We will be using two battery layers with as many cells as we can, up to 136. This will give us a minimum of 680 watt-hours and a maximum of 1,360 watt-hours of available electrical energy, and a battery weight between 80 and 160 pounds. The number of battery cells we can use will depend on the total weight of the driver-resonator assembly and its auxiliary equipment (vacuum can, gas reservoir, etc.) and electronics.

The use of the GAS can imposes certain restrictions. Since we are using batteries to supply the power, the refrigerator has to be energy efficient. Also, the GAS can setup requires the STAR to be compact and lightweight. Figure I-6 shows a photograph of Hofler's prototype refrigerator. This setup is approximately six feet high. In comparison, the maximum payload height for the GAS can is 28.25 inches, or less than 2.5 feet. These considerations played a major role in the choice of equipment for and the design of the STAR.

C. SCOPE

Chapter II discusses basic acoustical and thermodynamic theory as applied to STAR. The results of this theory determine the driver requirements. The theory of the selected electrodynamic driver is given next. Following the driver theory is a presentation and discussion of a computer program that models the coupled system, which consists of

16
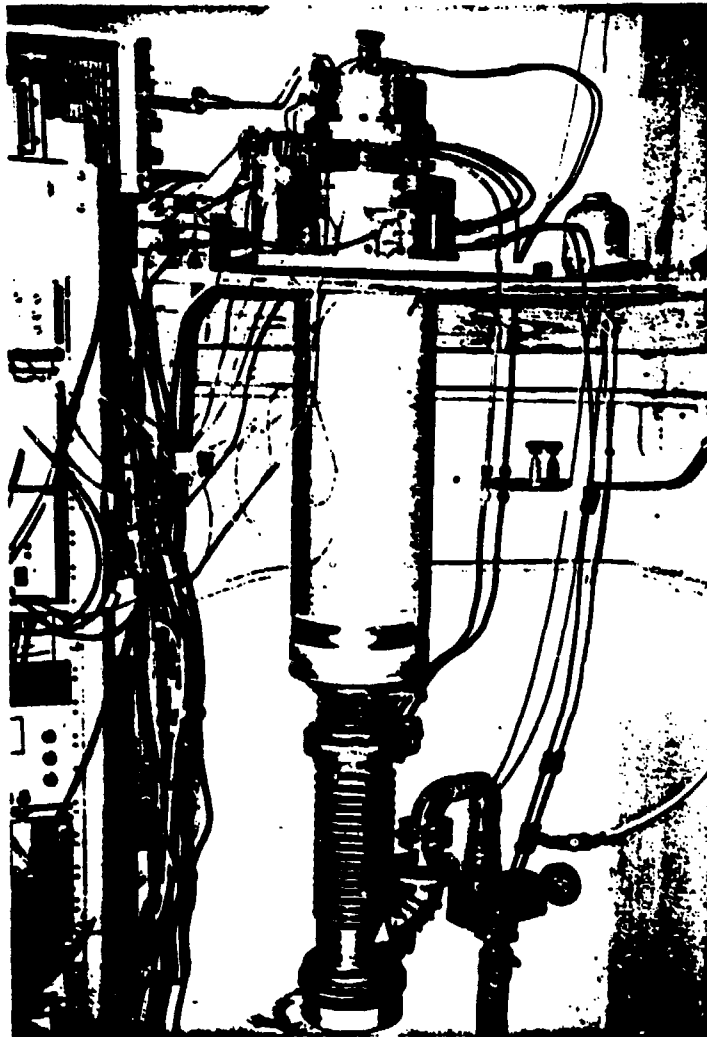
Figure I-6.   Photograph of Hofler's (1986)
             Prototype Refrigerator.

the electrodynamic driver and the resonator containing the gas mixture and stack.

Chapter III describes the technique for measuring the electrodynamic driver parameters. These parameters are used as input for the driver design, the computer model, and the efficiency calculations. This measurement technique was developed using an Altec 290-16K electrodynamic driver and was applied to the final driver.

Chapter IV describes the measurement of the STAR driver parameters. The driver chosen for STAR is a custom unit, built by Harmon-JBL!‹™›, which uses neodimium-iron-boron (NIB) magnets. The STAR driver is a minor modification of a new line of compression drivers using NIB magnets and has characteristics similar to the JBL 2450J.

Chapter V discusses the construction of the STAR driver, including the housing and accessories (reducer, stiffener, bellows, accelerometer, microphone, electrical feed-throughs, etc.) necessary to integrate it with the resonator and the GAS cannister system. Dimensional shop drawings for the parts are included in Appendix C.

Chapter VI gives conclusions and recommendations for further development.

II. THEORY

A. THERMOACOUSTIC THEORY

Thermoacoustic theory has been developed in detail by Rott (1969, 1974, 1975 and 1980) and adapted to the thermo-acoustic refrigerator by Wheatley et al. (1982, 1983a, 1983b, 1985 and 1986), Wheatley and Cox (1935), Hofler (1986) and Swift (1989).

The space thermoacoustic refrigerator (STAR) basically consists of an acoustic driver producing sound waves in a resonant tube (see Figure I-2). This resonator is filled with a mixture of helium-xenon gas (12.5% xenon) pressurized to ten atmospheres, and contains a stack of plastic plates. This Chapter will present a qualitative model for the thermoacoustic heat pumping process followed by a quantitative development for heat and work flow at a plate. The Chapter concludes with the efficiency of a stack of plates that are very much shorter than one quarter of a wavelength.

1. Qualitative Picture

Consider a parcel of gas that moves back and forth along one of the plates at the acoustic frequency (see Figure II-1). As it moves, the gas parcel will experience changes in temperature and volume. Part of the temperature changes come from the adiabatic compression and expansion of the gas by the sound pressure, and part as a consequence of

19
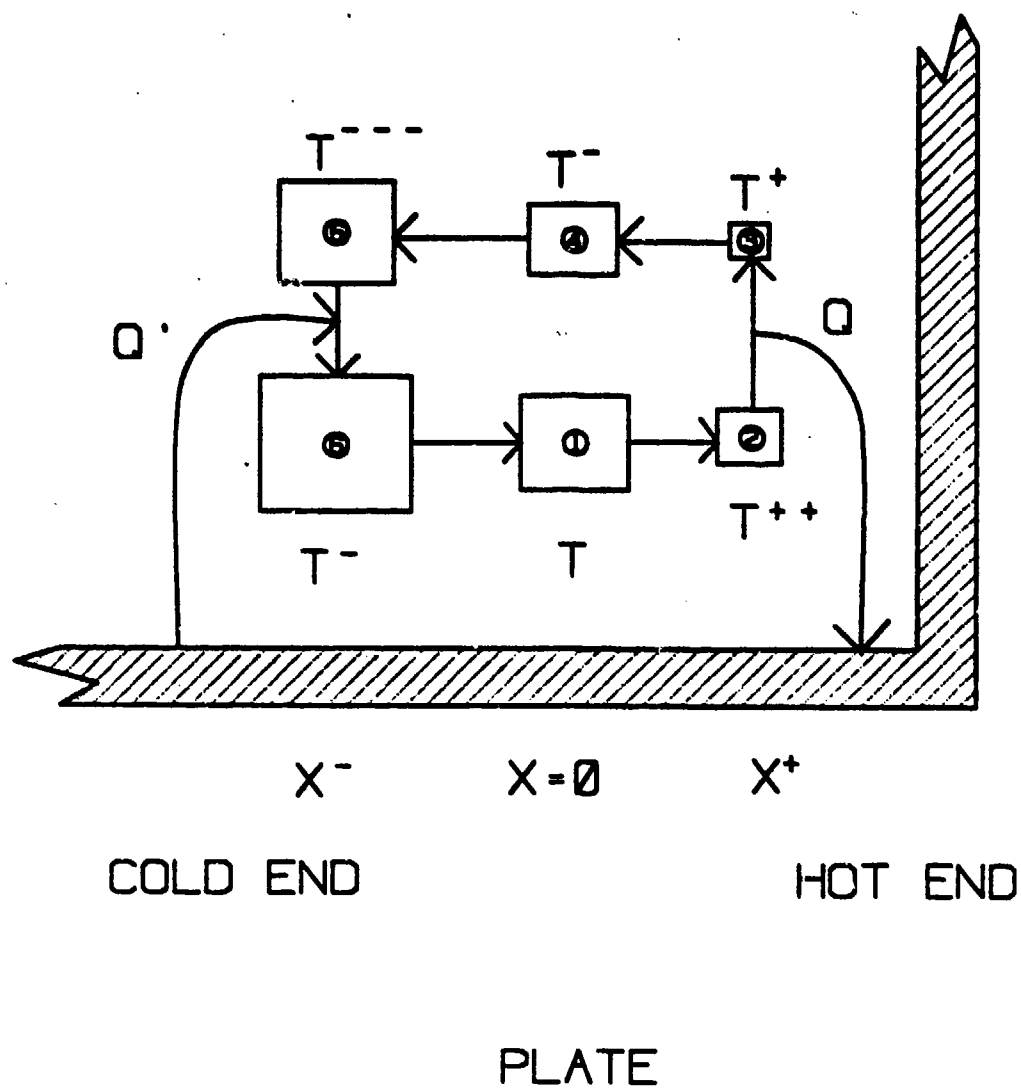
Figure II-1. Gas Parcel Diagram. (Note: Displacement
in the Vertical Direction is Shown for
Clarity--Parcel Moves in Horizontal
Direction Only.)

the local temperature of the plate itself. A temperature
gradient may develop along the plate as a result of the
operation of the refrigerator. The temperature and volume
changes can be described by six separate steps (the changes
in volume are indicated by the change in size of the square
parcel in the figure).

Assume the plate is at a uniform temperature, T. The
parcel starts at position 1 (X = 0) with a temperature of T.
The sound wave moves the parcel to the right to position 2.
The parcel has undergone adiabatic compression and its tem-
perature is now T^{++}. Since the temperature of the gas is
higher than that of the plate, heat (Q) will flow from the
gas parcel to the plate. The parcel's volume is decreased
and its temperature lowered to T^{+}. This heat flow also
causes the plate's temperature to increase at the position
X^{+}. Parcel position 3 is actually in the same location as
position 2, but it is displaced vertically in the figure for
clarity. The parcel now moves to position 4 and expands
adiabatically to a new temperature of T^{-}. A repeat of this
process puts the parcel in position 5 with a temperature of
T^{---}. Now the temperature of the gas is lower than that of
the plate and heat (Q') flows from the plate to the gas
parcel, expanding the parcel and raising its temperature to
T^{--}. This flow causes the plate's temperature to decrease at
position X^{-}. The parcel moves to the right again under
adiabatic compression and we are back where we started in

21

position 1 with temperature T (adapted from Wheatley, et al., 1985).

This gas parcel cycle is repeated at the resonator's operating frequency. For the STAR this frequency is between approximately 250 and 600 cycles per second, depending on the gas mixture (specifically the speed of sound in the gas mixture) and the length and shape of the resonator.

Notice that the temperature of the gas parcel at position X = 0 is different depending on which direction the gas parcel is moving. It is this phase shift in temperature relative to motion that produces the thermoacoustic effect, as we will show in the calculations that follow.

It is also important to note that in order for heat to flow between the gas parcel and the plate, the parcel must be vertically located within about a thermal penetration depth of the plate. The thermal penetration depth (δ_K) is the distance that heat can diffuse through the fluid during a time $1/\omega$, where ω is the acoustic angular frequency.

Wheatley et al. (1986) describe thermoacoustic engines as consisting of long trains of these gas parcels, all about a thermal penetration depth from the plate. The parcels draw heat from the plate at one extreme of their oscillatory motion and deposit heat at the other extreme. Adjacent heat flows cancel except at the ends. The net result is

that an amount of heat Q is passed from one end of the plate to the other.

2. Single Plate

Swift (1989) illustrated the basic principles of the thermoacoustic engine by examining a simple example of a single plate in a gas-filled tube such as we described above. In this example the acoustic and thermodynamic effects are nearly distinct. In the absence of the plastic plate, the plane standing wave sustained in the tube has well-known acoustic properties. It's pressure and x-direction velocity (along the length of the tube) are given as (using peak values):

$$P_1 = p_a \sin(x/\lambda) \qquad (II-1)$$

$$\text{and} \qquad u_1 = i(p_a/p_m a) \cos(x/\lambda) \qquad (II-2)$$

where P_a is the pressure amplitude at the pressure antinode, the reduced wavelength $\lambda = \lambda/2\pi = a/\omega$, λ is the wavelength, a is the speed of sound in the gas, ω is the angular frequency, and p_m is the mean density of the gas. The subscript 1 indicates the first order time oscillation, and the subscript m indicates the mean value. The total pressure can be given as

$$P = P_m + p_1 e^{i\omega t}. \qquad (II-3)$$

A similar expression represents the total velocity. Following Swift, we will assume that the first order in the acoustic amplitude is sufficient for all acoustic and thermo-

dynamic variables (pressure, velocity, temperature, density, and entropy).

The sound wave is adiabatic and has an oscillatory temperature given by:

$$T_1 = (T_m\beta/\rho_m c_p)\, p_1, \qquad (II-4)$$

where $\beta = -(d\rho/dT)_p/\rho_m$ is the isobaric thermal expansion coefficient and c_p is the isobaric (constant pressure) heat capacity per unit mass. Note that T_1 and p_1 are in phase. For ideal gases, thermodynamics tells us that

$$T_m\beta/\rho_m c_p = (\gamma-1)T_m/\gamma p_m, \qquad (II-5)$$

where γ = the ratio of isobaric to isochoric specific heats (5/3 for monatomic gases, smaller, but greater than one, for other gases). Combining Equations II-4 and II-5 gives us:

$$T_1/T_m = [(\gamma-1)/\gamma]\, p_1/p_m. \qquad (II-6)$$

The introduction of the plastic plate into the standing wave modifies the original, unperturbed temperature oscillations. This modification is due to the heat flow between the gas and the plate, as described previously. The temperature is modified in both magnitude and phase for gas about a thermal penetration depth away from the plate. According to Swift, this results in two important effects: 1) a time-average heat flow near the surface of the plate, along the direction of acoustic vibration, and 2) the generation or absorption of real acoustic power near the surface of the plate. In refrigerators the effect is an absorption of acoustic power. In prime movers the acoustic

power is generated by the temperature gradient present in the plate.

There are several assumptions we will make to simplify calculations, again following Swift. We assume that the plate is short enough compared to a reduced wavelength ($\Delta x \ll \lambda$) and far enough from both velocity and pressure nodes that p_1 and u_1 can be considered uniform over the entire plate. We assume the gas has zero viscosity, so that u_1 does not depend on y (we had already made this assumption by looking at u_1 in the x-direction only). We assume that the plate has a large enough heat capacity per unit area that its temperature does not change appreciably at the acoustic frequency. We assume that the plate has a mean temperature gradient in the x-direction ∇T_m. Finally, we neglect the plate's and gas' thermal conductivity in the x-direction.

Applying these assumptions, we see that the mean fluid temperature ($T_m(x)$) is the same as that of the plate. Swift calculated the oscillating fluid temperature using the general equation of heat transfer. He kept only first-order terms, neglected thermal conduction along x, and applied the boundary condition $T_1(0)=0$ imposed by the plate. The resulting equation is:

$$T_1(y) = [(T_m\beta/\rho_m c_p)p_1 - (\nabla T_m/\omega)u_1][1-\exp[-(1+i)y/\delta]]. \quad (II-7)$$

To interpret this equation, we look at it in the limit that

25

the gas is far enough from the plate ($y \gg \delta \kappa$) to make negligible thermal contact with the plate. This gives:

$$T_1(y) \rightarrow [(T_m \beta / \rho_m c_p) p_1 - (\nabla T_m / \omega) u_1] \qquad (II-8)$$

The first term in Equation II-8 is the temperature oscillation due to the adiabatic compressions and expansions of the gas (see Equation II-4). The second term comes from the mean temperature gradient in the gas. As the gas oscillates along x with displacement amplitude u_1/ω, the temperature at a given point in space oscillates by an amount $\nabla T_m u_1/\omega$ even if the temperature of a given piece of fluid remains constant. The actual temperature oscillations are a linear superposition of these two effects.

The y dependent part of equation II-7 is complex. It approaches 1 for $y \gg \delta \kappa$, as given previously. It approaches zero for $y \ll \delta \kappa$, where the plate imposes the condition $T_1 = 0$. Most importantly, for $y \approx \delta \kappa$, its magnitude is still of the order of 1, but it has a substantial imaginary part. This phase shift in the oscillating temperature of the standing wave at $y \approx \delta \kappa$, due to the thermal presence of the plate, is an important result because it leads directly to the time-averaged heat flow in the x-direction. It is the same phase shift we emphasized in the description of the gas parcel motion.

a. Heat Flow

Swift argues that since we are neglecting ordinary thermal conductivity in the x direction, the only way

26

heat can be transported along x is by the hydrodynamic
transport of entropy, carried by the oscillatory velocity
u_1:

$$q_2 = T_m \rho_m \overline{s_1 u_1} = 1/2 \, \rho_m c_m \, Im \, [T_1] \, u_1. \qquad (II-9)$$

The line above the quantity $s_1 u_1$ indicates the time-average
of the first-order entropy and velocity product. The heat
flow is a second order quantity, signified by the subscript
2.

The total heat flow Q_2 along the plate, in the x-
direction, is found by integrating q_2 over the y-z plane:

$$Q_2 = \Pi \int_0^\delta q_2 \, dy \qquad (II-10)$$

where Π is the perimeter of the plate in the y-z plane.
Substituting for T_1 and performing the integration gives:

$$Q_2 = -1/4 \, \Pi \delta \kappa (T_m \beta) p_1 u_1 (\Gamma - 1) \qquad (II-11)$$

where $\Pi \delta \kappa$ is the thermodynamically active area in a plane
perpendicular to the longitudinal acoustic motion, $T_m \beta$ is
the heat parameter of the gas, and Γ is defined as the ratio
of actual temperature gradient to the critial temperature
gradient ($\nabla T / \nabla T_{crit}$). The critical temperature gradient
occurs when the temperature change along the plate just
matches the temperature change due to the adiabatic
compression of the gas, and no heat flows between the gas
and the plate. It is the boundary between the refrigerator
and prime mover functions of the thermoacoustic engines.

Equation II-11 shows that when $\Gamma < 1$, heat flows
up the temperature gradient from cold to hot and work

27

(acoustic power) is absorbed, as for a refrigerator. When $\Gamma = 1$ there is no heat flow. When $\Gamma > 1$, heat flows down the temperature gradient from hot to cold and acoustic power is produced, as for a prime mover.

Note that the total heat flow is proportional to the area $\Pi \delta \kappa$, and to $T_m \beta$ ($=1$ for ideal gases). It is also proportional to the product $p_1 u_1$, and so equals zero if the plate is at either a pressure node or a velocity node of the standing wave. The maximum value of the product occurs halfway between the nodes. Finally, the heat flow is proportional to the temperature gradient factor $\Gamma - 1$. For $\nabla T_m > \nabla T_{crit}$, $\Gamma - 1 > 0$ and the heat flow is toward the pressure node, while for $\nabla T_m < \nabla T_{crit}$, $\Gamma - 1 < 0$ and the heat flow is away from the pressure node. If suitable heat exchangers at temperatures T_H and T_C are installed at the ends of the plate (with $T_H - T_C = \nabla T_m \Delta x$), this heat flow carries heat from one exchanger to the other.

The heat flow is small under ordinary circumstances. However, in closed resonators it is possible to achieve sound amplitudes many orders of magnitude higher than those of ordinary conversation. Since Q_2 is proportional to p_a^2, and since in practical acoustic engines the entire cross section of the standing wave is filled with plates (spaced roughly $4\delta \kappa$ apart), very high heat flows and/or a large $T_H - T_C$ may be achieved.

b. Work Flow

The work flow (i.e. acoustic power) is given by the work per cycle times the rate at which that work occurs (the acoustic frequency f). From thermodynamics, the average acoustic power produced per unit volume is:

$$\dot{W}_2 = -(\omega/\rho_m) \, \overline{ip_1\rho_1} = -1/2 \, \omega\beta \, p_1 \, Im[T_1]. \qquad (II-12)$$

The gas about a thermal penetration depth away from the plate "breathes," because of thermal expansion and contraction, with the right time phase with respect to oscillating pressure to do (or absorb) net work. This is exactly the same gas that we have seen is responsible for the heat flow. Gas elsewhere is ineffective in doing (or absorbing) work. The density oscillations for $y \ll \delta_K$ and for $y \gg \delta_K$ are in phase with the pressure oscillations, and hence do (or absorb) no net work.

The total acoustic power $\dot{W}_2$ produced is found by integrating $\dot{w}_2$ over all space, as with the heat flow:

$$W_2 = 1/4 \, \Pi\delta_K \, (\gamma-1) \, (p_1^2/\rho_m a) \, (\Gamma-1) \, \Delta x/\lambda, \qquad (II-13)$$

where all the terms have been defined previously.

The acoustic power is proportional to the volume $\Pi\delta_K\Delta x$ of fluid that is about a thermal penetration depth from the plate. It is proportional to p_1^2, and so is quadratic in the acoustic amplitude (as was the heat flow) and vanishes at pressure nodes. Finally, W_2 is proportional to $(\Gamma-1)$, the same temperature gradient factor as appeared in Q_2 (Equation II-11). When $\nabla T_m = \nabla T_{crit}$, $(\Gamma-1) = 0$, and there

29

are no temperature oscillations in the fluid other than those due to adiabatic processes, and no acoustic power is absorbed or generated. For $\nabla T_m > \nabla T_{crit}$, $\Gamma - 1 > 0$ and acoustic power is produced near the plate. Whether this power increases the amplitude of the standing wave, is radiated away to infinity, is simply absorbed, or flows through an acoustic-to-electric transducer to generate electric power depends on details of the resonator, not on the plate itself or on the standing wave near the plate. For $\nabla T_m < \nabla T_{crit}$, $\Gamma - 1 < 0$ and acoustic power is absorbed near the plate. For a tube without plates which has a diameter less than the wavelength, at constant temperature ($\nabla T = 0$), this work flow is responsible for the ordinary thermal attenuation of a sound wave (Kinsler, et al., 1982).

c. Efficiency

We combine Equations II-11 and II-13 to get the efficiency of the plate with no viscous or longitudinal conduction losses:

$$\eta = W_2/Q_2 = (\gamma-1)/(T_m\beta)\ (\omega\ \Delta x\ p_1)/(\rho_m a^2 u_1). \quad (II-14)$$

Since $u_1 = u_o \sin x/\lambda$, and $p_1 = \rho_m a\ u_o \cos x/\lambda$,

$$\eta = (\gamma-1)/(T_m\beta)\ (\Delta x/\lambda\ \tan x/\lambda). \quad (II-15)$$

For $x \ll \lambda$, $\quad \eta = (\gamma-1)/(T_m\beta)\ (\Delta x/x), \quad (II-16)$

$$\text{and} \qquad \eta = \eta_{carnot}/\Gamma \quad (II-17)$$

This efficiency approaches the Carnot efficiency as the power output and heat transfer rates approach zero.

We can make a similar calculation for the refrigerator mode of operation, where the relevant efficiency is the coefficient of performance, COP = $\dot{Q}_2/\dot{W}_2$. We find that

$$COP = \Gamma \ COP_{carnot}. \qquad (II-18)$$

3. Short Stack

After developing the basic principles of the thermo-acoustic engine using a simplified example, Swift developed a more realistic model by including viscosity, longitudinal thermal conductivity, finite (instead of infinite) plate heat capacity, and many plates. He still made the assumptions that the temperature spanned is much less than the absolute temperature, that the length of the plates is much shorter than the reduced wavelength, and that the spacing between the plates is greater than a few penetration depths.

Using the equation of motion for the gas, the boundary condition that the velocity at the gas-plate interface is zero, the continuity equation of the gas, the heat flows in the gas and plates, and basic thermodynamic properties, Swift derived a wave equation for pressure $p_1(x)$ in terms of dT_m/dx, material properties and geometry. Swift also derived an equation for enthalpy flow along x in terms of $p_1(x)$, $T_m(x)$, geometry, and material properties (including Prandtl number of the gas $\sigma = c_p\mu/\kappa$, where μ is the viscosity, and κ is the thermal conductivity of the gas).

31

In the boundary layer approximation, for a short ($\Delta x \ll \lambda$) stack of plates, and neglecting viscosity, the heat flux and acoustic power are given by expressions very similar to the simple results of the single plate example. Practical engines can be expected to have all available cross-sectional area filled with plates spaced about $4\delta_\kappa$ apart. The only effect of longitudinal (i.e., along x) thermal conductivity is to add to the heat flow in the x direction by simple conduction. For gases this effect is normally negligible.

The inclusion of viscosity adds considerable algebraic complication, and a little conceptual difficulty as now u_1 is a function of y.

Without viscosity, ∇T_{crit} is the temperature gradient for which the temperature oscillation at a given x-location is zero. But in the presence of viscosity, T_1 depends on x as well as y, so no well-defined ∇T_{crit} exists.

To the lowest order in $\sqrt{\sigma}$ (where σ is the fluid's Prandtl number), the hydrodynamic heat flow is increased by $1/(1-\sqrt{\sigma})$. This factor arises because the mean velocity $\langle u_1 \rangle$ underestimates the velocity with which entropy is convected along the stack. As we saw in the single plate calculations, the convective entropy transport occurs mostly at a distance δ_κ from the plate. The velocity there is higher than the mean velocity by $1/(1-\sqrt{\sigma})$.

32

The lowest order effect of viscority on the acoustic power is the power dissipated by viscous shear in the fluid within the boundary layer, a well-known fluid mechanical result.

For accurate calculations, the full general equation must be used; but for rough estimates, the results presented here are good approximations, and are much simpler to compute with. In addition, the results presented here are fairly easy to interpret physically. The expressions for arbitrary viscosity are complicated, but those to lowest order in viscosity are simple. It is easy to see the single plate expressions for heat flow and acoustic power about a thermal penetration depth from the plates, modified as longitudinal thermal conductance adds to the heat flow, as viscous shear dissipates acoustic power, and as non-ideal plate properties modify the thermal boundary condition at the fluid-plate interface.

4. Design Considerations

One of the important considerations in the design of a thermoacoustic refrigerator is the location of the stack of plates with respect to the pressure and velocity nodes and antinodes of the acoustic standing wave in the resonant tube. Experiments performed by Wheatley, et al. (1986) showed that the heat flow as a function of position fit a simple sine curve whose spacial period is half the wavelength of the acoustic standing wave. By noting how the sign

33

of the temperature difference varied with respect to the plate's location in the sound wave, they saw that heat always flows in the direction of the closest pressure anti-node. This effect is expected because a parcel of gas moving in the direction of a pressure antinode is compressionally warmed and will transfer heat to the plate. A parcel moving toward a pressure node is cooled by expansion and will draw heat from the plate. At both the pressure nodes (velocity antinodes) and antinodes (velocity nodes) heat flow drops to zero. Thus the acoustic heat flow depends on both the acoustic pressure and the fluid velocity.

As a plate or stack of plates is moved away from the pressure antinode, the temperature gradient developed becomes smaller. At a quarter of a wavelength, no gradient forms (the critical temperature gradient equals zero). This positioning effect is important in the design of a refrigerator, because, together with the length of the plates, it places an upper limit on the maximum temperature drop possible across the stack.

B. DRIVER REQUIREMENTS

In order to drive the thermoacoustic refrigerator we needed a device, a transducer, that would convert the electrical energy of a battery pack to acoustic energy, as discussed in Subsection I.A.3. We wanted as high a pressure (or force) and volume velocity (or motion) as possible to

get the most acoustic power provided to the system. There were several types of electroacoustic transducers to choose from: electro-static, electret, electrodynamic, magneto-strictive, electro-strictive, and piezoelectric. Only one of these, the electrodynamic transducer, can provide our system with both the large forces and velocities necessary. This transducer will be described in the next section. The remainder of this section describes the rest of the trans-ducers and explains why each was not appropriate for use in the thermoacoustic refrigerator.

The electrostatic transducer consists of a pair of charged electrodes, or capacitor plates, one of which is held stationary while the other, the diaphragm, moves in response to electrical excitation. The electret is a kind of electrostatic transducer that has a diaphragm of polarized plastic, and therefore does not need an external voltage supply to the diaphragm (Kinsler, et al, 1982, p. 350). If an alternating voltage is applied across the plates, the diaphragm moves, thereby radiating an acoustic wave. Unfortunately there is very little force (or pressure) and displacement associated with this motion. This type of transducer may be useful as a microphone but is not an appropriate choice to drive the thermoacoustic refrigerator.

In a magnetostrictive transducer a change in the magnetic polarization in the material causes an elastic strain (Wilson, 1985, p. 3.). Although the forces are more

than adequate the strain produces too little motion to be useful to us.

In electrostrictive and piezoelectric transducers an externally applied electric field causes a change in the dielectric polarization of the material, which in turn causes an elastic strain (Wilson, 1985, p. 3). Once again there is sufficient force but the displacement due to the strain is too small to be useful.

Because these techniques have sufficient force, it would be possible to overcome the displacement limitation using mechanical leverage or other forms of mechanical impedance transformation, but this was not considered due to the associated increase in device complexity.

C. ELECTRODYNAMIC THEORY

1. Physics

The electrodynamic driver is a moving coil transducer which converts electrical energy to kinetic energy (motion). It consists of a diaphragm attached to a cylindrical coil of wire (voice coil) that is suspended in a fixed magnetic field (see Figure II-2). If an alternating current is supplied to the coil, the interaction of the current and the magnetic field will induce a force on the coil so that the diaphragm moves. The magnitude of the force is $F = BlI$, where B is the magnitude of the magnetic induction, l is the length of the coil and I is the current. The
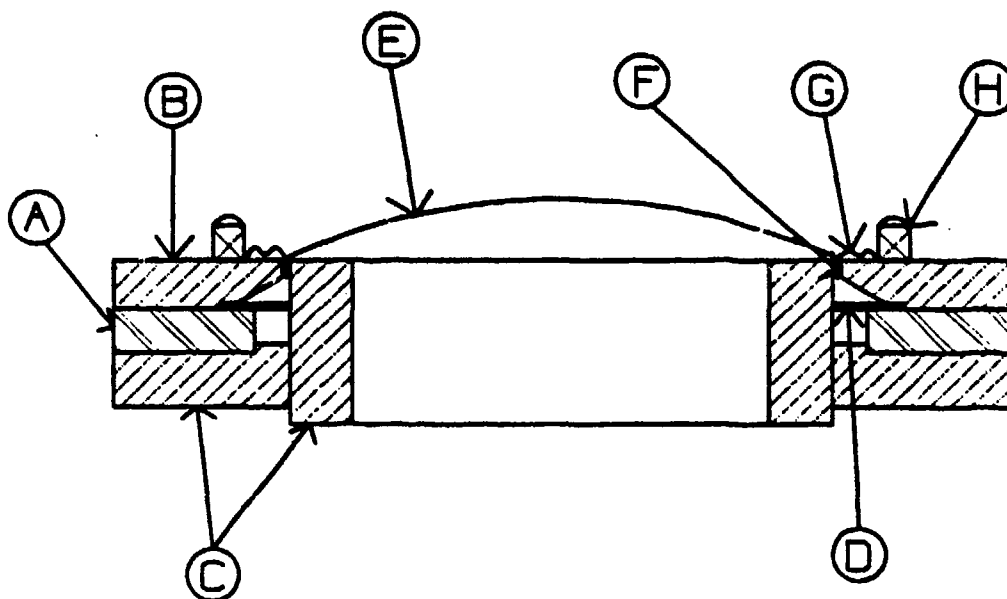
Figure II-2. Schematic of an Electrodynamic Transducer
Showing (A) Magnet, (B) Back Plate,
(C) Pole Piece, (D) Acoustic Seal,
(E) Diaphragm, (F) Voice Coil,
(G) Surround (Suspension), and
(H) Electrical Lead Connection.

37

direction of the force, given by the cross product of the current vector and the magnetic field (from Ampere's law $\underline{F}$ = $I\underline{l}$ X $\underline{B}$), is everywhere orthogonal to the current and the radial magnetic field. The motion of the diaphragm produces sound waves with a frequency equal to that of the alternating current. Another important property of the electrodynamic transducer is that the motion of the voice coil induces an electromotive force (emf) which equals Bl times the velocity of the voice coil (emf = Blv). This "back emf" increases the electrical impedance of the driver and can be used to monitor the driver motion as discussed in Section III.B.

The driver is attached to the resonator via a reducer and bellows. The reducer is a cone-shaped piece of aluminum mechanically connecting the driver voice coil which produces the force to the bellows, which in turn is in contact with the gas in the resonator. The reducer is designed to be lightweight, rigid, and strong for a direct transfer of motion and energy from the moving coil to the bellows. The bellows is a lightweight and flexible gastight seal between the driver and the tube. An aluminum plate is used as an interface between the reducer and the bellows to keep the bellows face rigid. For the STAR driver the reducer and plate are incorporated into a single unit machined from aluminum bar stock.

Figure II-3 shows a mechanical model of the electrodynamic transducer as a forced simple harmonic oscillator (SHO), which consists of a moving mass (m_o), stiffness (k), mechanical damping or resistance (R_m), and driving force (F). Included in the moving mass are the masses of the voice coil, reducer, stiffener, and bellows. The stiffness includes the suspension stiffness of the voice coil surround, the stiffness of the gas volume trapped behind the diaphragm, and the stiffness of the bellows. The equations governing the SHO can thus be used to determine the moving mass and stiffness of the driver. The primary relationship used is:

$$\omega_o^2 = k/m_o,\qquad\qquad (II-19)$$

or, the resonant angular frequency squared equals the stiffness divided by the moving mass. The use of this and other relationships will be discussed further in Chapter III, Driver Parameter Measurements.

2. Equivalent Circuit

An electrical circuit can be drawn that is equivalent to an electromechanical system if the values given for R_m, L_m, and C_m in the circuit produce the same electrical effects as the electromechanical system itself. In the case of the electrodynamic driver, the equivalent circuit is shown in Figure II-4 with the values given by Kinsler, et al. (1982) as:

Mechanical

$$R_{mech}$$

$$F \rightarrow \quad M_o \quad \rightarrow U$$

$$K$$

Acoustical

(P, Q, U)
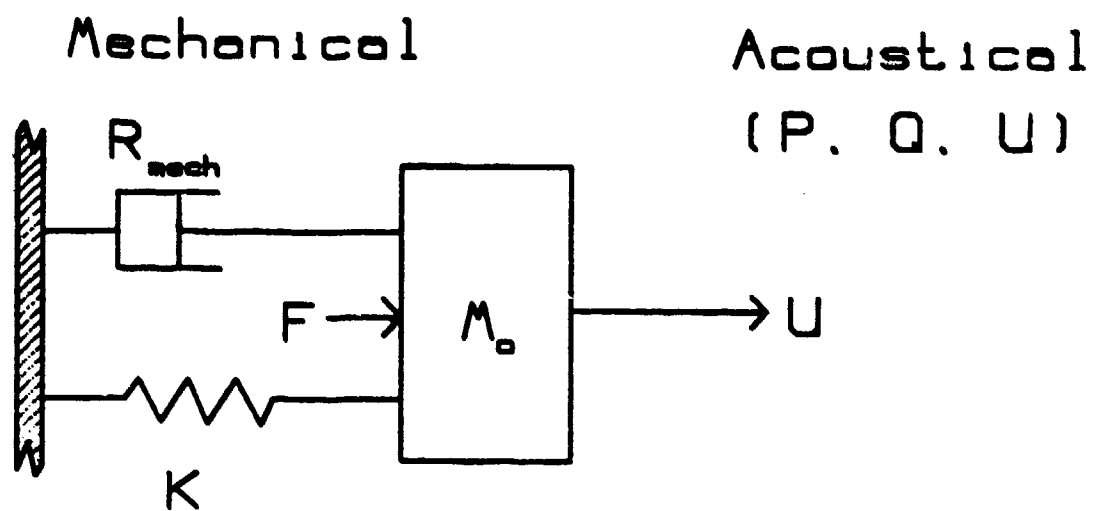
$$M_o = M_{coil} + M_{bellows} + M_{reducer}$$

$$K = K_{susp} + K_{bellows} + K_{gas\ vol.}$$

Figure II-3.   Electrodynamic Transducer--Forced Simple
Harmonic Oscillator Model.
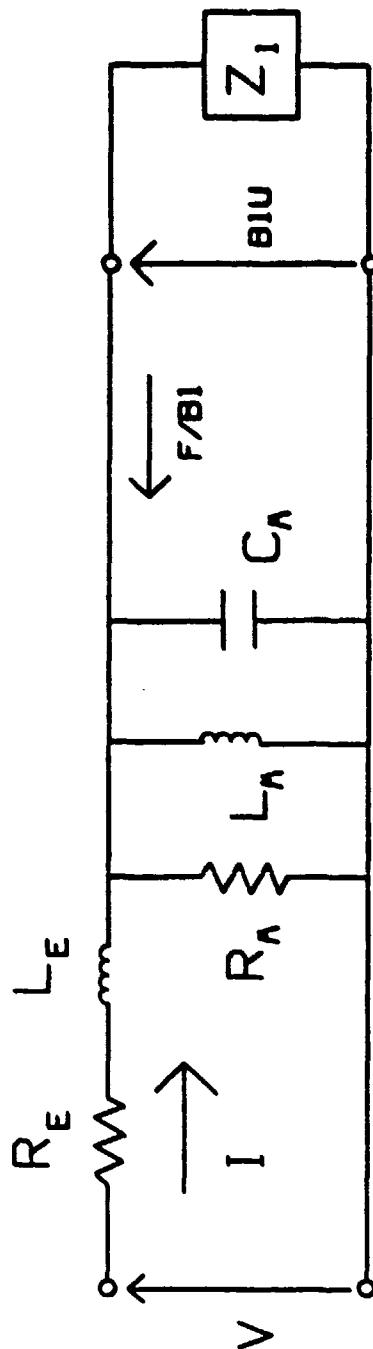
Figure II-4. Equivalent Electrical Circuit for the
Electrodynamic Transducer.

$$R_{m} = (Bl)^{2}/R_{m}, \tag{II-20}$$

$$L_{m} = (Bl)^{2}/k, \tag{II-21}$$

$$C_{m} = m_{m}/(Bl)^{2}, \tag{II-22}$$

where Bl is the transduction coefficient, R_{m} is the mechanical resistance, and k and m_{m} are the stiffness and moving mass as described previously.

The properties of the equivalent circuit allow us to evaluate the performance of the electrodynamic driver as if it were an entirely electrical system. The amount of power the driver generates will depend on the load it sees. Since one of the primary purposes of this thesis is to maximize the ratio of the acoutic power delivered to the electrical power provided (the electroacoustic efficiency), it is necessary to provide a load to the system in order to evaluate driver performance. This load is originally represented as a complex electrical impedence in the equivalent circuit. The actual value of the load will depend on the design of the resonator but can be characterized by an acoustic impedance which can be transformed to an equivalent electrical load impedance.

3. Losses

In our search for the highest electroacoustic efficiency it is useful to understand where possible losses may occur and do what can be done to minimize them. Losses that are an intrinsic part of the electrical driver are eddy current losses in the magnetic structure generated by the

current in the voice coil, Joule heating losses due to the drive current dissipated by the voice coil electrical resistance, and mechanical losses due to the internal friction of the surround and the viscosity of the gas in the "gap." These losses need to be taken into account. Very little can be done about the eddy current losses and the viscosity of the gas which is necessary to improve heat removal from the voice coil. The losses due to surround (suspension) mechanical resistance can be controlled by choice of the materials and removal of extraneous suspension material (see Section III.H).

D. COUPLED SYSTEM

1. Computer Model

Any discussion of the driver section of the thermoacoustic refrigerator is incomplete without some understanding of how the driver parameters are coupled to the resonator (acoustic load). The equivalent electro-mechanical circuit for the coupled system is the same as that shown in Figure II-4 with the acoustic load impedance:

$$Z_1 = -\rho_o c s j [(1+j\alpha/k)/(1+(\alpha/k)^2) \cdot \qquad (II-23)$$
$$((\cos(kL)\sin(kL) + j \sinh(\alpha L)\cosh(\alpha L)) \div$$
$$(\sin^2(kL)\cosh^2(\alpha L) + \cos^2(kL)\sinh^2(\alpha L)))],$$

where ρ_o is the density of the gas, c is the speed of sound (labeled "a" in previous discussions), s is the cross-sectional area of the resonator, k is the wave number

$(= \bullet/c)$, $\alpha = \omega_\bullet/(2Qc)$, Q is the quality factor of the reso-
nator, and L is the effective length of the resonator
(Kinsler, et al., 1982). This circuit combines the equiva-
lent circuit of the electrodynamic transducer with the com-
plex impedance load representing the resonator. One way to
examine this coupling is through computer modeling.

LT Michael P. Susalla, USN, developed a computer
program which models the thermoacoustic refrigerator as the
equivalent electrical circuit. The program models each of
the mechanical and acoustical components as equivalent
electrical components, as discussed above. Using the
electrical equation from the combined circuit we determine
the system performance as different parameters are varied.

a. Input

There are two sets of input parameters needed
for the model: (1) driver parameters and (2) resonator
parameters. The driver electrical parameters include the
voice coil inductance (LE) and resistance (RE), and the
current (I) supplied to the voice coil (which is held at one
ampere for all test cases). The driver mechanical parameters
used in the model are the same equivalent resistance, induc-
tance, and capacitance as those developed for the equivalent
circuit. Therefore the parameter values needed for input are
the transduction coefficient (BL), the mechanical resistance
(RM), the moving mass (M), the suspension stiffness (SSUP),

44

the volume of the gas behind the diaphragm (VOL), and the cross-sectional area of this volume (A).

The resonator parameters needed include the tube quality factor (Q), the speed of sound (c), the resonance frequency (FO), the density of the gas in the tube (RHO), the resonator cross-sectional area (S), and the equivalent length of the resonator (L). For this model the piston area is set equal to the resonator cross-section (S). For the tests reported here they were nearly equal but could differ sustantially in other designs.

b. Output

Four output plots are generated by the graph program that accompanies the model: (1) voltage across the driver vs. frequency (since we put unit current into the driver, this graph can also be read as the input electrical impedance), (2) piston velocity vs. frequency, (3) acoustic power delivered to the load (resonator) vs. frequency, and (4) electroacoustic efficiency vs. frequency. Each of these plots should produce peaks at both the driver and the tube resonant frequencies.

The model uses the electrical equation for the coupled equivalent circuit to calculate voltage directly (holding the current constant at one ampere) for the first output plot. It also directly calculates the force on the moving mass, $F = BlI$. From this force, the piston velocity for the second plot is found by dividing the force by the

45

mechanical impedence (Z_{mech}). Pressure is calculated as tube impedence times volume velocity, and acoustic power is pressure times volume velocity times the cosine of their phase difference (Equation I-8) for the third plot. For the final plot the electrical power is calculated as voltage times current times the cosine of their phase difference (Equation I-7), and the model takes a ratio of the electrical to the acoustical powers for the electroacoustic efficiency. Since the components of these powers are complex and have phase differences, the actual powers are calculated as one half the real part of [current times complex conjugate of voltage], and one half the real part of [pressure times the complex conjugate of volume velocity]. Each of the above mentioned plots is the discussed output parameter versus frequency.

2. Assumed Typical Parameters

Table II-1 lists the input parameters with sample values for the Altec 290-16K driver in air with a long straight resonant tube attached (see Chapter III). Sample outputs of the four plots using these input values are given in Figures II-5 through II-8.

Figure II-5 plots the driver voltage as a function of frequency. Since the current is held constant at one ampere, this plot actually gives us information on driver electrical input impedance vs. frequency. Notice that there are two peaks in this curve. The first peak occurs at a

TABLE II-1. MODEL INPUT VALUES--EXAMPLE DATA

Symbol	Meaning	Units	Value
RM	Mechanical resistance	kg/s	1.33
M	Moving mass	kg	0.0151
SSUP	Spring constant	N/m	9.2×10^3
RHO	Density of gas	kg/m^3	1.2
C	Sound speed	m/s	342.0
S	Resonator X-sec. area	m^2	9.35×10^{-4}
BL	Driver transduction factor	N/A	21.5
Q	Resonator quality factor		60.0
FO	Resonator resonance freq.	Hz	240.0
A	Back volume X-sec. area	m^2	7.92×10^{-4}
VOL	Back volume	m^3	1.0×10^{-2}
LE	Voice coil inductance	H	1.0×10^{-4}
RE	Voice coil DC resistance	Ω	10.6
I	Driver current	A	1.0
L	Resonator length	m	0.712
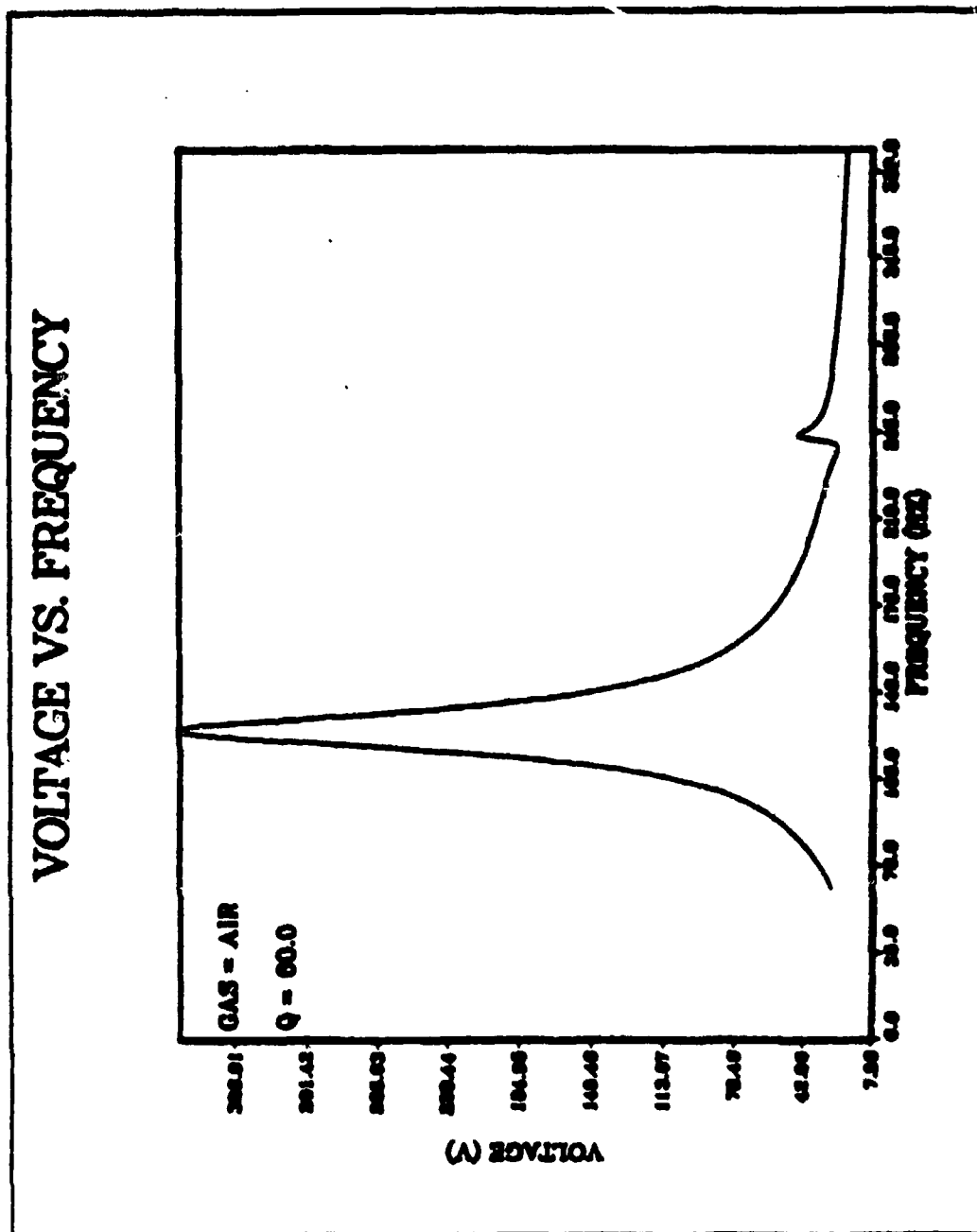
Figure II-5.   Computer Model Sample Output--Driver
Voltage vs. Frequency for One Ampere
Current into Driver.
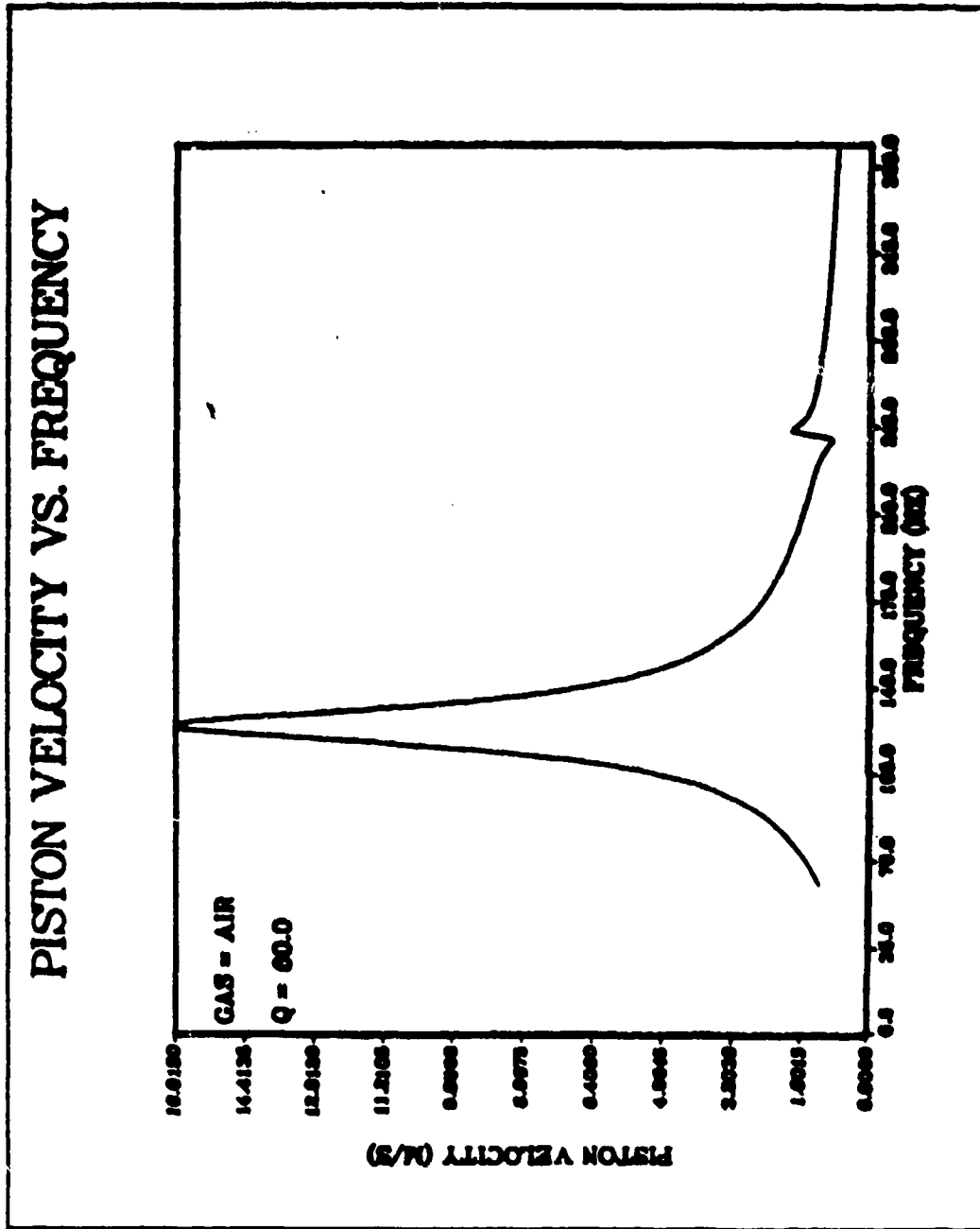
Figure II-6.   Computer Model Sample Output--Piston
Velocity vs. Frequency for One Ampere
into Driver.

49

ACOUSTIC POWER VS. FREQUENCY

GAS = AIR

Q = 60.0

ACOUSTIC POWER (W)
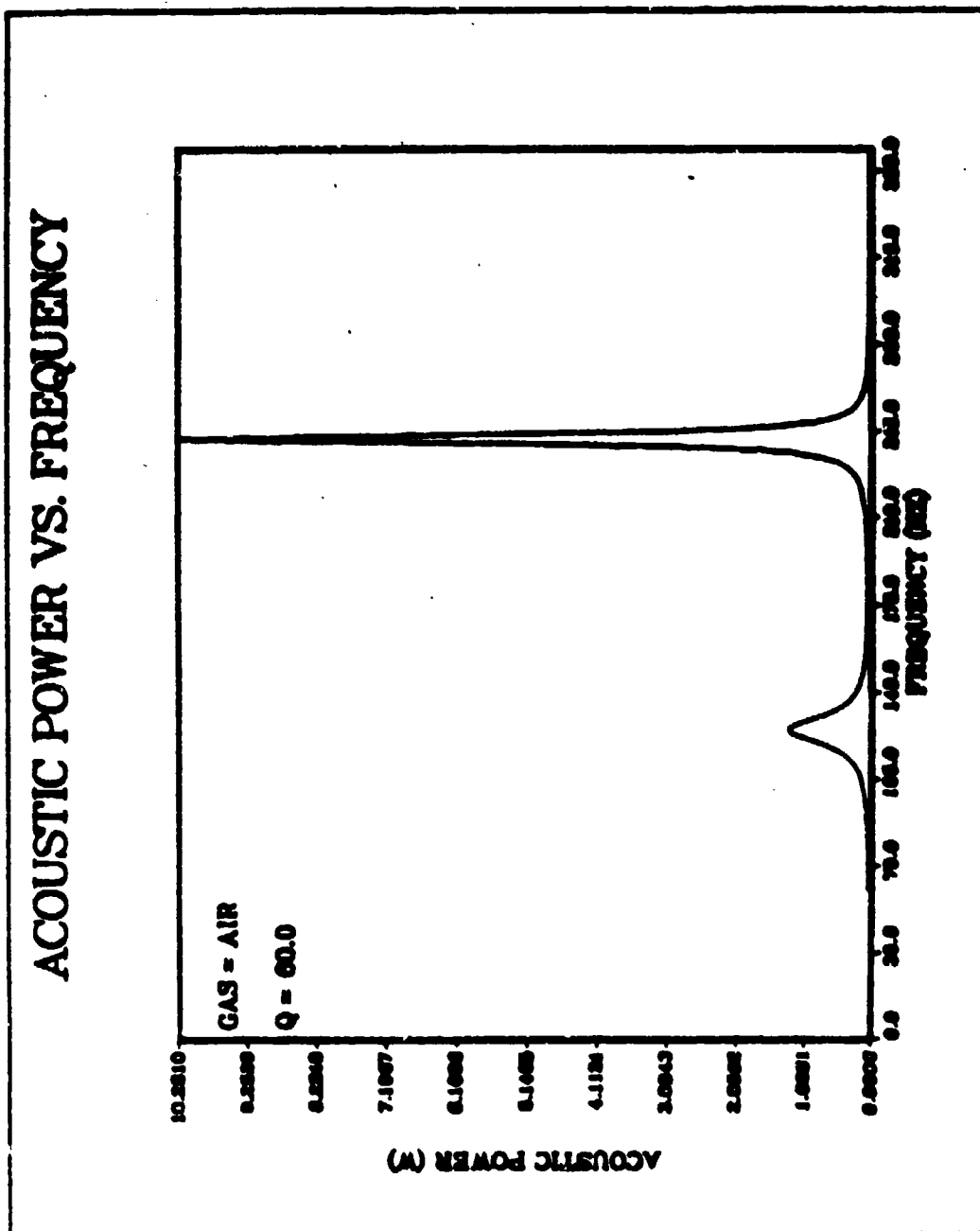
FREQUENCY (Hz)

Figure II-7.   Computer Model Sample Output--Acoustic
Power vs. Frequency for One Ampere.
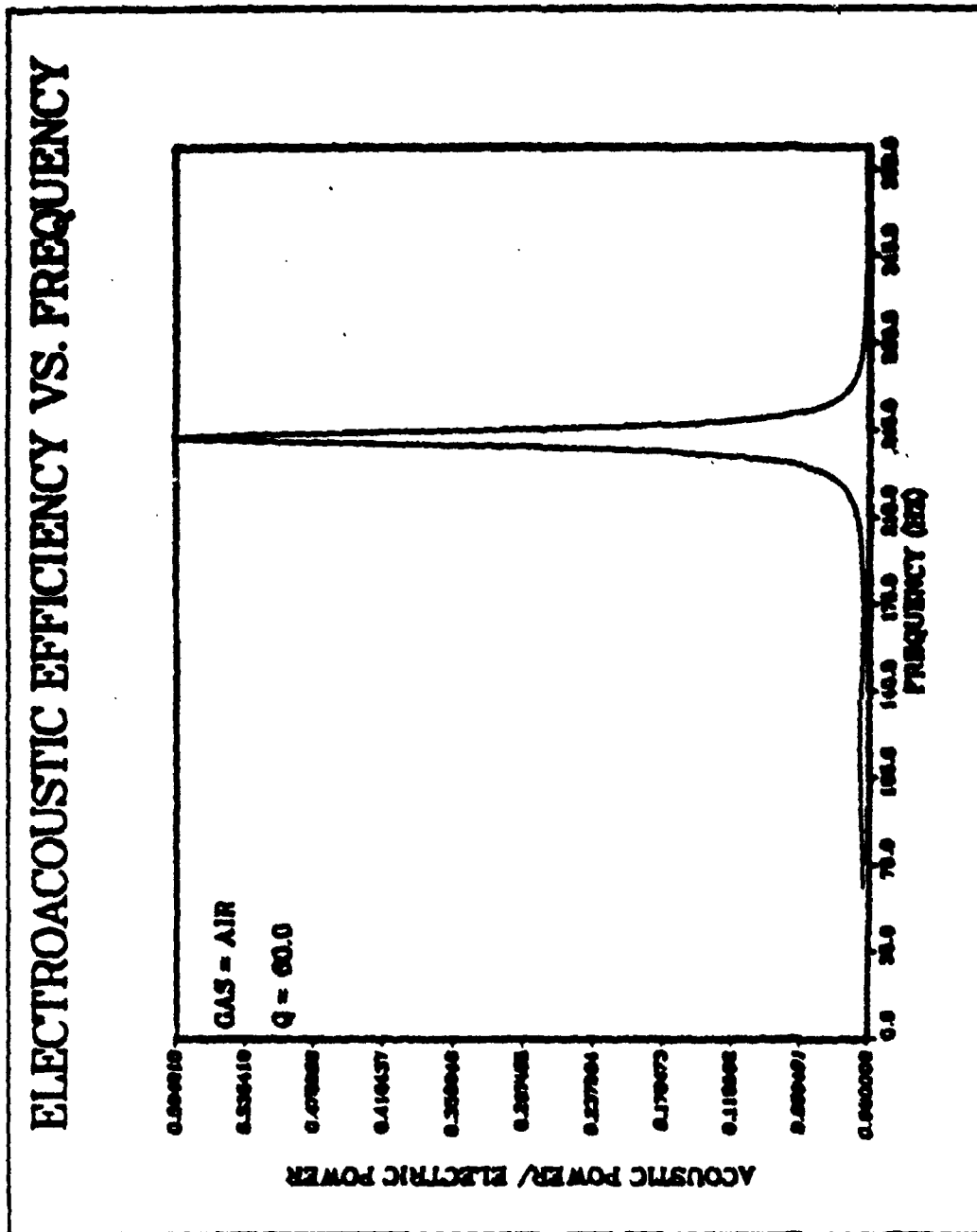
Figure II-8. Computer Model Sample Output--
Electroacoustic Efficiency vs.
Frequency.

51

lower frequency and has a much higher amplitude than the second. This higher amplitude peak occurs near the driver resonant frequency ($f_o = (1/2\pi)[k/m_o]^{1/2} = 124$ Hz). It dominates the curve because it is the driver impedance that we are plotting, and the voice coil motion, and consequently the "back emf," is the largest at that frequency. The fact that there is a second peak near the tube resonance (FO = 240 Hz) shows the effect of the coupling of the two parts of the system.

In the plot of piston velocity vs. frequency (Figure II-6), the dominant peak again occurs near the driver resonance for the reasons presented above. The smaller coupled peak at the tube resonance is due to the change in the load impedance which occurs near the tube resonance.

Figure II-7 shows the plot of the acoustic power vs. frequency. Now the dominant peak occurs at the tube resonance because acoustic power is primarily a function of the tube parameters. Here the secondary peak at the driver resonance is a consequence of the greatly increased piston velocity at the driver resonance putting energy into the smaller non-resonant acoustic load of the tube.

In the plot of electroacoustic efficiency vs. frequency, Figure II-8, the primary peak at the tube resonance is sharp and the secondary peak at the driver resonance is small but visible. It is important to note that the electroacoustic efficiency peaks at a value of nearly

52

60% even though the two individual resonances are separated by nearly an octave in frequency. The peak acoustic power for one amp as shown in Figure II-7 is 10.3 W. The losses (40%) are due primarily to Joule heating in the voice coil DC resistance ($P_R = 1/2$ ($I^2 R_{DC}$) $= 5.3$ W). This accounts for 34%. The remaining loss can probably be attributed to mechanical resistance losses in the suspension.

Appendix A contains a printout of the calculation program. Appendix B contains a printout of the graph program.

III. DRIVER PARAMETER MEASUREMENTS

A. INTRODUCTION

In Sections II.B and II.C we discussed the choice of the electrodynamic transducer to drive the thermoacoustic refrigerator. Given this choice, we needed to develop a system for measuring the mechanical parameters of this type of driver to be used in determining the electroacoustic efficiency. The relevant parameters (as discussed in Section II.D) are: (1) moving mass, (2) suspension stiffness, (3) transduction coefficient (Bl), and (4) mechanical resistance.

The driver we selected for the preliminary measurements is the Altec model 290-16K moving-coil loudspeaker. There are several pieces of equipment needed to interface the driver with the resonator. Three of these parts--the reducer cone, stiffener, and dynamic bellows--become an integral part of the driver, and their effects on the driver parameters must be taken into account. We first measured the parameters of the driver alone, then added the other parts and determined the new parameters for the entire system. The driver-bellows combination was then fitted to one end of a resonant tube. The actual resonator used in the thermoacoustic refrigerator will be a complex structure that is not easily modeled. For the purposes of the driver parameter

measurements we used a resonant tube of uniform cross-section to allow easy comparison of experimental values to theory. The non-driver end of the closed tube housed several microphones. The electroacoustic efficiency of the system at resonance was determined from measurements of electric power delivered to the driver and the acoustic pressure at the microphone. The acoustic power dissipation was determined from the quality factor of the tube at resonance and the microphone sensitivity (the relationship between the pressure that the microphone senses and its voltage output).

B. IMPEDANCE ANALYZER

The primary instrument used in the testing and evaluation of the electrodynamic driver was the Hewlett Packard Model 4192A LF Impedance Analyzer. According to the manufacturers Operation and Service Manual, the 4192A is a fully automatic, high performance test instrument designed to measure a wide range of impedance parameters as well as gain, phase, and group delay. Its two measurement display sections provide direct readout of the selected measurement parameters with 4.5 digit resolution along with the appropriate units. In normal mode operation, the 4192A performs approximately five measurements per second. It also provides an average measurement mode (one measurement per second) for higher resolution and noise rejection. A high speed mode can perform ten measurements per second.

The 4192A can provide measuring frequency, OSC voltage level, and DC bias voltage (impedance measurements only) equivalent to actual operating conditions. The sweep capability of the built-in frequency synthesizer and DC bias source permits quick, convenient, and accurate measurements. Measuring frequency or DC bias voltage can be automatically or manually swept in either direction. OSC level can be manually swept in either direction in 1mV increments. Actual test voltage across or test signal current through the device under test is also measured.

In amplitude/phase measurements, the 4192A can measure four transmission parameters - gain/loss, level, phase, and group delay. In impedance measurements, the 4192A can measure eleven impedance parameters - absolute value of impedance, absolute value of admittance, phase angle, resistance, reactance, conductance, susceptance, inductance, capacitance, dissipation factor, and quality factor. All impedence measurements have a basic accuracy of 0.1% and a resolution of 4.5 digits. Also, the circuitry of the 4192A provides direct and accurate impedance measurements of both grounded and floated devices.

C. MECHANICAL PARAMETERS

The most important parameters for a moving coil transducer are the moving mass, suspension stiffness, and the Bl (transduction) coefficient. The moving mass of the driver

includes the mass of the voice coil, the diaphragm, and the hydrodynamic mass of the air being pushed by the diaphragm. The masses of the reducer and stiffener are also important, as are the moving mass and suspension stiffness of the bellows. The moving mass and stiffness of the combined driver-reducer-bellows system is also important. The values for the combined system should equal the sum of the values of the individual parts. The stiffness, mass, and Bl coefficient give us the information we need to construct the equivalent electrical circuit, as discussed in Subsection II.C.2. Also, we have to insure that the stiffness of the driver system is just large enough to produce a mechanical resonance at the tube resonant frequency, at which point the driver piston looks like a soft (or open) tube end. This may appear to be contradictory to having a velocity node of the standing wave at the piston, but it is not. It is how we get high efficiency.

The important design parameters of the tube are its resonance frequency and quality factor. The length of the tube and the speed of sound in the contained gas determine the resonance frequency.

1. Dynamic Mass Loading of Driver

We used the driver's similarity to a simple harmonic oscillator to find the moving mass and suspension stiffness of the driver by taking advantage of the fact that the resonance frequency squared equals the stiffness divided by

57

the mass. If we add mass to the driver, it should linearly change the inverse of the frequency (or period) squared:

$$T^2 = 1/f^2 = 4\pi^2(m_o + m)/k, \qquad (III-1)$$

where m_o is the moving mass, m is the added mass, and k is the suspension stiffness. The instrument we used for this measurement was the HP 4192A Low Frequency Impedance Analyzer, described in section B. We added various masses of putty (one to nine grams) to the diaphragm and found the resonance frequency of the driver for each mass. The putty mass was measured on the Sartorius model 2403 mass balance (serial number 1287). This balance has an accuracy of ± 0.00005 g. However, the putty could be expected to gain or lose more mass than that due to handling. Based on mass measurements of the putty after use, we expect an experimental accuracy of ± 0.005 g for the masses. A more significant uncertainty involving the masses arises from the inability to place the masses evenly on the voice coil or to produce a perfectly rigid coupling between the masses and the voice coil. It is not possible to assign a specific numerical percentage error to this uncertainty, but we must take it into account when evaluating the data associated with mass loading. A typical plot of the period squared vs. added mass in air is shown in Figure III-1. We used the least squares method to fit a straight line through the data. We determined the suspension stiffness ($k = 4\pi^2/\text{slope}$) to be:

ALTEC 290-16K MASS LOADING

$y = 8.4947 + 1.4735x \quad R = 0.99$
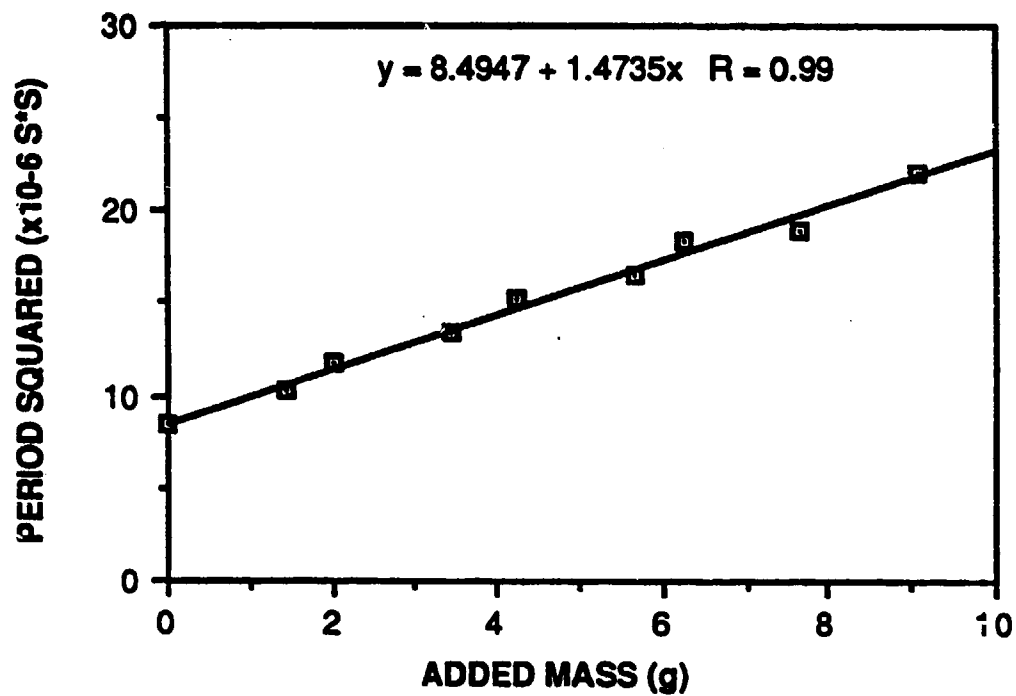
Figure III-1. Least Squares Fit of Period Squared vs. Added Mass to Determine Stiffness and Moving Mass of the Altec 290-16K Driver.

$$k = 2.7 \pm 0.1 \times 10^4 \text{ N/m}, \qquad \text{(III-2)}$$

and the moving mass $(m_o = \text{intercept/slope})$:

$$m_o = 5.8 \pm 0.1 \text{ g}, \qquad \text{(III-3)}$$

for this driver in air.

The moving mass of the driver in vacuum is expected to be less than the value in air because in vacuum the driver is not pushing a hydrodynamic mass. However, we did not take any measurements of this driver in vacuum.

2. **Bellows Parameters**

The Servometer custom-designed dynamic bellows (shown in Figure III-2 with test stand) is used to provide a flexible gas seal between the driver and the resonator.

The stiffness of the bellows was measured using two independent methods - static and dynamic. For the static method we used Hooke's law: $k = -F/x$. The force was determined by pulling a partial vacuum on the bellows and multiplying the vacuum pressure (read on a manometer) by the surface area of the bellows ($A = 1.1 \pm 0.1 \times 10^{-3} \text{ m}^2$). We used a G. L. Collins Corporation model LMS-119V22-01 Linear Variable Differential Transformer (LVDT) (serial 274674) connected to an EG&G 128A Lock-in Analyzer to determine the displacement of the bellows under a partial vacuum. Figure III-3 shows the LVDT in its calibration stand. The calibration curve for the LVDT is shown in Figure III-4. The least squares fit slope of this curve gives us the calibration constant for the LVDT:

60
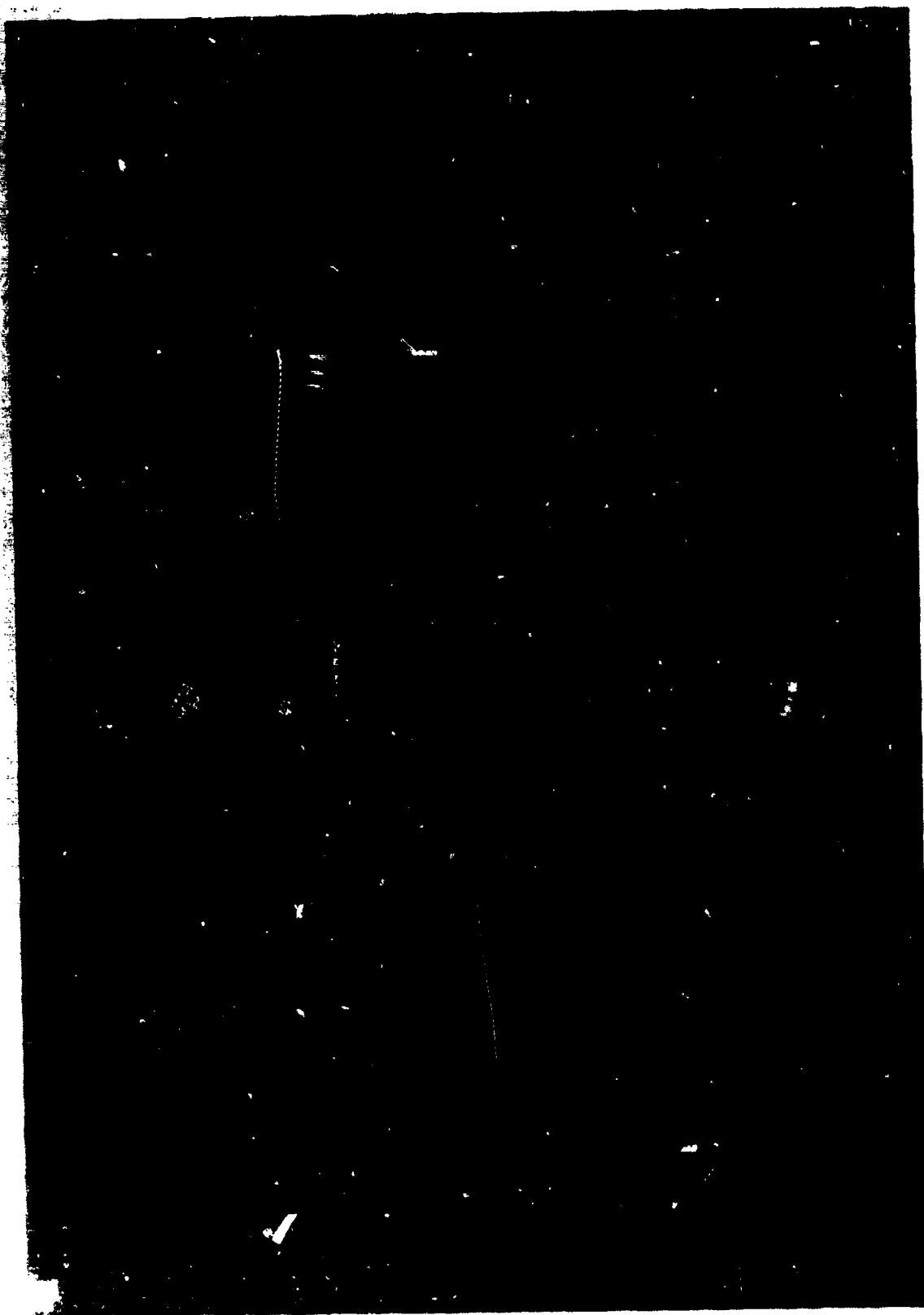
Figure III-2. Photograph of Servometer Custom-Designed
Dynamic Bellows--With and Without
Test Stand.

Figure III-3. Photograph of Linear Variable
Differential Transformer (LVDT)
in its Calibration Stand.

LVDT CALIBRATION

y = 187.9945 - 378.2689x   R = 1.00

Y-axis: LOCK-IN OUTPUT VOLTAGE (mV dc)
X-axis: LVDT DISPLACEMENT (INCHES)
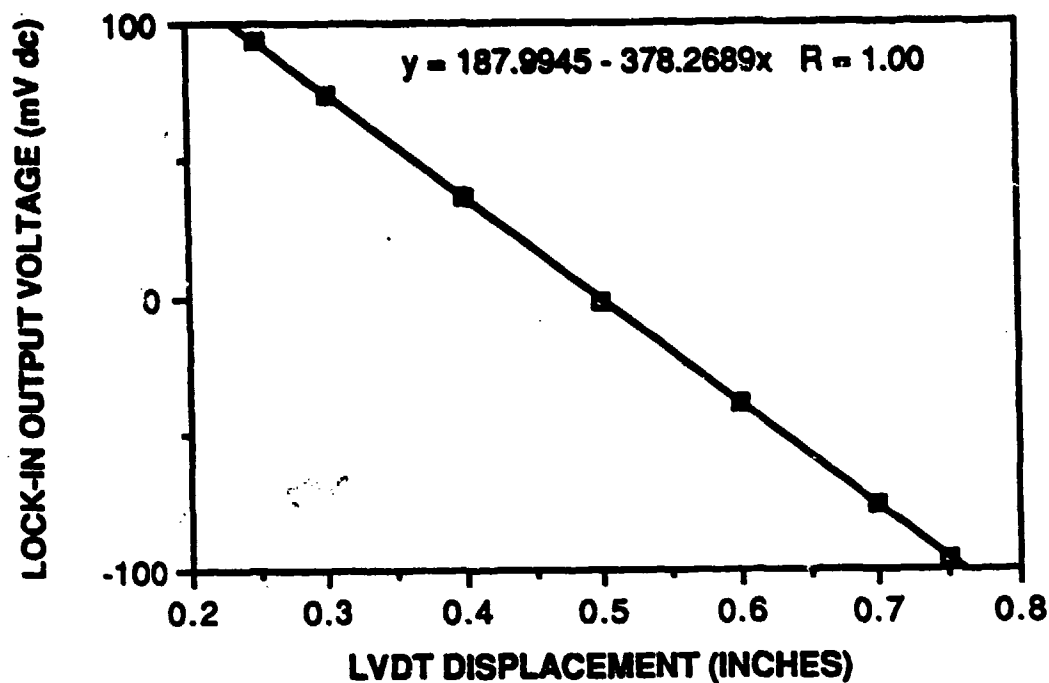
Figure III-4.   Calibration Data for LVDT Voltage
Output vs. Displacement.

BELLOWS DYNAMIC MASS LOADING

y = 50.5616 + 8.6609x   R = 1.00

Y-axis: PERIOD SQUARED (x10-6 S*S)
X-axis: ADDED MASS (g)
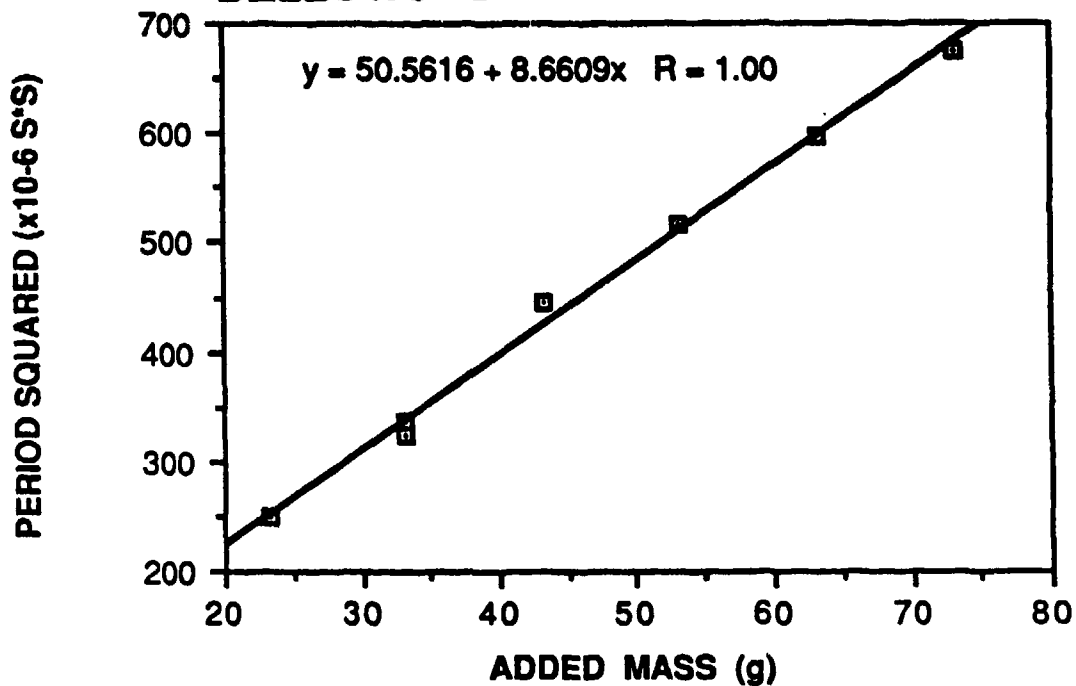
Figure III-5.   Least Squares Fit of Period Squared
vs. Added Mass for Dynamic Loading
of Bellows.

$$dV/dx = -0.378 \pm 0.0005 \text{ V/in} = -14.9 \pm 0.02 \text{ V/m}. \quad \text{(III-4)}$$

Table III-1 gives the static test data for the stiffness measurement. By averaging the values we obtained:

$$k = 4.3 \pm 0.2 \times 10^{9} \text{ N/m}. \quad \text{(III-5)}$$

TABLE III-1. BELLOWS STIFFNESS--STATIC MEASUREMENT RESULTS

LVDT Voltage (mV)	Pressure (cm Hg)	Pressure ($\times 10^{9}$ Pa)	Force ($=P \cdot A$) (N)	Stiffness ($\times 10^{9}$ N/m)
14.84	2.9	3.87	4.39	4.40
15.62	3.1	4.13	4.69	4.47
12.89	2.3	3.07	3.48	4.02

The dynamic measurement was a mass loading technique similar to that used for the driver. In this case, we measured the period as a function of added mass using un Endevco model 2225M2 accelerometer (serial FA80) and a Nicolet model 3091 digital storage oscilloscope to record the free decay of the bellows after it had been disturbed by the blunt wooden end of a cotton swab. We then plotted period squared versus added mass and found the stiffness and moving mass from the slope and intercept of the least squares fitted line (see Figure III-5) as discussed in the previous Section. This gave us values of:

$$k = 4.56 \pm 0.05 \times 10^{9} \text{ N/m} \qquad \text{(III-6)}$$

$$\text{and } m_o = 5.84 \pm 0.05 \text{ g.} \qquad \text{(III-7)}$$

This value for moving mass includes the accelerometer cable and is not representative of the actual moving mass of the bellows. Subtracting the weight of the accelerometer gives us a value of approximately:

$$m_o = 1.5 \pm 0.1 \text{ g.} \qquad \text{(III-8)}$$

for the bellows. We know the moving mass has to be less than 2.3 g, since that is the bellows' total mass--moving and static. The values obtained for bellows stiffness using the two different methods were within experimental error. We therefore felt confident using a value of $k_o = 4.5 \pm 0.1 \times 10^{9}$ N/m in our later calculations.

3. Combined System

After we glued the reducer (m = 4.8 g), stiffener plate (m = 4.4 g) and bellows to the driver, we wanted to find the stiffness and moving mass of the combined driver-reducer-bellows system. We first tried a dynamic mass loading measurement (same procedure as with the driver alone), but found that the period squared versus added mass plot (see Figure III-6) gave unrealistic results. So instead we used the relationship:

$$F = -kx = BlI \qquad \text{(III-9)}$$

$$\text{or} \qquad k = -BlI/x = Bl \, (di/dV)(dV/dx) \qquad \text{(III-10)}$$

and made a static measurement using the LVDT. We expected the additional equipment (reducer, stiffener, and bellows)

MASS LOADING DRIVER-CONE-BELLOWS

y = 1.8358 + 0.0724x   R = 0.99

PERIOD SQUARED (x10-6 s^2)
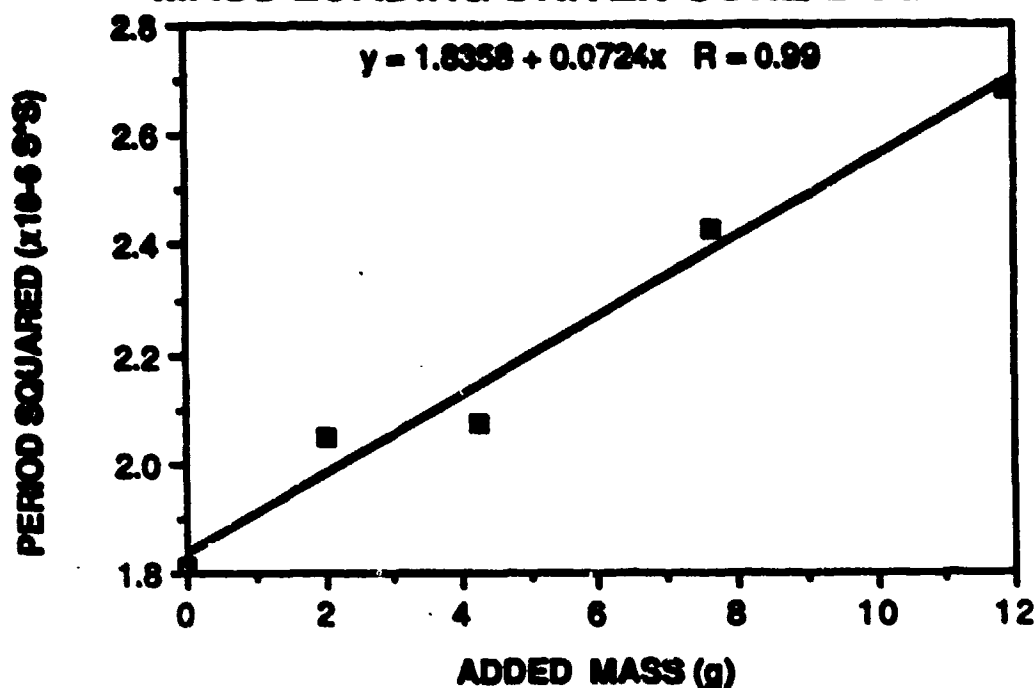
ADDED MASS (g)

Figure III-6.   Least Squares Fit of Period Squared
vs. Added Mass for Combined Driver-
Reducer-Bellows System.

ALTEC 290-16K STATIC DISPLACEMENT

y = 3.6095 + 0.0118x   R = 1.00

LVDT OUTPUT VOLTAGE (mV)

CURRENT IN VOICE COIL (mA dc)
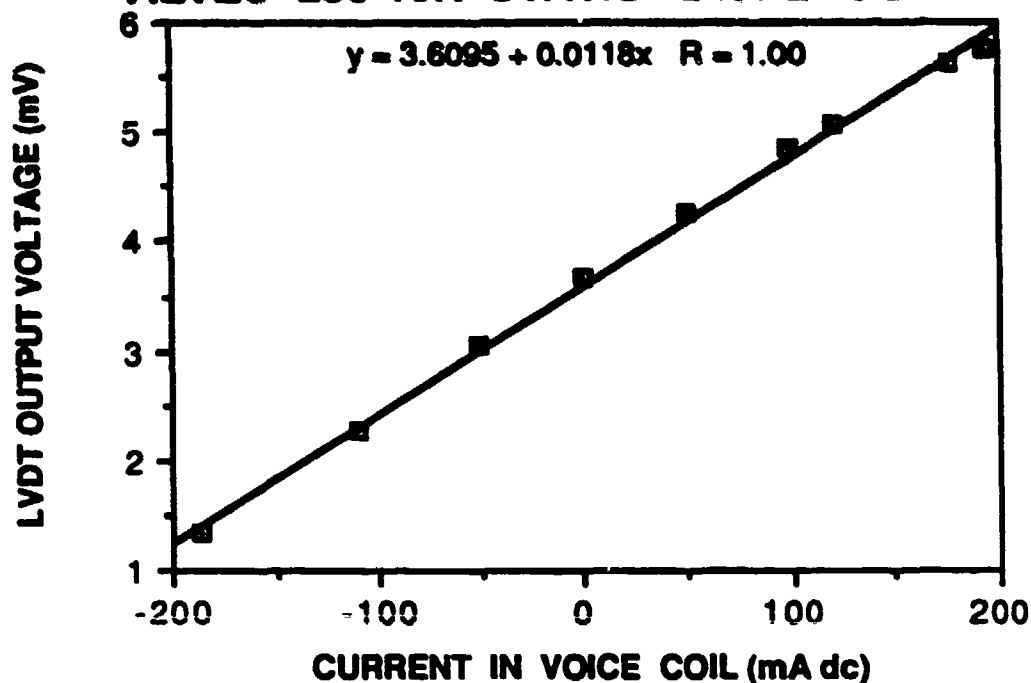
Figure III-7.   Driver Displacement vs. Voice Coil
Current as Measured with LVDT/
Lock-in Analyzer.

66

to change the moving mass and suspension stiffness of the system but not the transduction coefficient (Bl). We applied a DC current to the driver and recorded the LVDT voltage output, then changed the current and recorded the new voltage. This process produced the values: $\Delta I = 283 \pm 0.5$ mA and $\Delta V = 2.58 \pm 0.005$ mV. We substitute these values and the value of Bl $= 21.5 \pm 0.5$ N/A (experimental measurement of this quantity is discussed in the next section) into Equation III-10 for a combined stiffness value of:

$$k = 3.5 \pm 0.1 \times 10^4 \text{ N/m}. \qquad \text{(III-11)}$$

If we add the stiffness values for the driver and bellows together a total stiffness of $k = 3.2 \pm 0.1 \times 10^4$ N/m for the system is obtained. Thus the total experimental stiffness for the combined system differs by about 10% from the sum of the individual stiffnesses. Using the relationship $m_o = k/(2\pi f)^2$, and a measured resonance frequency of 235 ± 0.5 Hz, the combined moving mass is:

$$m_o = 16.2 \pm 0.5 \text{ g}, \qquad \text{(III-12)}$$

compared to $m_o = 15.9 \pm 0.5$ g for the individual masses added together. The two types of mass measurement agree within 2%.

D. TRANSDUCTION COEFFICIENT (BL)

We determined the Bl coefficient of the driver using three independent methods. The first method was to remove the voice coil from the magnet and directly measure the

magnetic induction using a Dowdy RFL Industries model 912 Guassmeter (serial 808) using a Hall effect probe model 912015 (serial 21122) (B = 2.2 ± 0.05 Tesla). We then measured 1 (the length of the wire) by counting the number of turns of wire in the coil (under a microscope) and multiplying this number (44) by the circumference of the coil (1 = 44 X π X diameter = 9.98 ± 0.005 m). Combining these two measurements gave us the value:

$$Bl = 22.0 \pm 0.7 \text{ N/A}. \qquad \text{(III-13)}$$

In the second method we used the relationship:

$$F = BlI = -kx \quad \text{or} \quad Bl = -kx/I = -k(dx/dV)(dV/dI). \quad \text{(III-14)}$$

We previously determined k for the driver alone (Equation III-2), and now used the LVDT and lock-in analyzer to find dx/di. The LVDT calibration was discussed in the previous Section, with a calculated value of dV/dx = -14.9±0.05 V/m. We then measured the diaphragm displacement as a function of DC-current through the voice coil. This gave us a value of dV/dI = 11.75 ± 0.05 mV/A (see Figure III-7). Using the relation in Equation III-14 we obtain the value:

$$Bl = 21.2 \pm 0.1 \text{ N/A}. \qquad \text{(III-15)}$$

In the third method we used the relationship:

$$F = Bli = mg \quad \text{or} \quad Bl = mg/i. \qquad \text{(III-16)}$$

For this we measured the change in DC-current through the coil as a function of added mass, using the LVDT as a monitor to keep the displacement of the diaphragm constant.

Three different mass/current combinations (see Table III-2) produced an average value of:

$$Bl = 21.4 \pm 0.5 \text{ N/A}. \tag{III-17}$$

Averaging the results of these three methods gave us a value of $Bl = 21.5 \pm 0.5$ N/A with 2% deviation among the three methods.

TABLE III-2. STATIC MEASUREMENT OF ALTEC 290-16K
TRANSDUCTION COEFFICIENT (BL)

Δm (g)	ΔI (mA)	Bl = mg/I (N/A)
132.5	64.4	20.2
157.5	74.0	20.9
257.5	108.2	23.3

E. MICROPHONE CALIBRATION

Microphone calibration is an important part of the process leading to the measurement of the electroacoustic efficiency. A microphone is used to measure the acoustic pressure inside the resonator by converting the acoustic pressure to an output voltage. The ratio of the open circuit voltage to the pressure is called the open circuit microphone sensitivity.

We used three microphones for the calibration: (1) a General Radio (GR) model 1962-9611 half-inch electret

69

condenser microphone (serial 11811) with GR preamplifier model 1560-P42 (serial 4061); (2) an Endevco model 8510B-5 piezoresistive bridge microphone (serial 73MJ); and (3) an 1/8 inch B&K model 4138 microphone (serial 19683). We first calibrated the GR using a GR type 1562-A sound-level calibrator (serial 19683, 114dB SPL, 250 Hz), and obtained a GR sensitivity of M_o = 7.42 mV/Pa. This compares within about 1% of the calibration certificate provided by the manufacturer of 7.50 mV/Pa. Additional checks were made with a B&K pistonphone calibrator which substantiated the GR calibration results.

To calibrate the other two microphones we attached the resonator tube to the 290-16K driver. We used an HP 3325A Synthesizer/Function Generator to excite the driver at 240 Hz, the resonant frequency of the tube. We recorded the output voltages for all three microphones and used the comparison relationship:

$$M_1/V_1 = M_2/V_2 \qquad\qquad (III-18)$$

to determine the sensitivities of the B&K and Endevco. The B&K sensitivity was determined to be M_o = 0.463 mV/Pa, comparing within 2% of the manufacturer's specification value of 0.470 mV/Pa (adjusted to include the capacitance of the B&K model VA0160 1/8" to 1/4" adapter with an expected 4 dB "line loss"). The sensitivity of the Endevco microphone was calculated to be 8.17 X 10^{-6} V/Pa, comparing within 1% of the manufacturer's specification of 8.09 X 10^{-6} V/Pa. For

all three microphones we measured sensitivity values within 2% of the manufacturers' specifications.

F. ELECTROACOUSTIC EFFICIENCY

The electroacoustic efficiency is the ratio of the acoustic power dissipated in the resonator to the electric power delivered to the driver. The electric power was determined using the relationship:

$$P_{elec} = V I \cos \theta, \qquad (III-19)$$

where V is the voltage across the driver terminals, I is the current flowing in the driver, and θ is the phase angle between the voltage and the current. The values for voltage, current and phase angle delivered to the driver were obtained using the HP 4192A.

Calculation of the acoustic power was a little more complex. We started with the basic relationship for the quality factor of the tube:

$$Q = 2\pi E_{ST}/E_{LC}, \qquad (III-20)$$

where E_{ST} is the energy stored in the tube and E_{LC} is the energy lost per cycle. The acoustic power generated in the tube is the energy lost per cycle times the number of cycles per second, or frequency:

$$P_{AC} = E_{LC}f = 2\pi f E_{ST}/Q. \qquad (III-21)$$

Following Burmaster (1985) the energy stored in a plane standing sound wave is equal to the energy density integrated over the volume of gas in the tube (VOL):

$$E_{ST} = (P_{rms}^2/2\gamma P_o) \cdot VOL, \qquad (III-22)$$

where P_{rms} is the root mean square acoustic pressure in the tube, γ is the ratio of the specific heats of the gas in the tube (1.4 for air), and P_o is the ambient pressure (one atmosphere or 1.013×10^5 Pa for these measurements). The r.m.s. acoustic pressure is the r.m.s. microphone output voltage divided its sensitivity (V/M) as discussed in the previous Section. The expression for the acoustic power becomes:

$$P_{ac} = (\pi f V^2 VOL)/(QM^2 \gamma P_o). \qquad (III-23)$$

The only remaining quantity in Equation III-23 that needs to be calculated separately from the efficiency measurement is the quality factor of the tube (Q). To determine Q we removed the 290-16K driver from the resonator and replaced it with an electret transducer to drive the tube. This was necessary because there were losses due to the 290-16K that made the tube Q appear to be lower than it actually is (we discovered this problem while investgating the reasons for the calculated efficiency to be greater than one). We used the B&K microphone for the pressure (converted to voltage) readings at the other end of the tube. We plotted voltage as a function of frequency, and determined the resonant frequency (f_o) and frequencies of the half power points (f_u and f_1). Using the relationship:

$$Q = f_o/(f_u - f_1) \qquad (III-24)$$

we obtained a value of $Q = 60 \pm 1$ for the tube.

To determine the electroacoustic efficiency we returned the tube to the 290-16K driver (see Figure III-8) and drove the tube at resonance. We recorded the voltage, current, and phase angle for the driver and the B&K output voltage. The electroacoustic efficiency was then calculated using:

$$\eta_{ea} = P_{ac}/P_{elec}. \qquad (III-25)$$

Table III-3 lists the electric power, acoustic power, and efficiency for five test runs at driver currents ranging from 3-38 mA (with corresponding voltages 0.15-1.43 V). The electroacoustic efficiency ranged from 84.2 for the lowest driver current to 75.9 for the highest.

TABLE III-3. ALTEC 290-16K ELECTROACOUSTIC

EFFICIENCY MEASUREMENTS

P_{elec} (mW)	P_{ac} (mW)	η_{ea} (%)
0.56	0.47	84.2
3.41	2.70	79.2
10.0	7.79	77.9
17.0	13.1	77.2
54.2	41.2	75.9

G. COMPARISON TO COMPUTER MODEL

The final task in the evaluation procedure for the electrodynamic driver is to compare the measured electro-acoustic efficiency to that predicted by the computer model

73
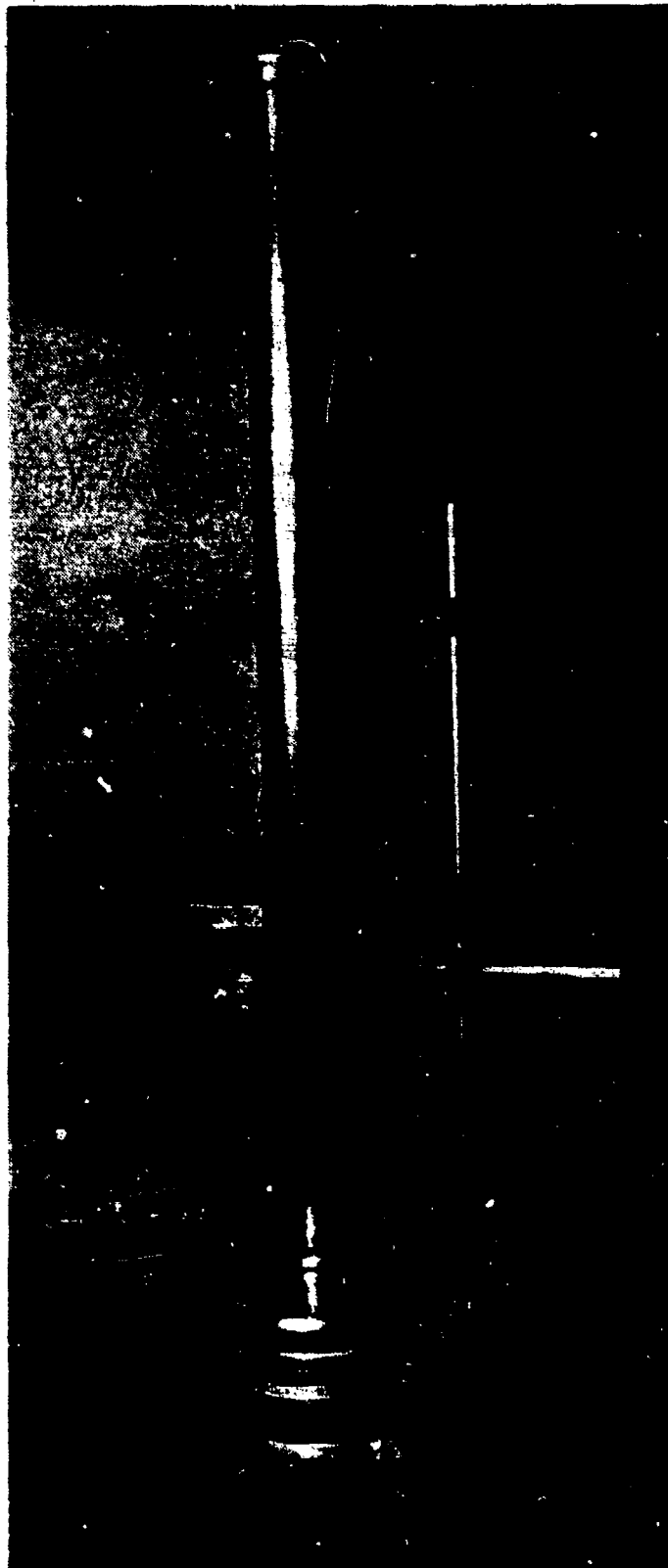
Figure III-8. Photograph of Altec 290-16K Driver
Assembly with Resonator Tube and
Endevco Microphone.

discussed in Section II.D. We have already measured or calculated all the input values for the model except for the driver's mechanical resistance (R_m).

1. Mechanical Resistance

We can determine R_m by using the relationship:

$$R_m = 2\pi f_o m_o / Q, \qquad \text{(III-26)}$$

where f_o is the resonant frequency, m_o is the moving mass and Q is the quality factor of the driver. There are several methods available for determining the driver's quality factor. One is to plot the magnitude of the modified driver impedance vs. frequency and pick the half power points off the graph. Then, as with the tube, Q is given by:

$$Q = f_o / (f_u - f_l), \qquad \text{(III-27)}$$

where f_u and f_l are the frequencies associated with the upper and lower half power points (located at $[Z]_{max} / \sqrt{2}$, where [Z] is the magnitude of the driver impedance which is modified by subtracting the direct current (DC) resistance from the measured complex impadance).

Another method is to use the relationship [Hofler, 1986]:

$$Q = \frac{1}{2} f_o \, d\theta/df, \qquad \text{(III-28)}$$

where θ is the phase angle between driver resistance (R) and reactance (X), the two components of modified impedance (Z = R + iX, where R is the measured resistance minus the DC (direct current) resistance). This modified impedance is proportional to the voice coil velocity. The quantity $d\theta/df$

is the slope of the phase angle versus frequency curve evaluated at the resonant frequency (where the curve is a straight line). We used the HP4192A to obtain the data for these measurements.

Figure III-9 shows a plot of modified impedance vs. frequency for the Altec 290-16K in air. From this graph we find f_o=235.2 Hz, f_u=249.6 Hz and f_1=222.0 Hz. The Q for these values is 8.52. Figure III-10 shows a plot of phase angle vs. frequency for the same data set. Over this large range of frequencies the phase angle curve approximates an arctangent. At resonance, however, where $d\theta/df$ is evaluated, the curve is linear (see Figure III-11). Equation III-28 is the slope of the arctangent at resonance (f_o). The slope of the plotted data is 71.8×10^{-3} sec ($d\theta$ was converted from degrees to radians). The Q calculated from this method is 8.44. These values for Q agree within 1%. From these values we get R_m=2.77 kg/s.

We tried yet another method for determining driver Q. This third method measures the decay constant, τ, using a digital storage oscilloscope to record the "ring down" of the driver. This technique takes less time to run the experiment and reduce the data using the relationship:

$$Q = \omega\tau/2 \quad \text{or} \quad \tau = 2Q/\omega = QT/\pi \qquad \text{(III-29)}$$

where ω is the resonant angular frequency in radians/sec, T is the period in seconds, and τ is the free decay time

76

ALTEC 290-16K IMPEDANCE
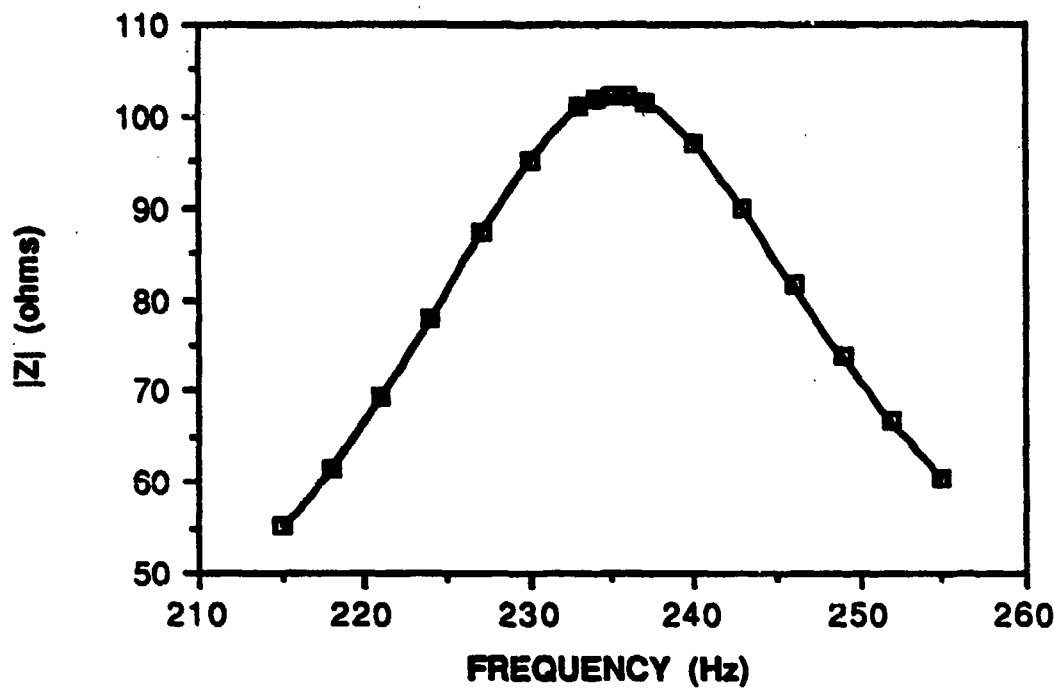
Figure III-9. Altec 290-16K Modified Impedance
Magnitude vs. Frequency.

ALTEC IMPEDENCE PHASE ANGLE
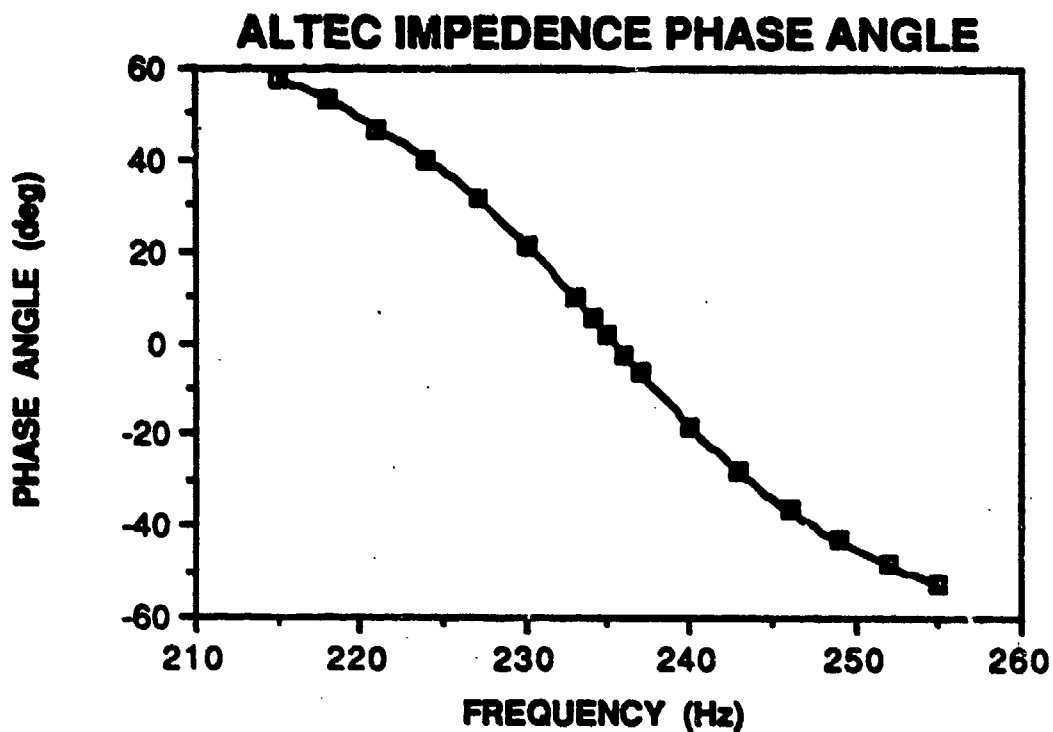
Figure III-10.   Altec 290-16K Modified Impedance
Phase Angle vs. Frequency--Full
Frequency Range.

ALTEC PHASE ANGLE - LINEAR SEGMENT

$y = 910.9193 - 3.8697x$ $R = 1.00$
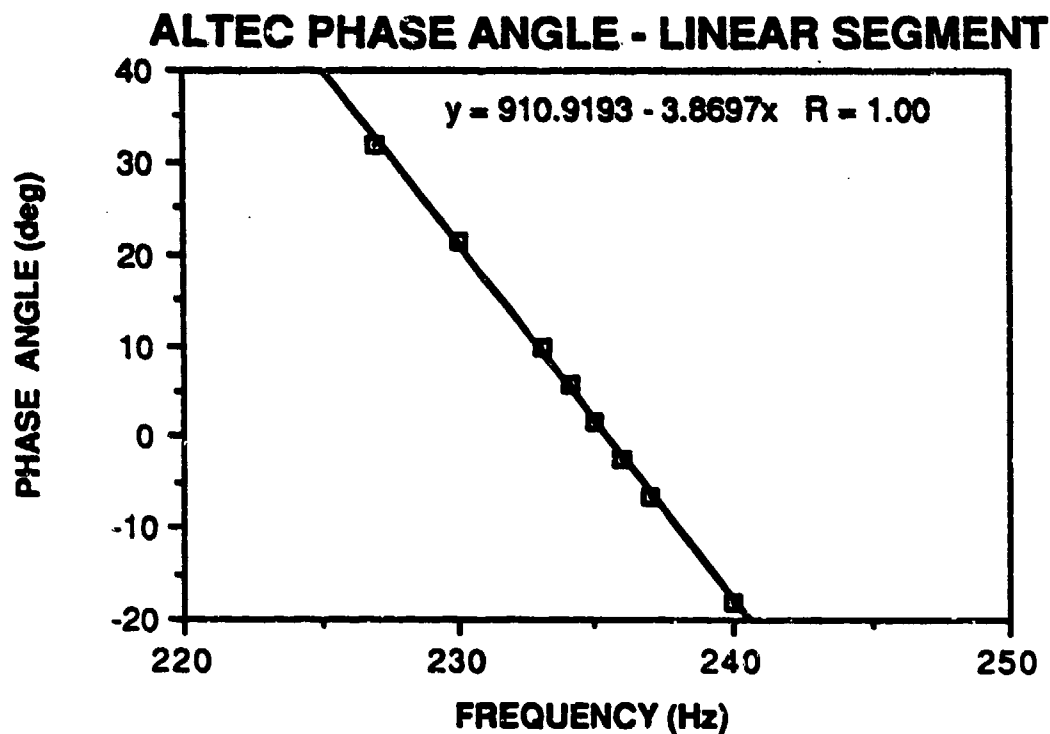
Figure III-11.   Least Squares Fit of Altec 290-16K
Modified Impedance Phase Angle as a
Function of Frequency Near Resonance.

78

constant in seconds. This method will be discussed in greater detail in Chapter IV.

2. Model Results

Table III-4 lists the computer model input values for the Altec 290-16K. Figures III-12 through III-15 show the output plots for these values as discussed in Section II.D. In this case the resonance peaks are much closer together, and the magnitude of the secondary peak is closer in value to the primary peak. Once again the driver resonance is at a lower frequency than the resonator resonance. It is interesting to note that the modeled efficiency (about 60%) is 15-20% less than the measured efficiency reported in the previous Section. We believe that this results from the fact that for the computer model, a high tube Q means that the driver losses, represented by R_m, play a more important role in the efficiency calculation, and the results are very sensitive to small errors in R_m. The primary ways for the driver energy to be dissipated are: (1) Joule heating due to DC resistance in voice coil and eddy currents induced in the magnet structure due to the time-varying magnetic fields generated by the AC voice coil current (small but not negligible); (2) mechanical resistance of driver (R_m); and (3) energy transferred to acoustic load. Another possible reason for the different efficiencies is that the efficiency is not independent of current hence the real physical system has some non-linearity, as Table III-3 clearly shows. The

79

TABLE III-4. COMPUTER MODEL INPUT--ALTEC 290-16K DRIVER

Symbol	Meaning	Units	Altec
RM	Mechanical resistance	kg/s	2.77
M	Moving mass	kg	0.0162
SUP	Spring constant	N/m	3.52×10^4
RHO	Density of gas	kg/m³	1.2
C	Sound speed	m/s	342.0
S	Resonator X-sec. area	m²	9.35×10^{-4}
BL	Driver trans. factor	N/A	21.5
Q	Resonator quality factor		60.0
FO	Resonator resonance freq.	Hz	240.0
A	Back volume X-sec. area	m²	4.13×10^{-3}
VOL	Back volume	m³	2.8×10^{-4}
LE	Voice coil inductance	H	1.0×10^{-3}
RE	Voice coil DC resistance	Ω	10.6
I	Driver current	A	1.0
L	Resonator length	m	0.712
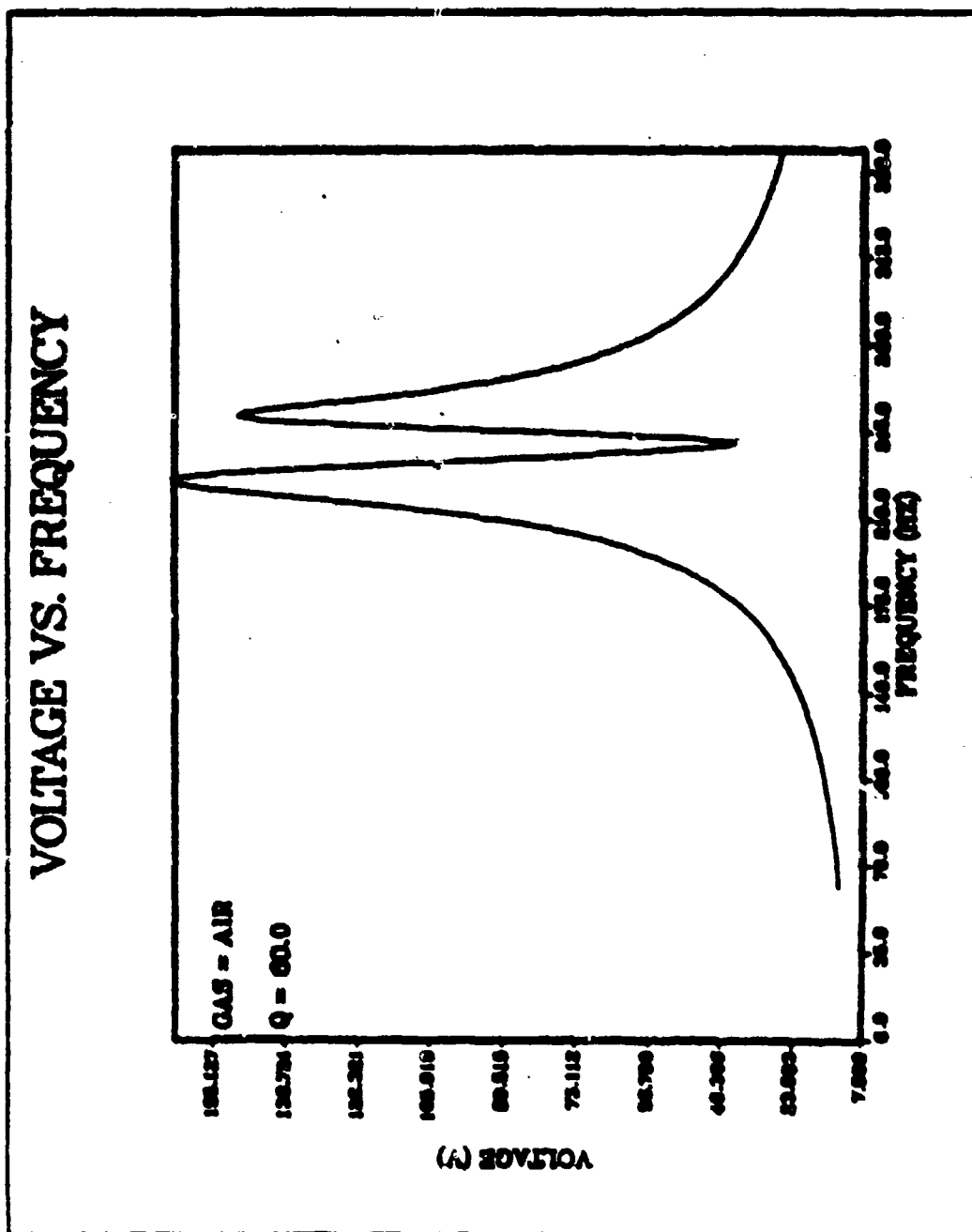
Figure III-12. Computer Model Output for
Altec 290-16K--Driver Voltage
vs. Frequency for One Amp.

81
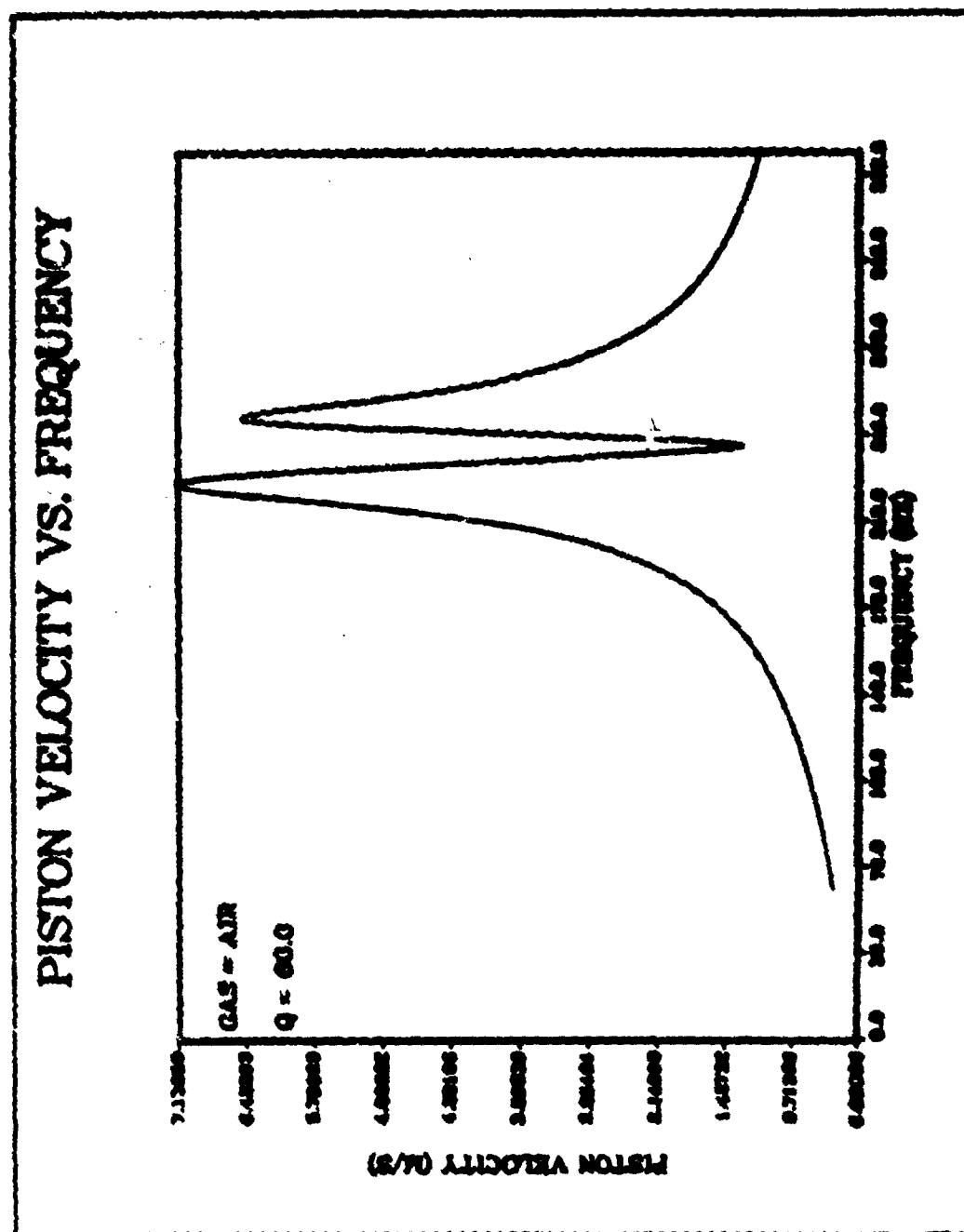
Figure III-13. Computer Model Output for Altec 290-16K--Piston Velocity vs. Frequency for One Amp.

82
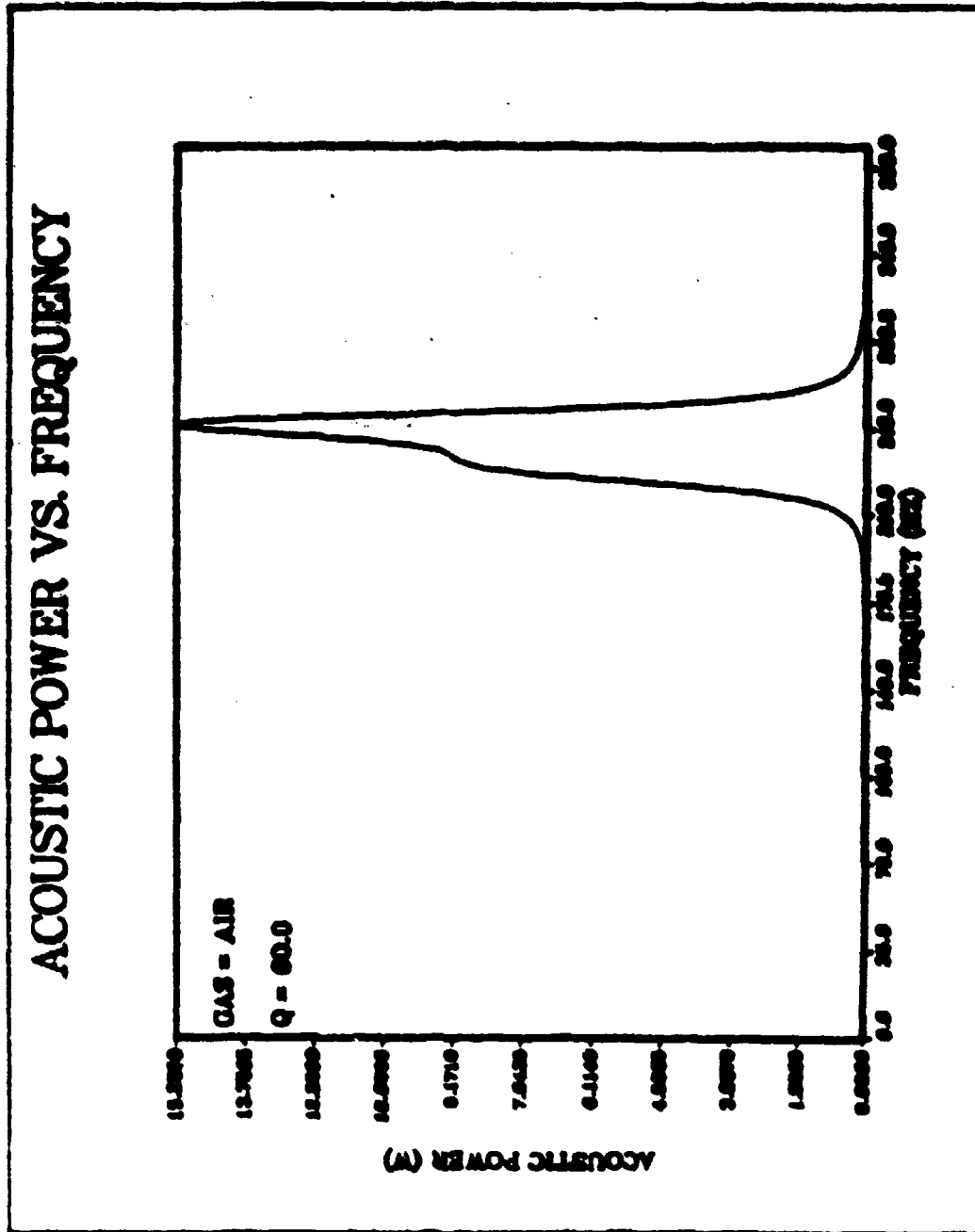
Figure III-14.   Computer Model Output for
Altec 290-16K--Acoustic Power
vs. Frequency for One Amp.
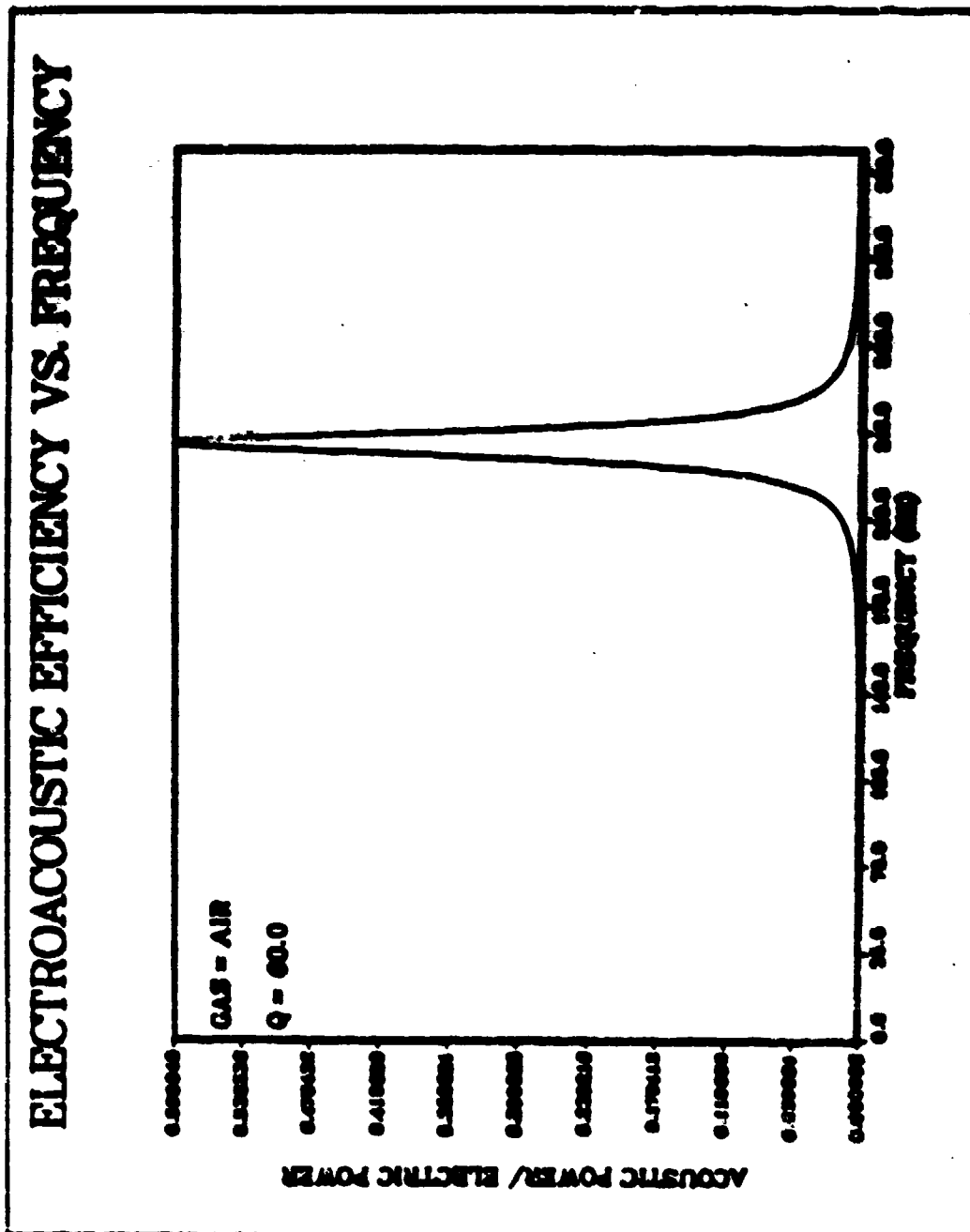
Figure III-15.   Computer Model Output for
                  Altec 290-16K--Electroacoustic
                  Efficiency vs. Frequency.

computer model is based on a linear theory and will have an
efficiency which is independent of drive current.

H. DRIVER RESONANCE ALTERATION

The refrigerator must operate at the resonant frequency
of the resonator to obtain the highest electroacoustic effi-
ciency and to maintain stack position with respect to the
standing acoustic wave (discussed in Sub-section II.A.4). It
appears from the computer model results and our experiments
so far that the operating frequency should also be near the
driver's resonance to get the most power out of the driver.
The resonant frequency of the resonator is determined by the
effective length of the resonator and the speed of sound in
the contained gas. The effective length for a tube of uni-
form cross-section and closed end is the actual measured
length. For the STAR resonator, however, the effective
length is the length that would produce the measured reso-
nant frequency for the given sound speed if the resonator
were a uniform cross-section closed-ended tube (see Figure
I-2 for approximate shape of resonator). The sound speed can
be altered by changing the percentage of xenon in the
helium-xenon mixture, since the sound speed depends on the
density of the mixture, and the density depends on the
percentages of the individual gases present (see Equations
IV-24 and IV-26). The gas mixture and effective resonator
length will be chosen to maximize the coefficient of

85

performance of the refrigerator. Therefore if we want to match the resonances, we will have to alter the resonance of the driver once the resonant frequency of the resonator has been determined.

The resonant frequency of the driver is proportional to the square root of the stiffness divided by the moving mass. If we want to raise the resonant frequency of the driver we can either increase the stiffness or decrease the mass. Conversely, to lower the resonant frequency we can either decrease the stiffness or increase the mass. Generally we prefer to decrease stiffness and mass to get a larger velocity. Reduction of stiffness usually also reduces the mechanical resistance.

For the Altec 290-16K attached to the uniform cross-section resonant tube in these preliminary experiments, the frequencies were already well matched (note the closeness of the peaks in Figures III-12 through III-14) and changing the driver frequency was not required. However, we know that in future applications we may need to alter, most probably lower, the driver resonant frequency. We developed an experimental procedure to do this.

Adding moving mass to the driver would appear to be the easiest way to lower the driver resonance. Unfortunately the added mass would also reduce the velocity by increasing the mecahnical impedance above resonance. We therefore chose to experiment with decreasing the driver stiffness. Recall that

the driver-reducer-bellows system stiffness includes the stifffness of the bellows (4.5 X 10⁹ N/m) and the suspension stiffness of the driver phenolic surround (29 X 10⁹ N/m). The driver suspension was the obvious choice for experimental alteration for two reasons: (1) it is over six times as large as the bellows stiffness, and (2) it would be very difficult for us to change the bellows stiffness without affecting its performance.

Since the 290-16K voice coil surround is made of a phenolic material, it was relatively easy to cut through it with an ordinary scalpel. We made a series of successive cuts in the surround material and ran measurements of the driver resonant frequency after each cut. The results of this experiment are given in Table III-5. We plotted the phase angle between the driver's electromotive force (emf) and the voice coil displacement as a function of frequency. For the emf we measured the voltage across the driver terminals in channel A of the HP 4192A Impedance Analyzer and assumed that the emf was in phase with the driver current and hence force. We used the photonic sensor to measure the displacement by connecting its voltage output to channel B. The 4192A then displayed the phase angle between the two voltages representing force and displacement. The driver is at resonance when this phase angle equals 90 degrees. The quality factor (Q) is equal to one-half the resonant frequency times the slope of the phase angle vs. frequency

curve evaluated at resonance (see Equation III-28). Using the previously determined values for moving mass (16 g) and bellows stiffness, we calculated the suspension stiffness:

$$k_{susp} = k_{tot} - k_{bellows} \qquad \text{(III-30)}$$

where $k_{tot} = 4\pi^2 f_o^2 m_o$. We calculated the mechanical resistance (R_m) using equation III-26. We stopped cutting the surround when its stiffness was approximately equal to that of the bellows and therefore the total stiffness was no longer suspension dominated.

TABLE III-5. RESULTS OF
DRIVER RESONANT FREQUENCY ALTERATION

Percent Surround Remaining (approx.)	Resonant Frequency (Hz)	Quality Factor	Suspension Stiffness (X10⁻⁹N/m)	Mechanical Resistance (kg/s)
100	241.0	8.55	32.2	2.83
100 (six slits)	229.5	8.09	28.8	2.85
80	213.5	5.17	24.3	4.15
50	183.5	8.65	16.8	2.13
20	119.5	8.56	4.52	1.40

Despite the anomoly at the 80% data point, we feel that this experiment shows that partial removal of the surround can reduce stiffness, resonant frequency, and mechanical resistance. It appears from the above data that the flexing

of the phenolic surround is responsible for the majority of the mechanical losses in the driver.

IV. STAR DRIVER PARAMETERS

A. INTRODUCTION

This chapter discusses the selection of the electro-dynamic driver, describes the parameter measurements on the chosen driver, and estimates the electroacoustic efficiency of the STAR using the computer model described in Section II.D.

1. Interface with NASA GAS Cannister

In addition to the maximum weight of 200 pounds discussed in Section I.B, restrictions due to the Get Away Special (GAS) cannister dimensions give us a maximum payload height (28.25 inches) and diameter (19.75 inches). In our allowed height we must fit two battery layers, the driver with its housing, the resonator assembly, and its associated vacuum space and thermal insulation. The battery layers are each about four inches high, for a total battery height of eight inches. This leaves about 20 inches for the driver and resonator assemblies (see Figure I-4 for approximate configuration). The electronics package and gas reservoir should fit in the area radially surrounding the resonator, and will therefore not add to the height. Although the diameter of the cannister volume is 19.75 inches, the driver housing must attach to the standard GAS can lid at a 9.5 inch diameter bolt circle, otherwise we would need a lid

90

specially designed for our project. As far as weight is concerned, approximately every pound we save elsewhere allows us to carry an extra battery cell, which results in an extra ten watt-hours of available energy.

2. Maximizing Electroacoustic Efficiency

In addition to the space and weight restrictions, we want to maximize the electroacoustic efficiency of the driver. We can do this by obtaining the maximum value for the combination of parameters $Bl/R_m m_m$. A larger Bl will give us a larger driving force ($F=Bli$), which in turn gives us a larger acoustic volume velocity, one of the components of acoustic power. For a given value of magnetic induction (B), a longer voice coil (achieved by having a larger voice coil diameter with the same number of turns, or the same diameter and more turns) will result in a larger Bl. This longer l would also result in a greater voice coil electrical resistance, so the two effects cancel. We also want to minimize the moving mass (m_m) to allow greater velocities and minimize the driver's mechanical resistance (R_m) in order to minimize mechanical losses in the driver.

3. Driver Selection

We had two off-the-shelf drivers available for consideration. The Altec 260-16K was discussed in Chapter III. The other driver was a JBL 2445J. Both drivers were designed for applications somewhat different from the STAR. Figure IV-1 shows a side view of the 2445J driver. The hatched
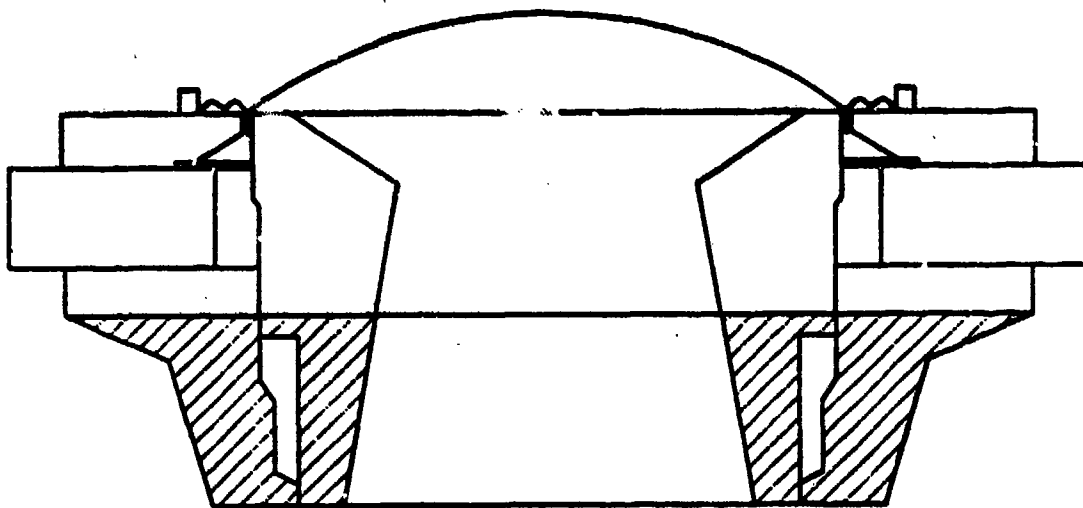
Figure IV-1.   Schematic Drawing of JBL 2445J Driver.
Hatched Area Shows Unnecessary Throat
Section.

area, known as the throat of the driver, is considered
unnecessary for our application, and adds a lot of extra
weight to the driver. The Altec 290-16K has a similar excess
throat volume. We contacted JBL and asked if they would
custom-design a driver which would eliminate this excess
weight. Fortunately for our project, JBL was in the process
of designing a new driver, the 2450J, which uses neodymium-
iron-boron magnets instead of the traditional ceramic. They
agreed to custom-design a version of the 2450J for our use.
The resulting driver (hereafter referred to as NIB) is shown
in Figure IV-2. The NIB driver accepts the same voice coils
(four inch diameter, aluminum wire, and titanium suspen-
sion/diaphragm) as the 2445J (ceramic magnet) driver. JBL
claims that it should also have the same properties,
including Bl.

In the remainder of this chapter we describe the
parameter tests on the NIB driver. We then compare the NIB
driver to the 290-16K driver. The results of the 2445J
parameter measurements are given for comparison. Finally we
present results generated by the computer model for the NIB
driver given various acoustic load impedances.

B. NIB DRIVER PARAMETERS

For the measurement of the NIB driver parameters, we
used the techniques we developed in Chapter III for the
measurement of the 290-16K driver parameters.
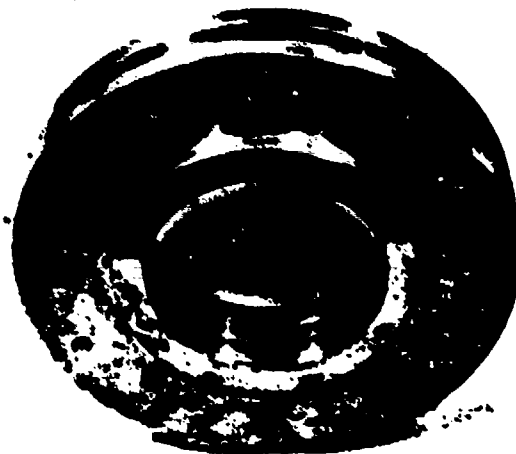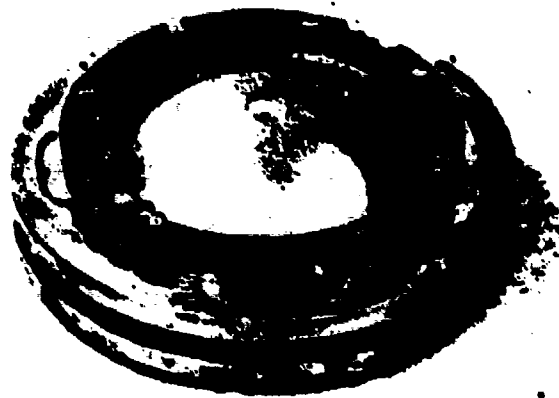
Figure IV-2. Photographs of JBL Neodymium-
Iron-Boron Driver.

1. Moving Mass and Suspension Stiffness

The moving mass and suspension stiffness were calculated using the mass loading technique. We placed small masses (0.5 to 3.5 grams) of black putty on top of the voice coil in half-gram increments. For each added mass the resonant frequency of the driver was found using the HP 4192A LP Impedance Analyzer (see Section III.B for a description of this instrument). Figure IV-3 shows a sample plot of period squared vs. added mass for the NIB driver in air. The stiffness was found by calculating four pi squared divided by the slope. The moving mass is equal to the intercept divided by the slope. For the NIB in air these values are:

$$k = 9.8 \pm 0.1 \times 10^4 \text{ kg/s}^2 \qquad \text{(IV-1)}$$

$$\text{and} \qquad m_o = 7.8 \pm 0.1 \text{ g}, \qquad \text{(IV-2)}$$

with a resonant frequency of 564 Hz. We repeated the measurement in a vacuum chamber and found:

$$k = 8.6 \pm 0.1 \times 10^4 \text{ kg/s}^2 \qquad \text{(IV-3)}$$

$$\text{and} \qquad m_o = 3.2 \pm 0.1 \text{ g}, \qquad \text{(IV-4)}$$

with a resonant frequency of 833 Hz (see Figure IV-4).

The moving mass is greater in air because of the driver having to move the air itself. The discrepancy in the stiffness is not as easy to explain. To determine the actual value of k, we used the static mass loading method. This gave us a value of:

NIB MASS LOADING - AIR

$y = 3.1368 + 0.4022x \quad R = 1.00$
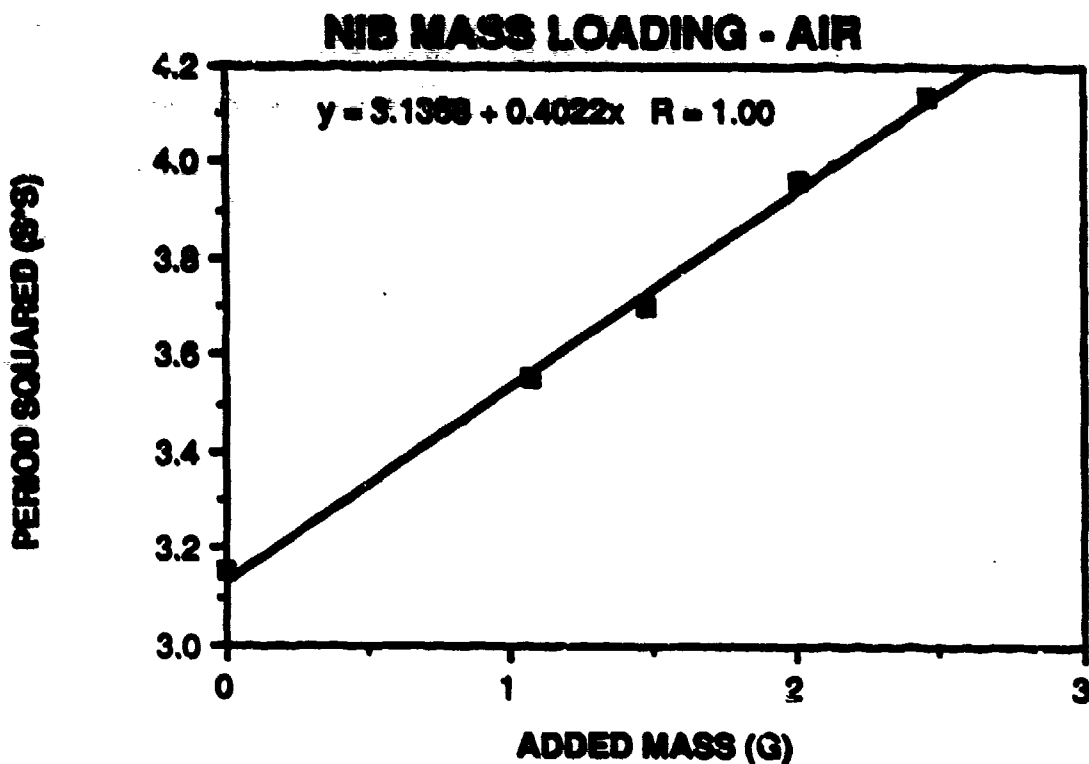
Figure IV-3. Least Squares Fit of Period Squared vs. Added Mass for NIB Driver in Air.

NIB MASS LOADING - VACUUM

$y = 1.4403 + 0.46x \quad R = 0.99$
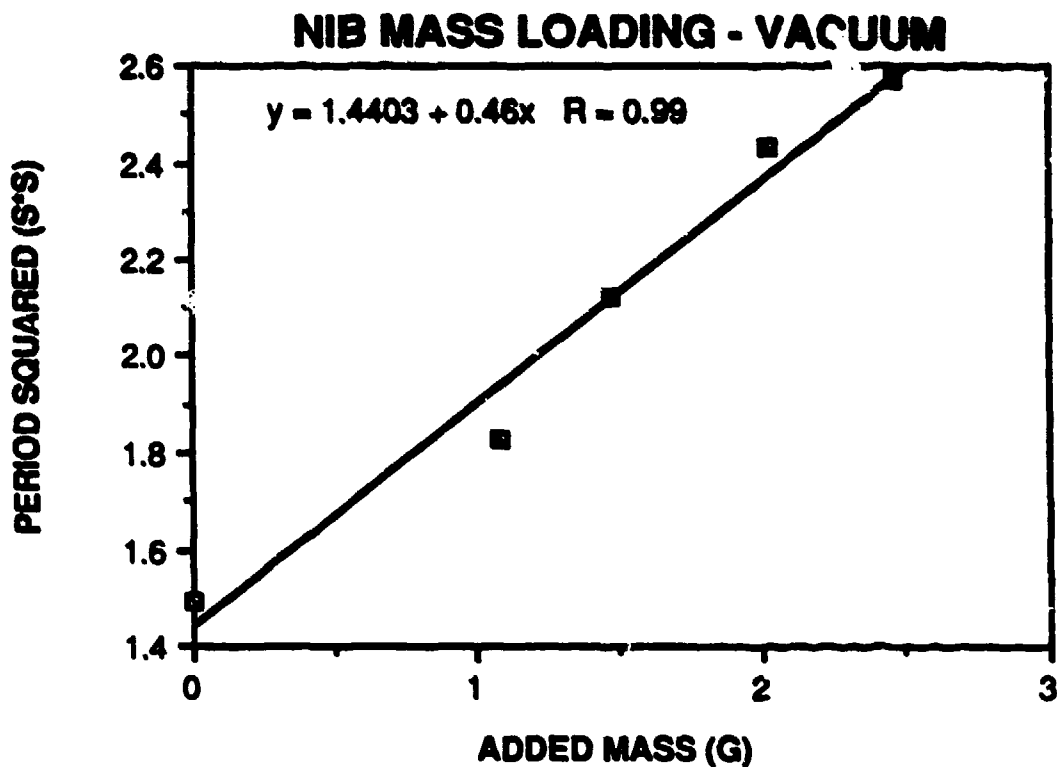
Figure IV-4. Least Squares Fit of Period Squared vs. Added Mass for NIB Driver in Vacuum.

$$k = 6.4 \pm 0.2 \times 10^4 \text{ kg/s}^2. \qquad \text{(IV-5)}$$

(The static loading measurements will be discussed in the next Sub-section.)

This last value for suspension stiffness differs by about 40% from the first two. We did not have sufficient time to test this driver until we were sure we had the "correct" value for the stiffness. We recommend that the follow-on students do so. Lacking the correct value, we ran the computer model for two sets of data: one set representing the "high" k (9.0×10^4 kg/s^2) and one using the "low" k (6.4×10^4 kg/s^2).

2. Transduction Coefficient (Bl)

The transduction coefficient (Bl) was calculated using two methods. The first method was to measure B (magnetic induction in the voice coil gap) and l (length of the voice coil) directly. We measured B with the Dowty RFL Industries model 912 Guassmeter (serial 808) using a Hall effect probe model 912015 (serial 21122). The maximum reading using this probe was 18.7 kGauss = 1.87 Tesla (T). This value differs by less than one percent from the value stamped on the driver by the manufacturer: 1.858 T. We will therfore use a value of B=1.86 $\pm$ 0.01 T for this driver. We then counted the turns of aluminum wire on the voice coil (n, = 30 $\pm$ 1 turns) and calculated l using the relationship:

$$l = \pi \, d \, n. \qquad \text{(IV-6)}$$

For the 9.98 ± 0.005 cm diameter coil we calculated a value of l = 9.4 ± 0.3 m. Multiplying these two values together gives us for the transduction coefficient:

$$Bl = 17.5 \pm 0.6 \text{ N/A.} \qquad (IV-7)$$

The other method used to determine Bl used the relationship:

$$F = BlI = -kx \qquad or \qquad Bl = -kx/I, \qquad (IV-8)$$

where I is the direct current applied to the coil, k is the spring constant measured earlier, and x is the displacement of the voice coil produced by the current. For this measurement on the 290-16K driver we had used a Linear Variable Differential Transformer (LVDT). For the NIB driver, however, we used Mechanical Technology Incorporated's MTI-1000 photonic sensor (serial 38010818) with plug-in cartridge model MTI-3812 (serial 1366) and probe model 125R. Figure IV-5 shows the photonic sensor with the NIB driver. One major advantage of the photonic sensor over the LVDT is that the photonic does not need to make physical contact with the surface it's measuring (it uses light) whereas the LVDT does. With the Altec 290-16K's rigid phenolic diaphragm, the contact with the LVDT probably did not affect the measurement. The NIB diaphragm, however, is made of thin titanium and is quite flexible. It would have been impossible to get an accurate reading of the displacement of this diaphragm using the LVDT. We calibrated the photonic sensor using calibration fixture KD-CH-III A. The output voltage
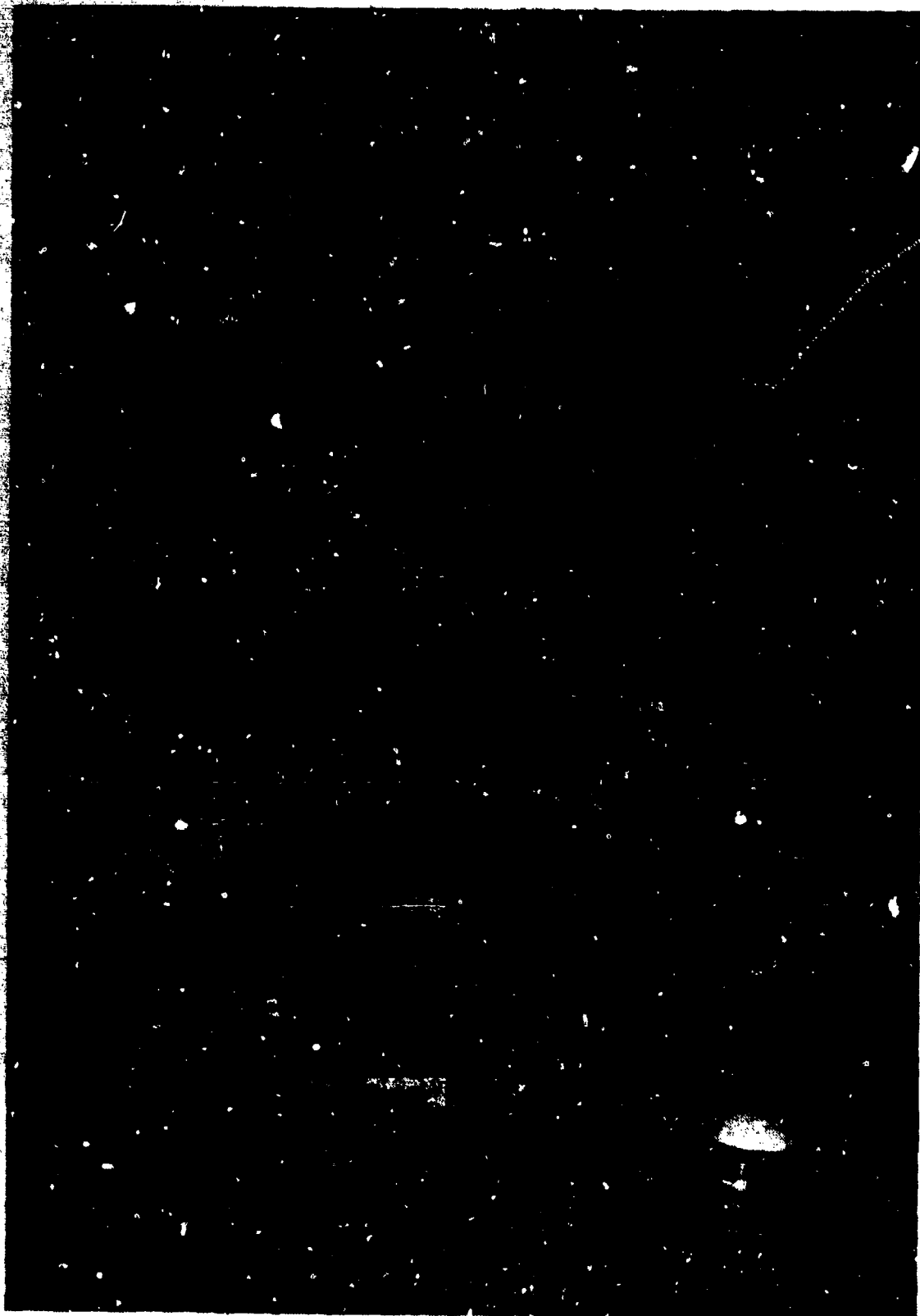
Figure IV-5.   MTI-1000 Photonic Sensor with NIB Driver.

from the sensor was read on a HP 3478A multimeter (serial A110136). We then plotted DC voltage vs. displacement in millimeters. The resulting graph is shown in Figure IV-6. The slope of this line gives us the calibration constant:

$$dV/dx = -2.086 \pm 0.001 \text{ V/mm.} \quad \text{(IV-9)}$$

This value is within two percent of the calibration value provided by the manufacturer of $dV/dx = 2.045$ V/mm (back slope).

The next step was to run DC current through the coil and record the displacement of the diaphragm (via a voltage reading from the photonic sensor). For the voltage supply we used the HP 467A power amplifier (serial 444-00243). We found the current by measuring the voltage (with the HP 3476A digital multimeter, serial 292162) across a ten ohm (10_Ω) resistor placed in series with the circuit, and dividing the voltage by ten ohms. The resulting graph is shown in Figure IV-7. The slope of the line gives us:

$$dI/dV = 2.10 \pm 0.005 \text{ A/V.} \quad \text{(IV-10)}$$

Combining the values in Equations IV-9 and IV-10 with the previously calculated high end value for the suspension stiffness $k = 9.2 \pm 0.6 \times 10^4$ kg/s^2 gives:

$$Bl = k(dx/dV)(dV/dI) = 21.5 \pm 1.4 \text{ N/A.} \quad \text{(IV-11)}$$

This 15% difference between the values of Bl using the two independent methods is what prompted us to test for Bl and k using the static loading method. Our primary concern is that we would expect the direct measurements of B

PHOTONIC CALIBRATION

$$y = 11.0854 - 2.0353x \quad R = 1.00$$
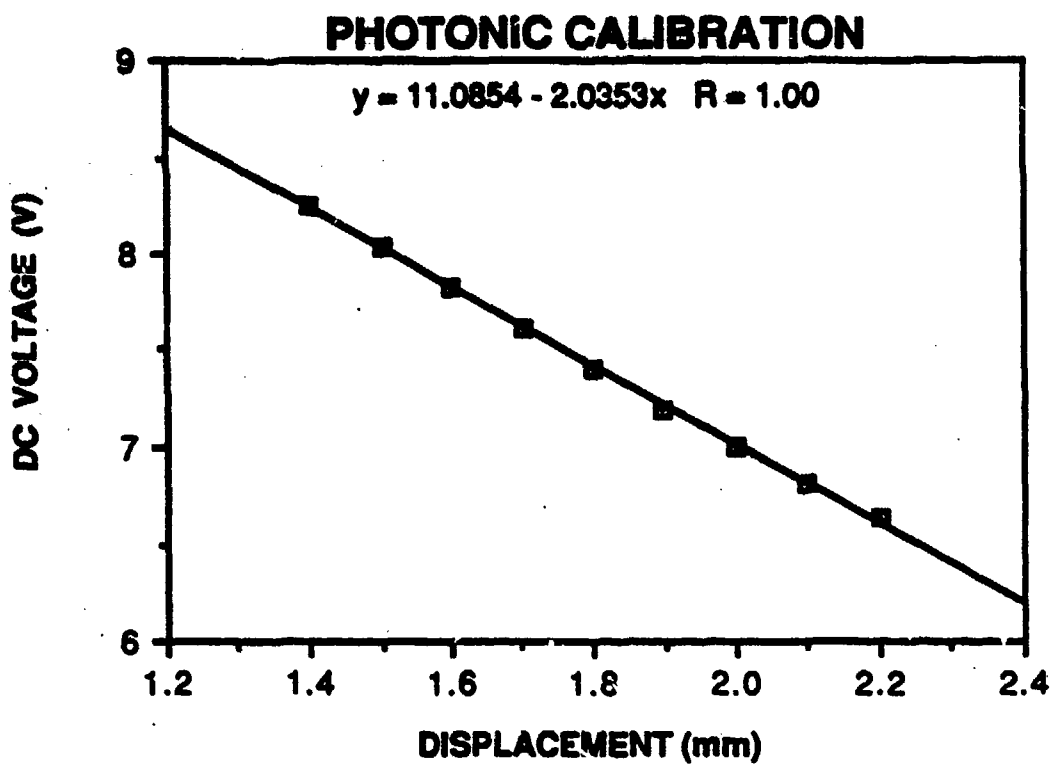
Figure IV-6. Calibration Data for Photonic Sensor Voltage Output vs. Displacement.

NIB - PHOTONIC CURRENT CALIBRATION

$$y = -15.2167 + 2.1004x \quad R = 1.00$$
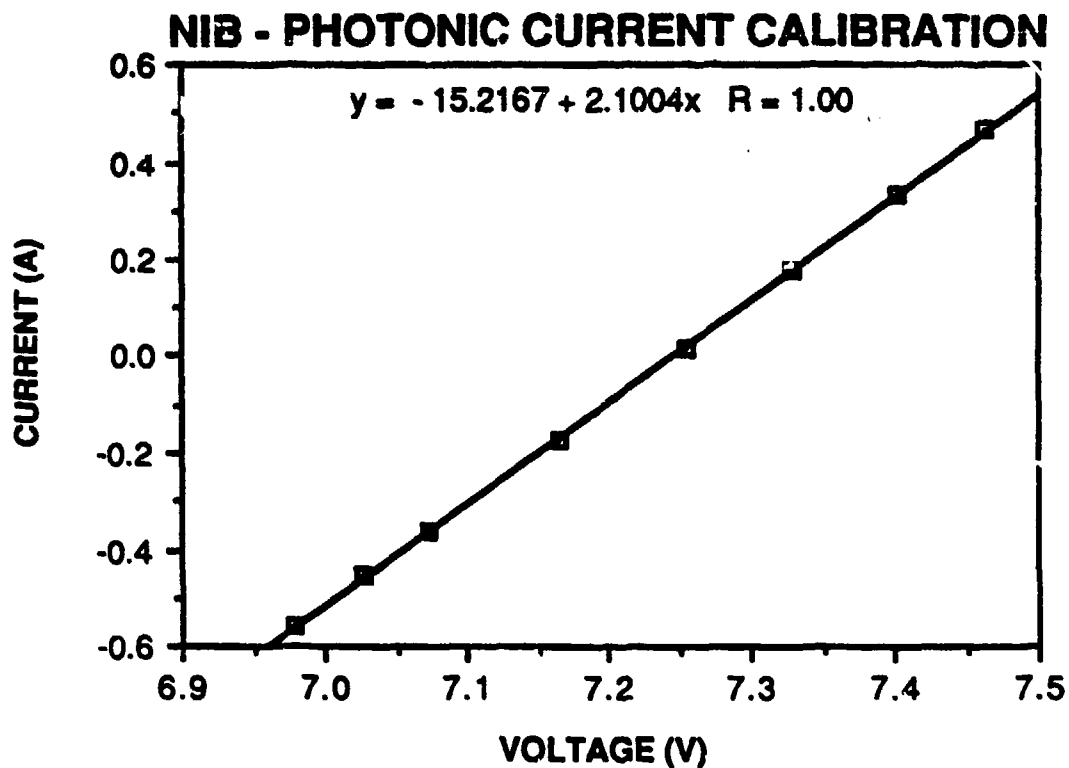
Figure IV-7. Least Squares Fit of DC Current Through Voice Coil vs. Photonic Voltage Output.

101

and 1 to give us the highest possible value for Bl. This is because the maximum magnetic field may not be acting on the full length of the coil. We did not expect the value of Bl calculated using the spring constant to be 15% higher than the direct measurement value.

We were able to obtain static loading values for both Bl and k using the same equipment setup and the formulas:

$$Bl = \Delta mg/\Delta I \quad \text{and} \quad k = -\Delta mg/\Delta x \qquad (IV-12)$$

For these measurements the voice coil is driven with a DC current. We then add previously measured masses (putty and soldering wire) to the voice coil, and measure the resulting displacement of the diaphragm using the photonic sensor. To measure Bl we determine how much current is needed to bring the voice coil back to its null displacement (original output voltage reading from the photonic sensor) after the mass is added. We measure k by keeping the current constant and measuring the difference in photonic output voltage (multiplied by the calibration constant to get displacement) resulting from the added mass. Table IV-1 lists the results of these measurements.

The bracketed value in each k and Bl pair was calculated using the measured value in the pair and the relationship:

$$BlI = -kx. \qquad (IV-13)$$

From these measurements we get the value k = 6.7 ± 0.2 kg/s² as reported earlier, and the transduction coefficient:

$$Bl = 15.0 \pm 0.2 \text{ N/A}. \qquad (IV-14)$$

For the model runs we used a value of Bl = 19.0 for the high k and Bl = 15.0 for the low k.

TABLE IV-1. STATIC LOADING OF NIB DRIVER TO DETERMINE
SUSPENSION STIFFNESS AND TRANSDUCTION COEFFICIENT

Δm (g)	ΔI (mA)	ΔV (V)	k (X10⁴ kg/s²)	Bl (N/A)
17.1	--	5.2	6.7	[15.3]
17.1	--	5.5	6.4	[14.6]
34.7	23.3	--	[6.4]	14.6
34.7	22.3	--	[6.7]	15.3
34.7	--	.288	6.1	--

(front slope)

3. Mechanical Resistance

The next parameter we measured was the mechanical resistance (R_m) using the relationship:

$$R_m = 2\pi f_o m_o / Q. \qquad (IV-15)$$

We attempted to find the driver quality factor (Q) using the same modified impedance technique described in Section III.G. As can be seen in Figure IV-8, the graph of the modified impedance magnitude vs. frequency is not a smooth resonance curve, as it was for the 290-16K (see Figure III-9). In fact, it looks like the superposition of two

NIB IMPEDANCE MAGNITUDE
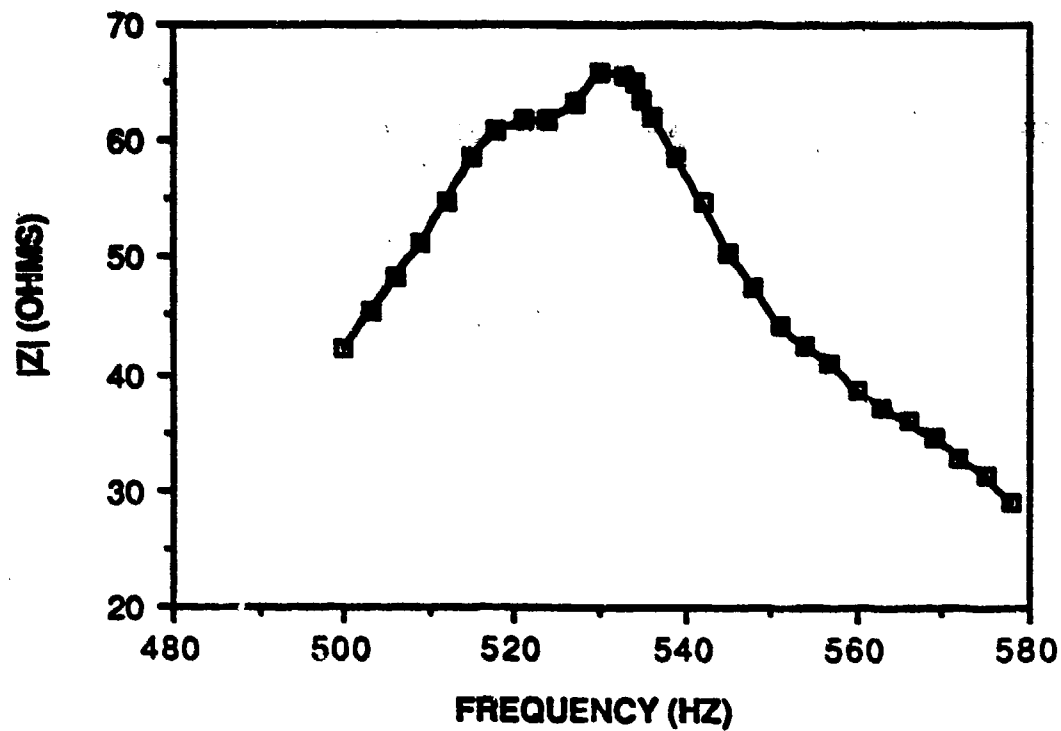
Figure IV-8. NIB Modified Impedance Magnitude
            vs. Frequency.

104

different impedance curves, the first one shorter and fatter and the second one taller and thinner. It was impossible to accurately measure half-power points from this curve, so we chose the phase angle method. (It is interesting to note that the JBL 2445J (ceramic) driver did have a smooth modified impedance curve similar to that of the 290-16K.) Figure IV-9 shows the graph of phase angle vs. frequency over a wide range of frequencies. Although this curve generally approximates an arctangent, the segment of the line immediately adjacent to the resonant frequency (assumed to be the frequency where $\theta=0$, in this case 534.5 ± 0.5 Hz) is linear (for a frequency range of about ten Hz). This segment is plotted in Figure IV-10. The slope of the line is $d\theta/df$ = - 42.0 ± 0.5 X 10^{-3}s (after converting degrees to radians). As in Section II.G, Q is given by:

$$Q = -(f_o/2)(d\theta/df) = 11.2 \pm 0.2. \qquad (IV-16)$$

This gives a value for R_m (using the moving mass in air m_o = 7.8 ± 0.1 g):

$$R_m = 2.34 \pm 0.05 \text{ kg/s.} \qquad (IV-17)$$

We decided that a more accurate measurement of Q and R_m could be found by making the Q measurement in vacuum. For this we used the open circuit free decay method. This method consists of sending a signal to the driver at resonance with an HP 3314A function generator (serial A342044), then simultaneously switching off the signal and triggering a Nicolet model 310 storage oscilloscope (serial 88004641) to

NIB IMPEDANCE PHASE ANGLE

y = 784.8911 - 1.4576x   R = 0.98
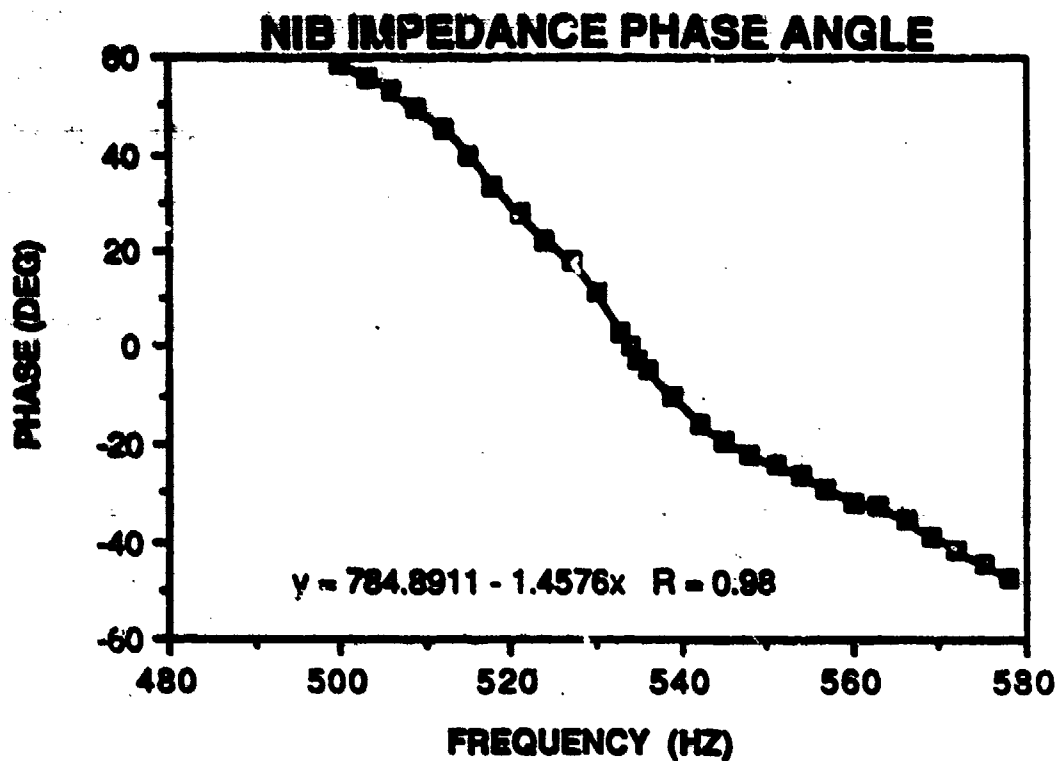
FREQUENCY (HZ)

Figure IV-9.   NIB Modified Impedance Phase Angle
as a Function of Frequency--Full
Frequency Range.

NIB PHASE ANGLE - LINEAR SEGMENT

y = 1219.5242 - 2.2815x   R = 1.00
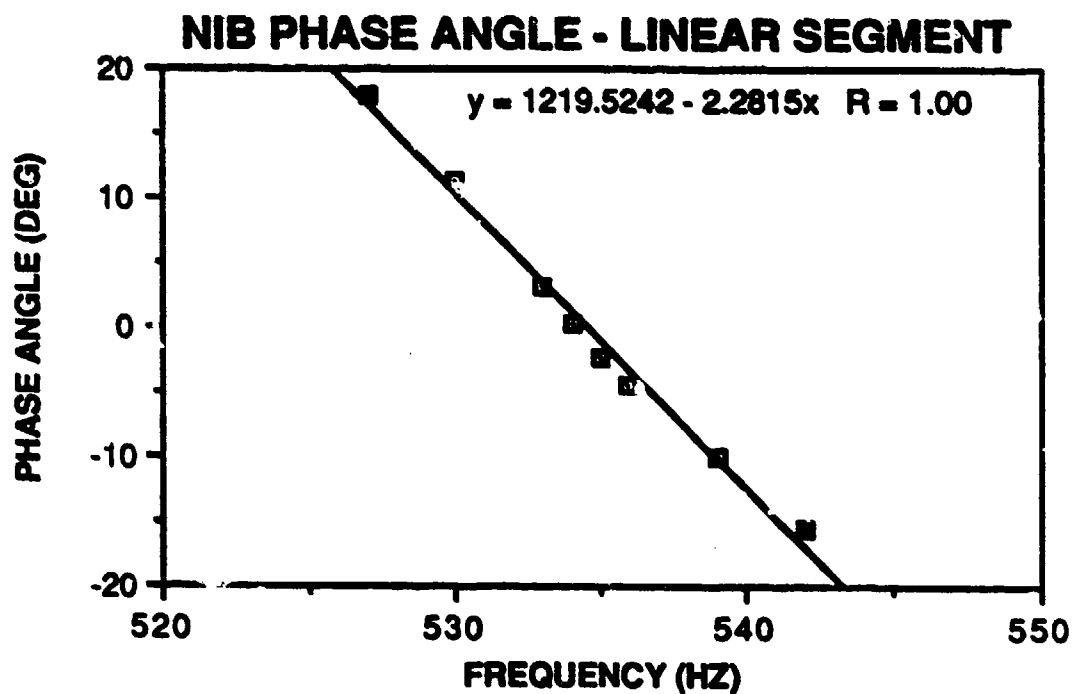
FREQUENCY (HZ)

Figure IV-10.   NIB Modified Impedance Phase Angle
as a Function of Frequency--Linear
Segment Near Resonance.

106

record the free decay. A sample of the output from this process is shown in Figure IV-11. The equation for a simple harmonic oscillator experiencing free decay is:

$$A(t) = A_o \exp(-t/\tau) \sin(\omega_o t + \phi), \qquad \text{(IV-18)}$$

where $A(t)$ is the amplitude as a function of time, A_o is the initial (maximum) amplitude, t is the time ($= nT$, or the number of periods times the period), τ is the free decay constant ($= QT/\pi$, see Equation III-29), ω_o is the angular resonant frequency, and ϕ is the phase angle. We recorded the peak amplitude as a function of period number, and plotted the natural logarithm of the peak amplitude vs. period number. The equation representing this line is:

$$\ln A(T)_{peak} = \ln A_o - nT/\tau. \qquad \text{(IV-19)}$$

The slope of this line is $t/\tau = nT/\tau = n\pi/Q$. Therefore Q can be found by dividing π by the slope of the line. Figure IV-12 shows a semi-log plot for the NIB driver in air. The value of Q for this plot is 21.5, which is almost twice the value we found using the modified impedance phase angle measurements (Q = 11.2). Obviously the air strongly affects the measurements. The scattering of the data points in this figure is probably due to the same phenomena that causes the double peaks in the impedance curve. Figure IV-13 shows the semi-log plot of the amplitude vs. period number for vacuum. This curve is much smoother and, we assume, more reliable. The Q for this data is:

$$Q = \pi/\text{slope} = 19.8 \pm 0.05. \qquad \text{(IV-20)}$$
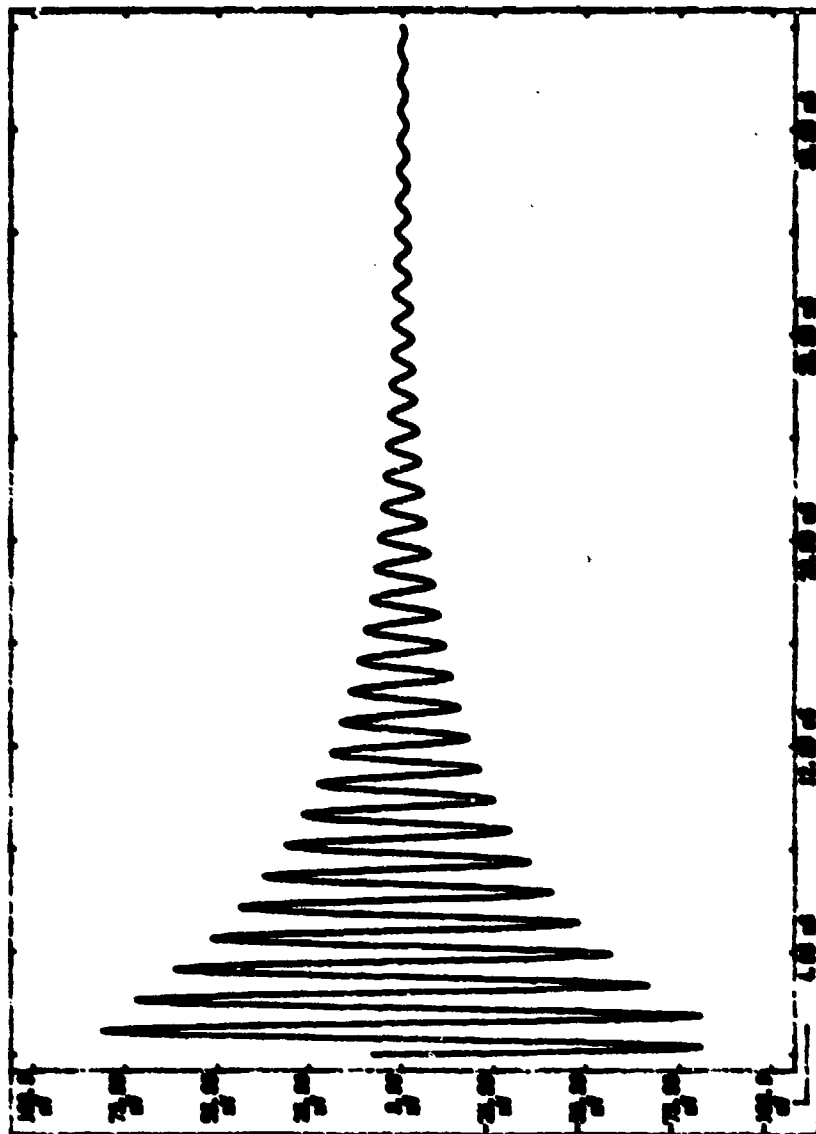
Figure IV-11. Sample of Free Decay Output from
Nicolet 310 Storage Oscilloscope.

108

NIB FREE DECAY - AIR

$$y = 3.5792 - 0.1464x \quad R = 1.00$$
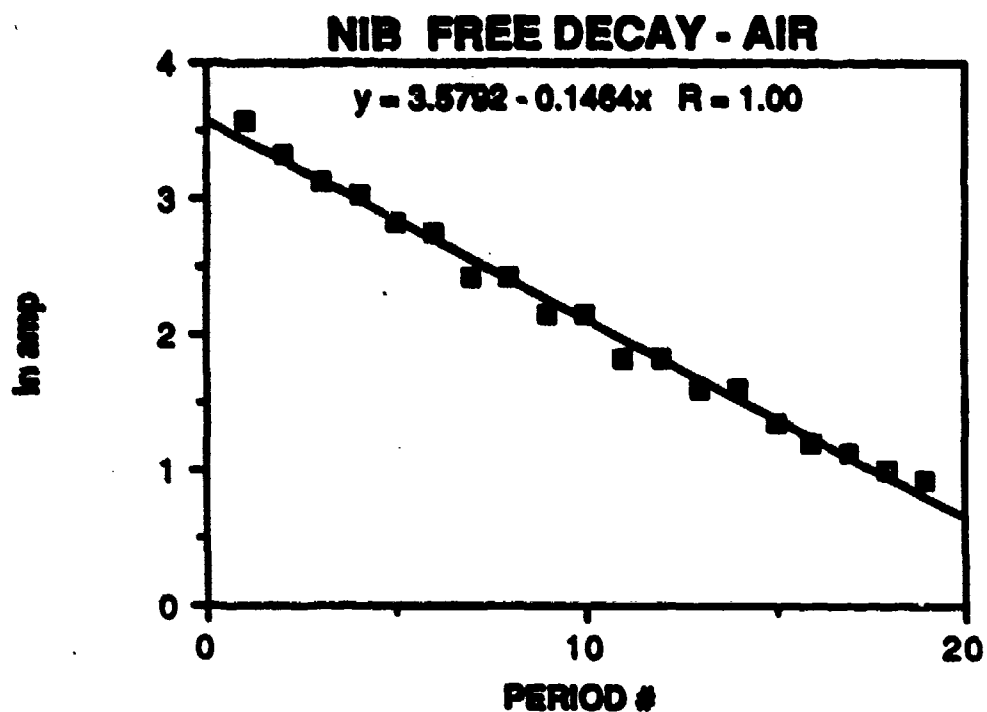
Figure IV-12.   Semi-log Plot of Amplitude
vs. Period Number for NIB
Free Decay in Air.

NIB FREE DECAY - VACUUM

$$y = 4.5606 - 0.1585x \quad R = 1.00$$
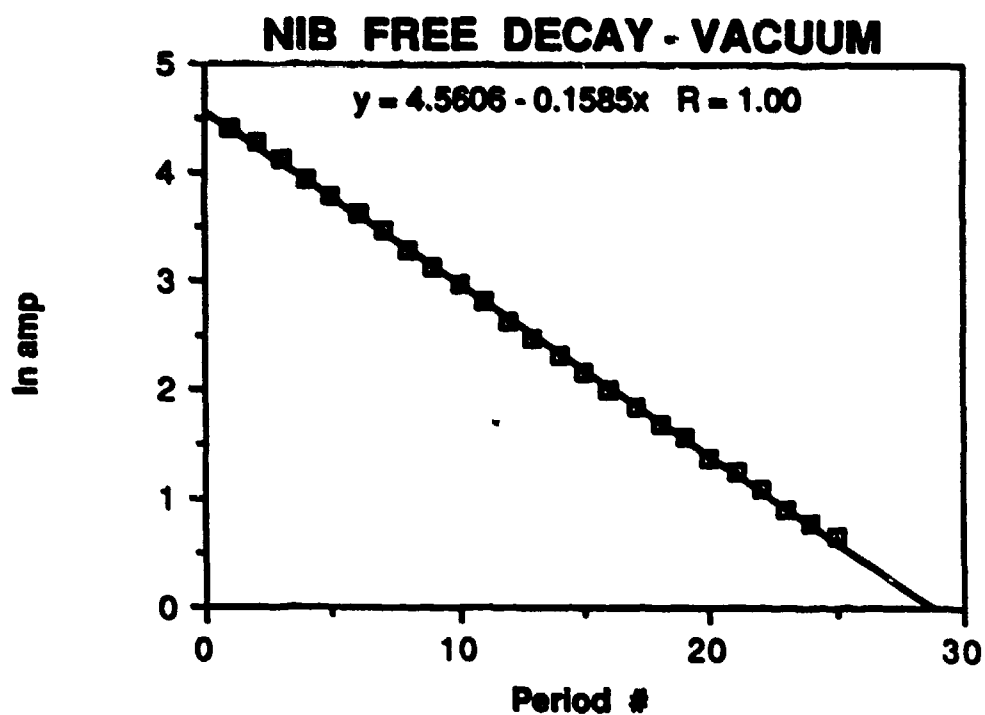
Figure IV-13.   Semi-log Plot of Amplitude
vs. Period Number for NIB
Free Decay in Vacuum.

109

We can also find the period from the free decay curve (and thus the resonant frequency as the inverse of the period). We use the oscilloscope to measure the time for ten cycles and divide this number by ten. For the vacuum run the resonant frequency was 839 ± 0.5 Hz. These values (and the moving mass = 3.2 g in vacuum) give us the mechanical resistance in vacuum:

$$R_m = 2\pi f_o m_o / Q = 0.83 \pm 0.01 \text{ kg/s}. \qquad (IV-21)$$

This is the value we used for the model.

Table IV-2 gives a comparison of applicable parameters for the three drivers. Notice that the parameter $Bl/R_{m\_\_\_\_m_o}$ is almost three times greater for the NIB driver than the 290-16K. This is the parameter that we said (Subsection IV.A.2) we wanted to maximize to get the highest thermoacoustic efficiency. Thus the driver that gives us the best height and weight characteristics (see photograph of the three drivers in Figure IV-14) also gives us the best electroacoustic efficiency.

C. MODELED EFFICIENCY

In order to model the electroacoustic efficiency of the driver, we need to know what acoustic load (impedance) it will see. The final resonator and stack composition will not have been determined by the time this thesis is completed. We therefore assumed a range of possible values for the

110

TABLE IV-2. COMPARISON OF PARAMETERS FOR THE THREE DRIVERS

Property (units)	Altec 290	JBL 2445J	JBL N18
Moving mass, m_o (kg)	0.0151	0.015	0.015
Spring constant (N/m)	3.52×10^4	$\sim 8.5 \times 10^4$	$\sim 9.0 \times 10^4$
Magnetic Induction, B (Tesla)	2.1	1.97	1.87
Voice Coil Diameter (cm)	7.22	9.98	9.98
Bl (N/A)	21.5	18.5	17.5
Voice coil DC resistance (Ω)	10.6	7.1	7.6
Mechanical resistance (kg/s)	2.77	~ 1.0	0.83
Voice coil inductance (H) (at 20 kHz)	1.0×10^{-4}	1.14×10^{-4}	1.14×10^{-4}
Mass (kg)	14.5	13.8	3.1
Height (in)	6.0	5.5	2.5
Magnetic energy density (J/cm^3)	~ 0.5	~ 0.5	3.2
$Bl/R_{mech}m_o$ (m/Coul-kg)	510	1230	1410

Figure IV-14. Photographic Comparison of the Three Drivers--Altec 290-16K, JBL 2445J, and JBL NIB.

acoustic load based on the experimental data acquired to date.

The model parameters that relate to the acoustic load are the density of the gas (RHO), the speed of sound in the gas (C), the resonator quality factor (Q), the resonator resonant frequency (FO), and the resonator length (L). The model was designed for a closed-ended tube of uniform cross-section. The STAR resonator has an open tube (with a bulb attached) and nonuniform cross-section. The problem of applying the existing computer model to the STAR resonator was solved by scaling the STAR parameters to make it look like a closed-ended uniform cross-section tube.

1. Input Values for Pure Helium

For pure helium, the experimental data available was the range of resonator quality factor values (10-20), and the speed of sound and gas density at room temperature (about 300K) and ten atmospheres (c_{RT} = 1024 m/s, ρ_{RT} = 1.618 kg/m^3). Also available were four resonant frequencies, two for a short resonator at warm (580 Hz) and cold (520 Hz) temperatures, and two for a long resonator at warm (520 Hz) and cold (470 Hz) temperatures. Using this information, we first calculated the effective lengths of the resonators at room temperature as if they were closed-ended, uniform cross-section tubes. For this we used the relationship:

$$\lambda = 2L = c/f, \quad \text{or} \quad L_{eff} = c/2f, \qquad \text{(IV-22)}$$

113

where λ is the wavelength, L is the length of the tube, c is the speed of sound, and f is the resonant frequency. This calculation gave us effective lengths for the resonators: $L_\bullet$ = 0.883m and L_1 = 0.985m. For the computer runs we use a convenient value of L_{eff} = 0.90m. We then calculated the speed of sound for the operating temperature of approximately 250K using the relationship:

$$c(T) = c_{RT} [T/T_{RT}]^{1/2}. \qquad (IV-23)$$

This gives us a speed of sound c_{250} = 935 m/s. If we use this sound speed and the effective resonator lengths to estimate the resonant frequencies for 250K, we get $f_\bullet$ = 529 Hz and f_1 = 474 Hz, which agree with the measured values. We calculated the gas density at the operating temperature using the relationship:

$$\rho = \gamma P/c^2 = 1.94 \text{ kg/m}^3, \qquad (IV-24)$$

where γ is the ratio of the specific heats (1.667 for helium) and P is the pressure.

Table IV-3 lists the input parameters for the pure helium computer runs. Note that for the computer model, the moving mass must take the mass of the reducer cone and bellows into account (see Figure IV-15). The total moving mass is expected to be approximately 15 g.

2. Input Values for Helium-Xenon

There was somewhat less data available for the helium-xenon mixture (12.5% Xe). We had the sound speed at 300K and ten atmospheres (c_{RT} = 472 m/s). We also had

114

TABLE IV-3. COMPUTER MODEL INPUT--
NIB DRIVER WITH HELIUM AT TEN ATMOSPHERES
AND TEMPERATURE = 250K

Symbol	Meaning	Units	NIB
RM	Mechanical resistance	kg/s	0.83
M	Moving mass	kg	0.015
SSUP	Spring constant	N/m	6.6, 9.0 X10^4
RHO	Density of gas	kg/m^3	1.94
C	Sound speed	m/s	935.0
S	Resonator X-sec. area	m^2	1.14X10^{-3}
BL	Driver transduction factor	N/A	15.0, 19.0
Q	Resonator quality factor		10,15,20
FO	Resonator resonance freq.	Hz	519.4
A	Back volume X-sec. area	m^2	4.42X10^{-3}
VOL	Back volume	m^3	3.28X10^{-4}
LE	Voice coil inductance	H	1.14X10^{-4}
RE	Voice coil DC resistance	Ω	7.6
I	Driver current	A	1.0
L	Resonator length	m	0.90
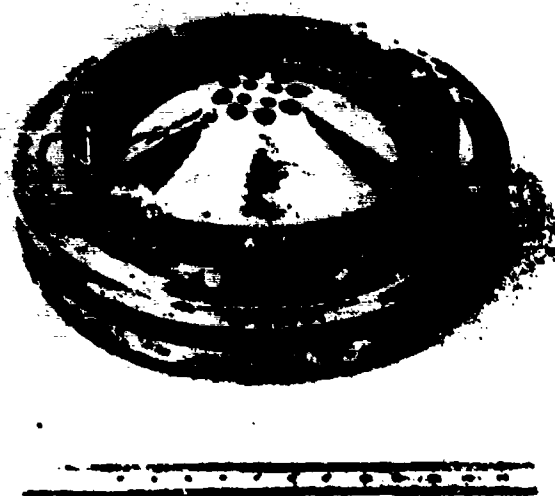
(a)
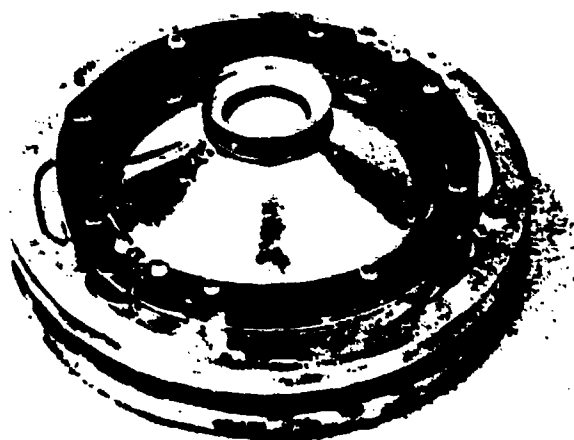
(b)

Figure IV-15. Photograph of JBL NIB Driver
with (a) Reducer and (b) Bellows.

resonant frequencies for the same four conditions as for the pure helium: short-warm (265 Hz), short-cold (230 Hz), long-warm (235 Hz), and long-cold (215 Hz). We used Equation IV-22 to find the effective resonator lengths (L_w = 0.891m and L_1 = 1.004m). However, once again we used a convenient effective length of 0.90 m for the computer runs. We used Equation IV-23 to find the sound speed for He-Xe at the operating temperature, $c_{\text{He-Xe}}$ = 431 m/s. The estimated resonant frequencies for the cold temperature were f_w=242 Hz and f_1=215 Hz, once again comparing favorably with the measured values. To find the density of the mixture at the operating temperature we used a form of the ideal gas law:

$$\rho = PM/RT, \qquad\qquad (IV-25)$$

where M is the atomic mass of the mixture, R is the universal gas constant, and P and T are the pressure and temperature. We calculated the atomic mass of the mixture using the equation:

$$M_{He-Xe} = M_{He}X_{He} + M_{Xe}X_{Xe}, \qquad\qquad (IV-26)$$

where the M's are atomic masses (4 for helium and 131.3 for xenon) and the x's are percentages of the gases in the mixtures. This equation gives us an atomic mass for the 12.5% Xe mixture of 19.9 g/mol, and a density of 9.70 kg/m^3 at 250K and ten atmospheres. Table IV-4 lists the computer input values for He-Xe, including a range of Q's from 5 to 30. (We are not sure what to expect for the actual value of Q, since a new stack will also be used.)

TABLE IV-4. COMPUTER MODEL INPUT--
NIB DRIVER WITH HELIUM-XENON AT TEN ATMOSPHERES
AND TEMPERATURE = 250K

Symbol	Meaning	Units	NIB
RM	Mechanical resistance	kg/s	0.83
M	Moving mass	kg	0.015
SSUP	Spring constant	N/m	6.6, 9.0 $\times 10^4$
RHO	Density of gas	kg/m^3	9.70
C	Sound speed	m/s	431.0
S	Resonator X-sec. area	m^2	1.14×10^{-3}
BL	Driver trans. factor	N/A	15.0, 19.0
Q	Resonator quality factor		5,10,15,20,25,30
FO	Resonator resonance freq.	Hz	239.4
A	Back volume X-sec. area	m^2	4.42×10^{-3}
VOL	Back volume	m^3	3.28×10^{-4}
LE	Voice coil inductance	H	1.14×10^{-4}
RE	Voice coil DC resistance	Ω	7.6
	Driver current	A	1.0
L	Resonator length	m	0.90

3. Computer Model Results

Figures IV-16 through IV-19 are sample output plots for pure helium with $Bl = 15$ N/A, $k = 6.4 \times 10^4$ kg/s^2, and $Q = 20$. Notice that the peak values for the driver and resonator are almost matched (the driver resonance is at the lower frequency). The thermoacoustic efficiency for this set of values is about 70.4%. Figures IV-20 through IV-23 show the corresponding plots for the helium-xenon mixture. This time the peaks are not matched (the driver peak is off the scale) and the electroacoustic efficiency is about 16.6%. The primary reason for the difference between the two gases is the lower sound speed, and therefore lower resonant frequency, in the He-Xe mixture.

Table IV-5 lists the maximum value of electroacoustic efficiency for each of the test runs. The consistently low efficiencies for the He-Xe emphasize the importance of matching the two resonant peaks. We recommend that the driver frequency be adjusted to match the resonator operating frequency. This can best be done by reducing the stiffness of the titanium surround (see Section III.H).
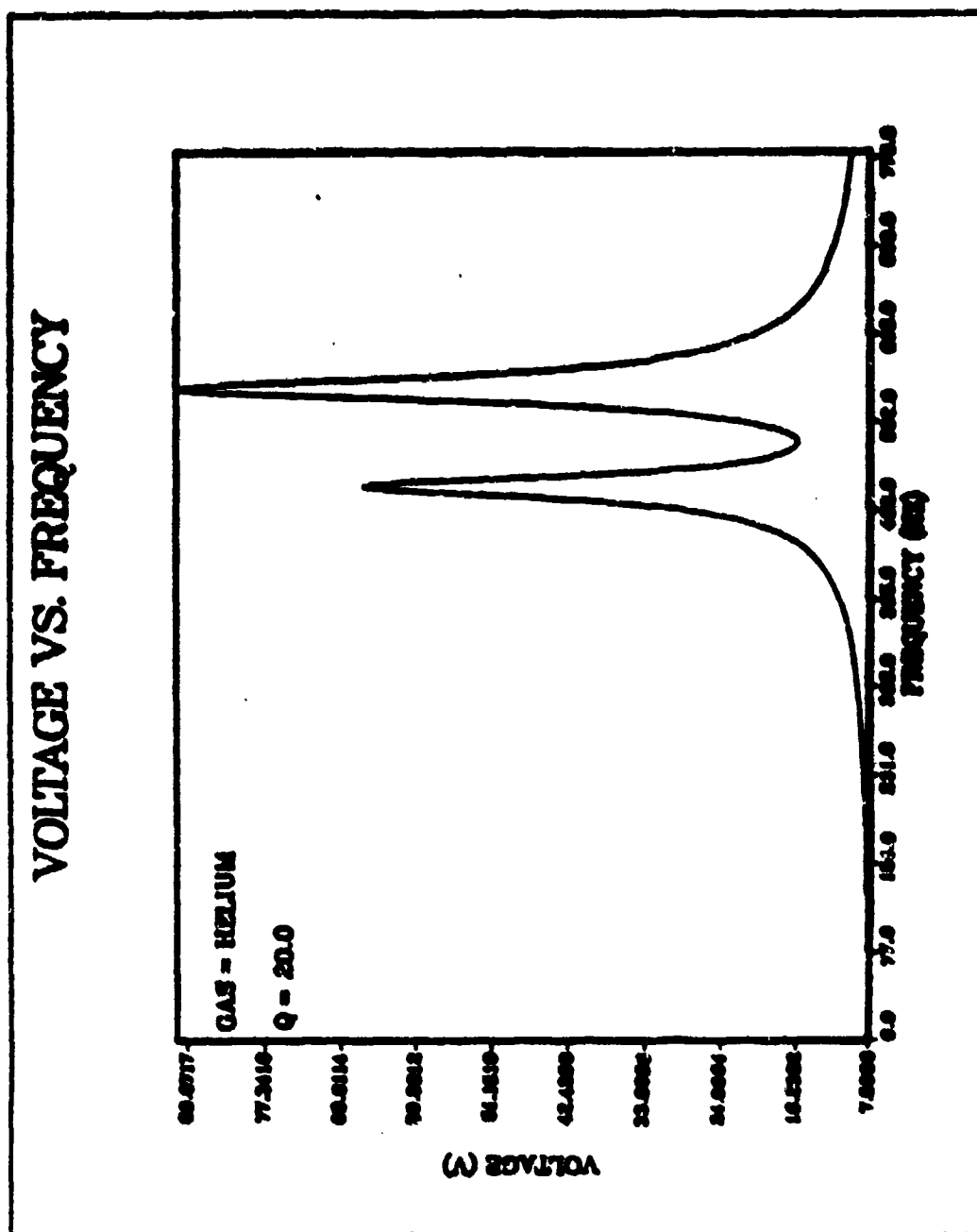
Figure IV-16.   Computer Model Output for NIB with
                Helium (Bl = 15, Q = 20)--Driver
                Voltage vs. Frequency for One Amp.

120
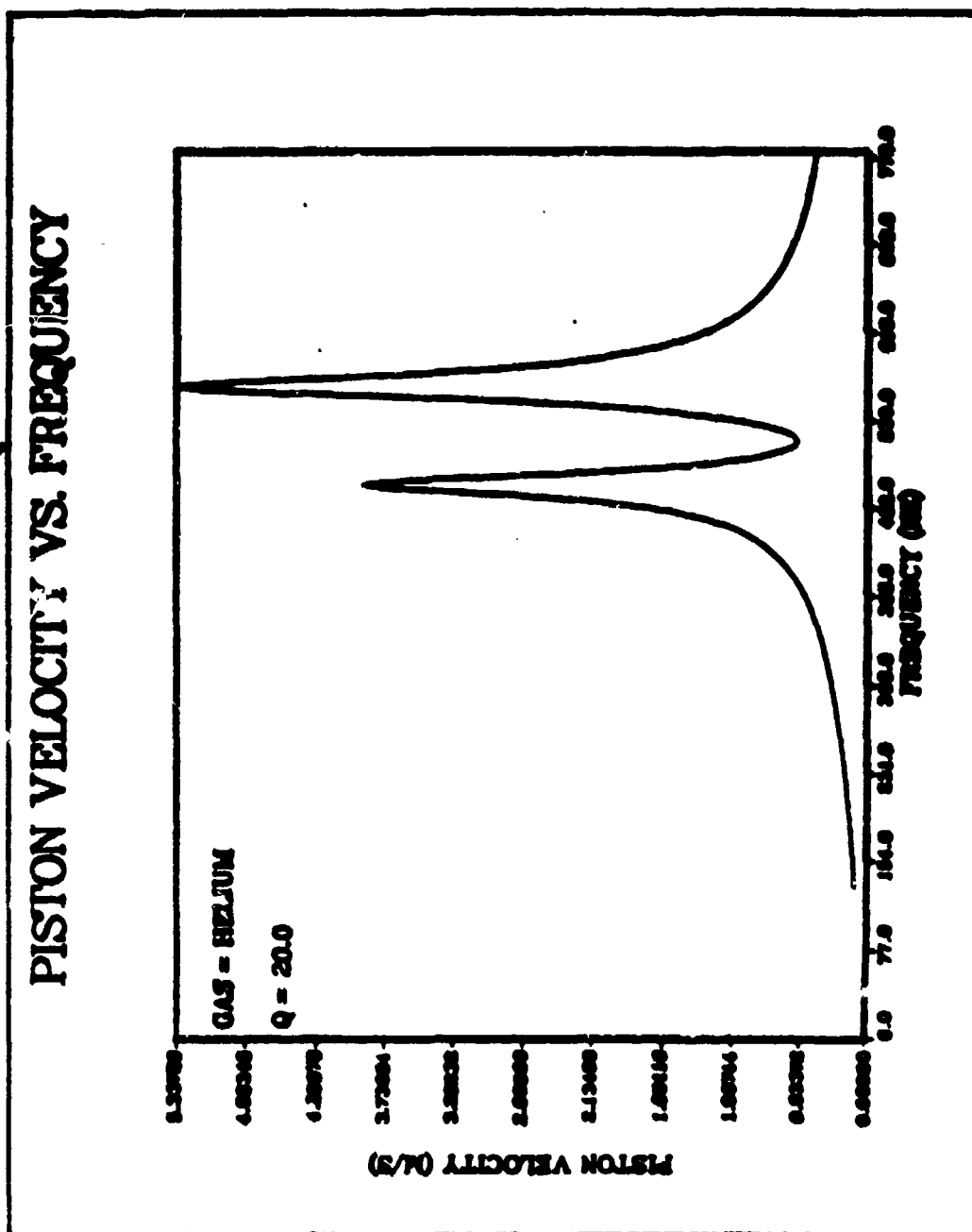
Figure IV-17. Computer Model Output for NIB with
              Helium (Bl = 15, Q = 20)--Piston
              Velocity vs. Frequency for One Amp.

121
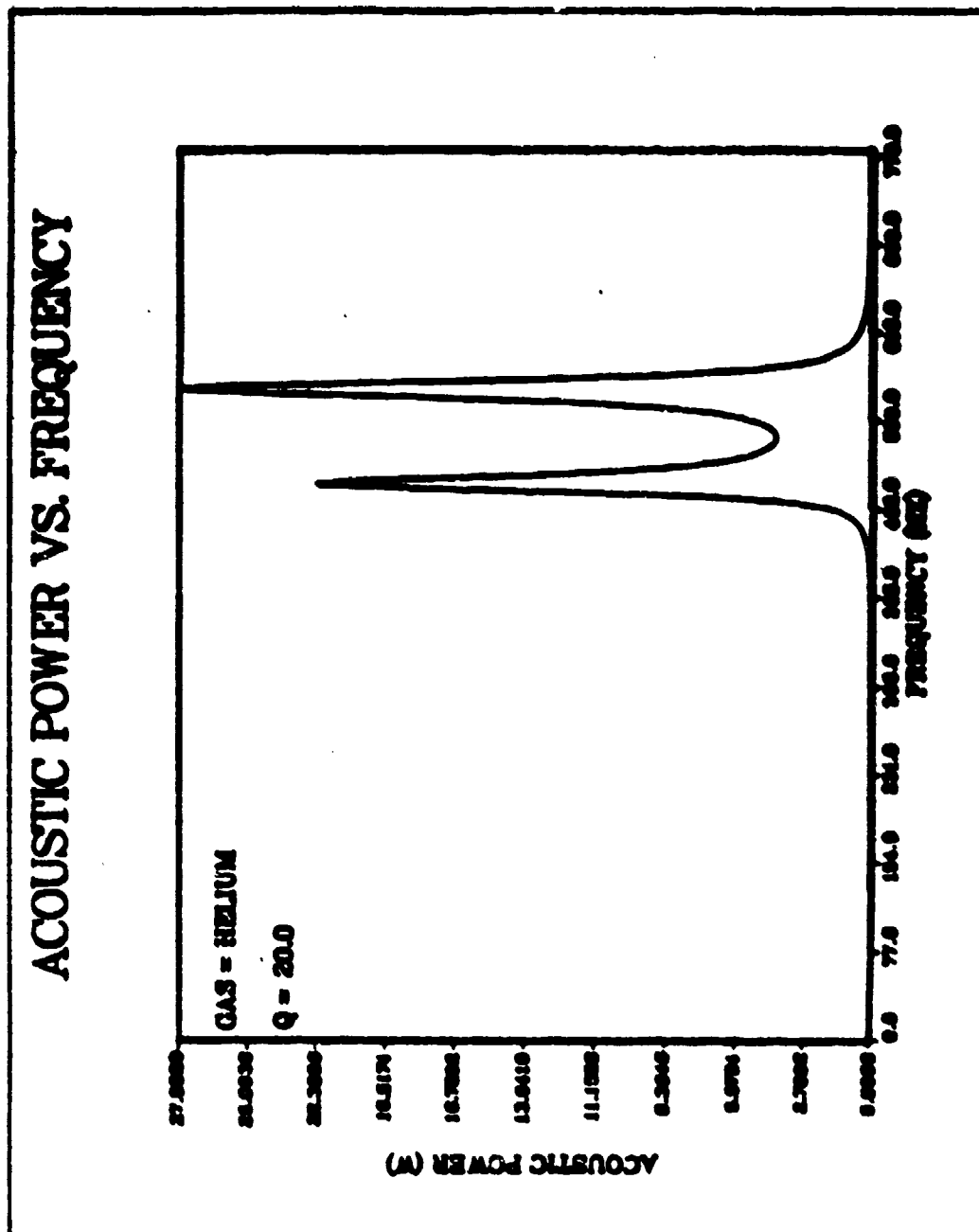
Figure IV-18.   Computer Model Output for NIB with Helium (Bl = 15, Q = 20)--Acoustic Power vs. Frequency for One Amp.
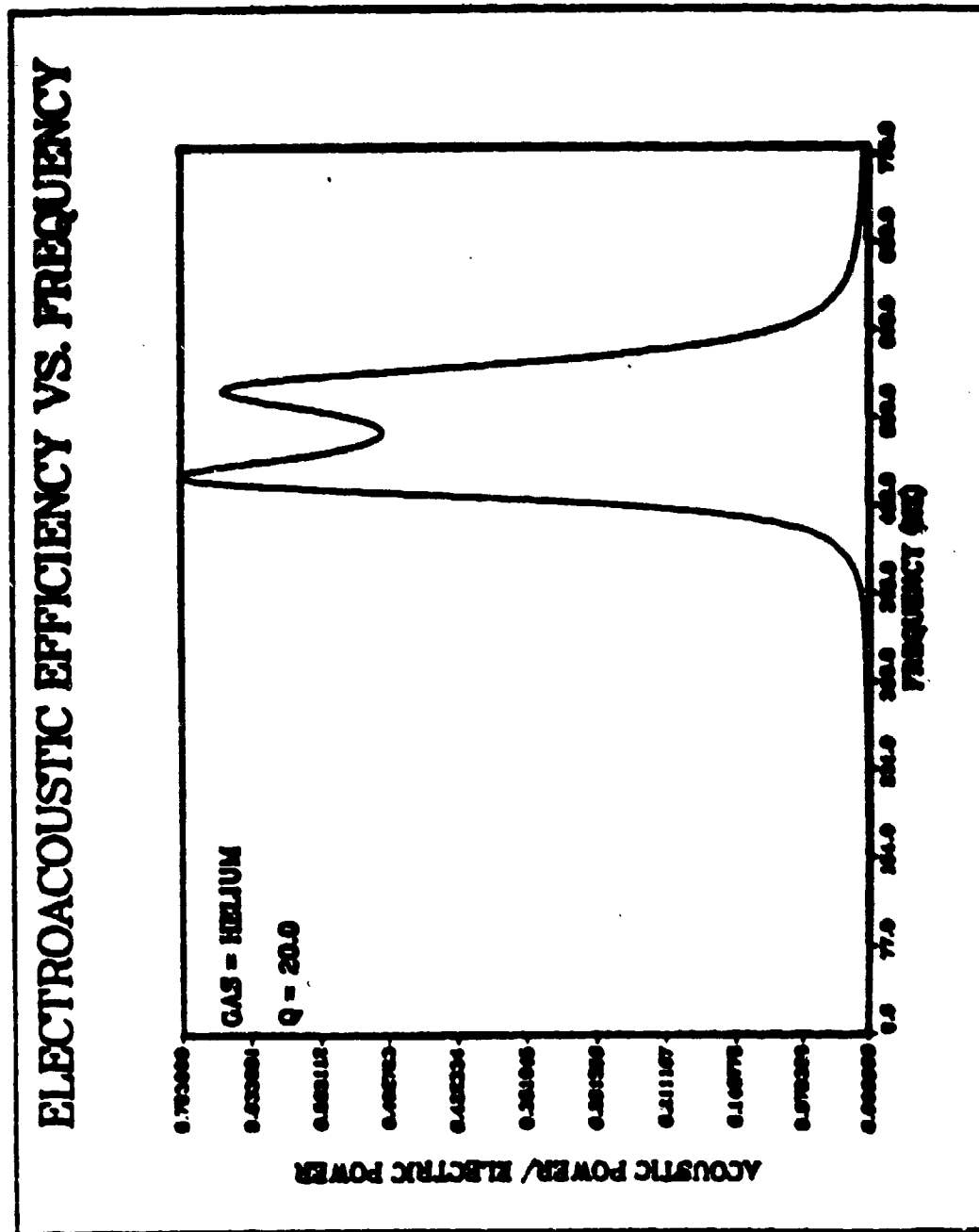
Figure IV-19. Computer Model Output for NIB with Helium
(Bl = 15, Q = 20)--Electroacoustic
Efficiency vs. Frequency.

123

Figure IV-20. Computer Model Output for NIB with Helium-
Xenon (B1 = 15, Q = 20)--Driver Voltage
vs. Frequency for One Amp.
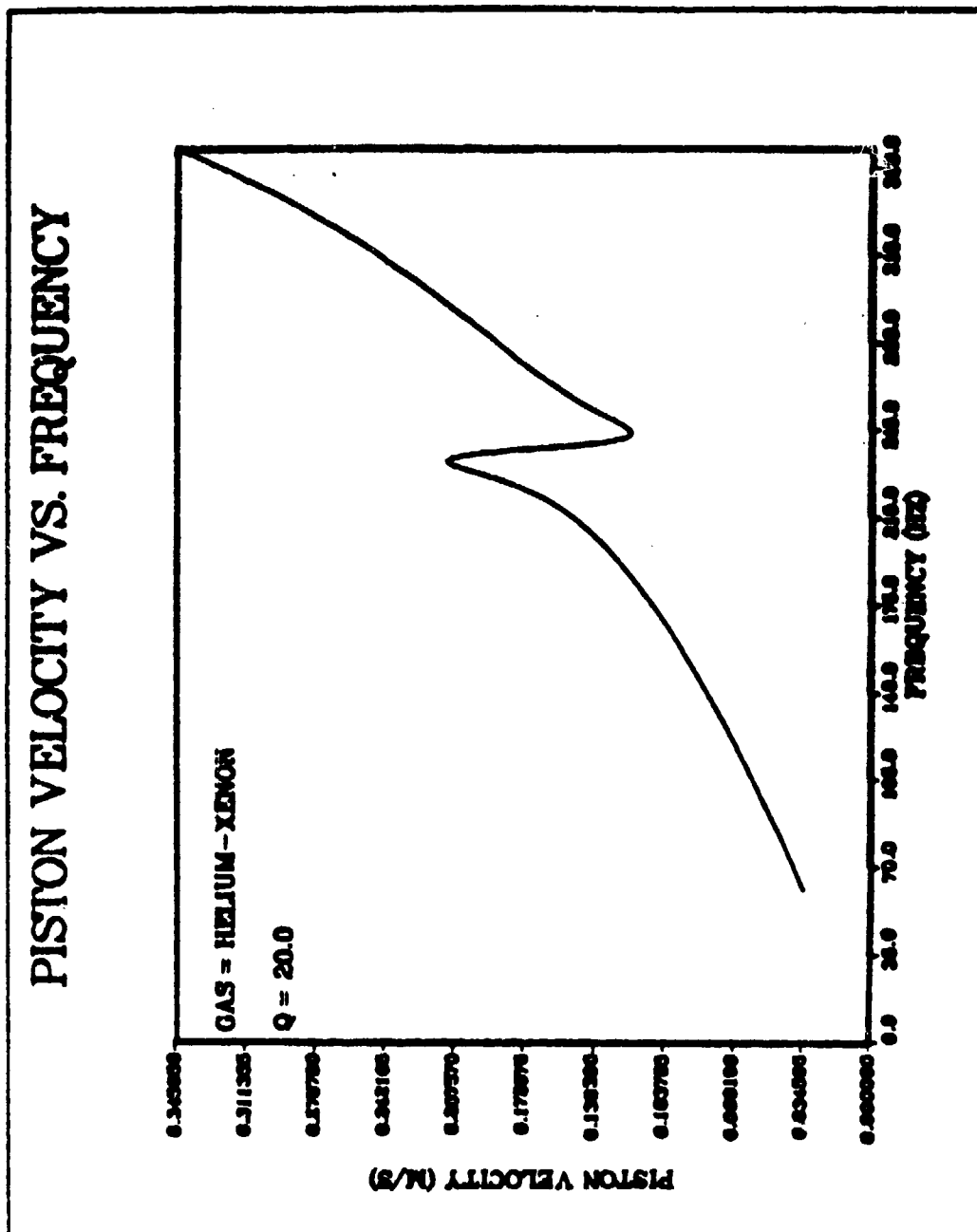
Figure IV-21. Computer Model Output for NIB with Helium-
Xenon (Bl = 15, Q = 20)--Piston Velocity
vs. Frequency for One Amp.
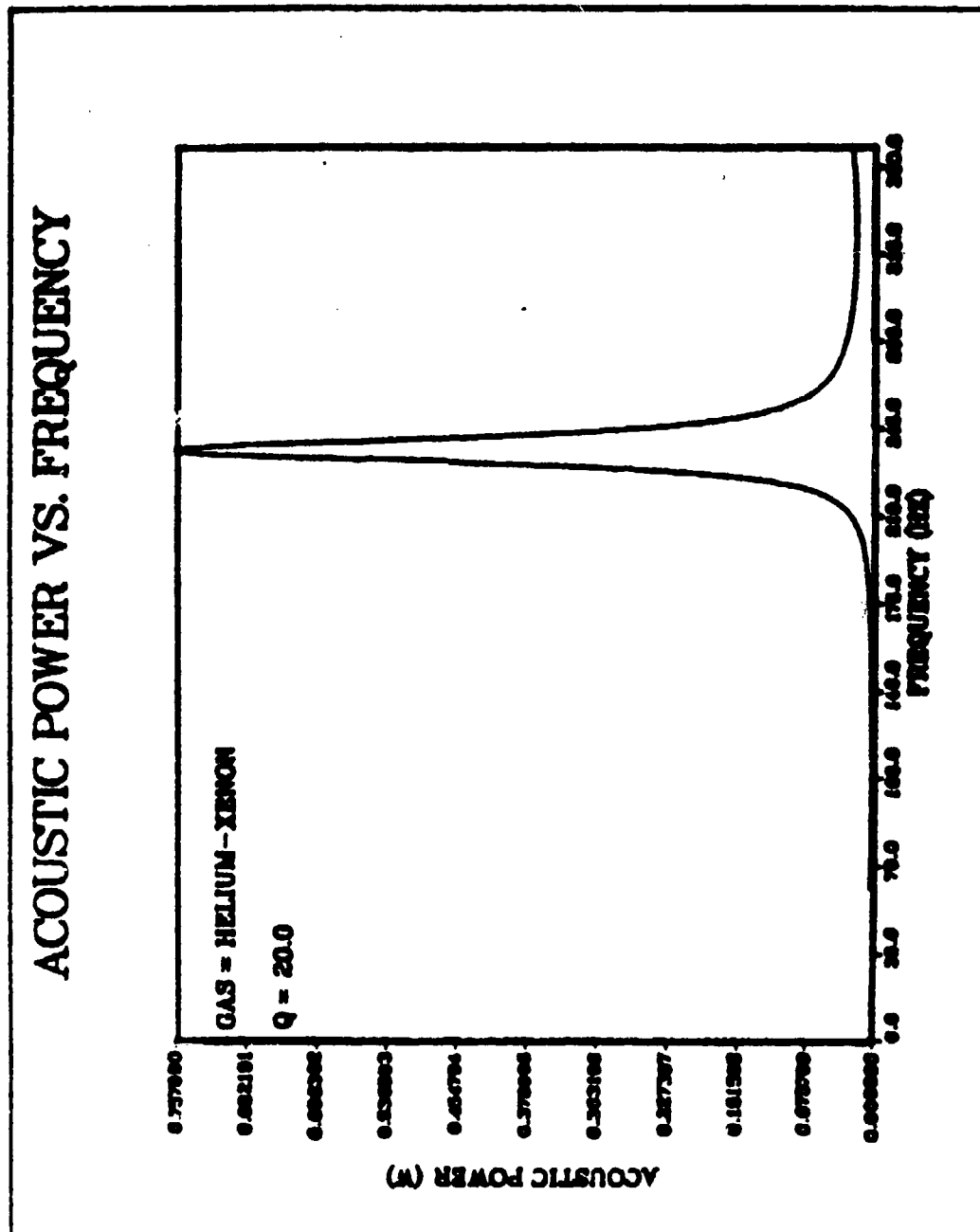
Figure IV-22. Computer Model Output for NIB with Helium-
Xenon (Bl = 15, Q = 20)--Acoustic Power
vs. Frequency for One Amp.

126
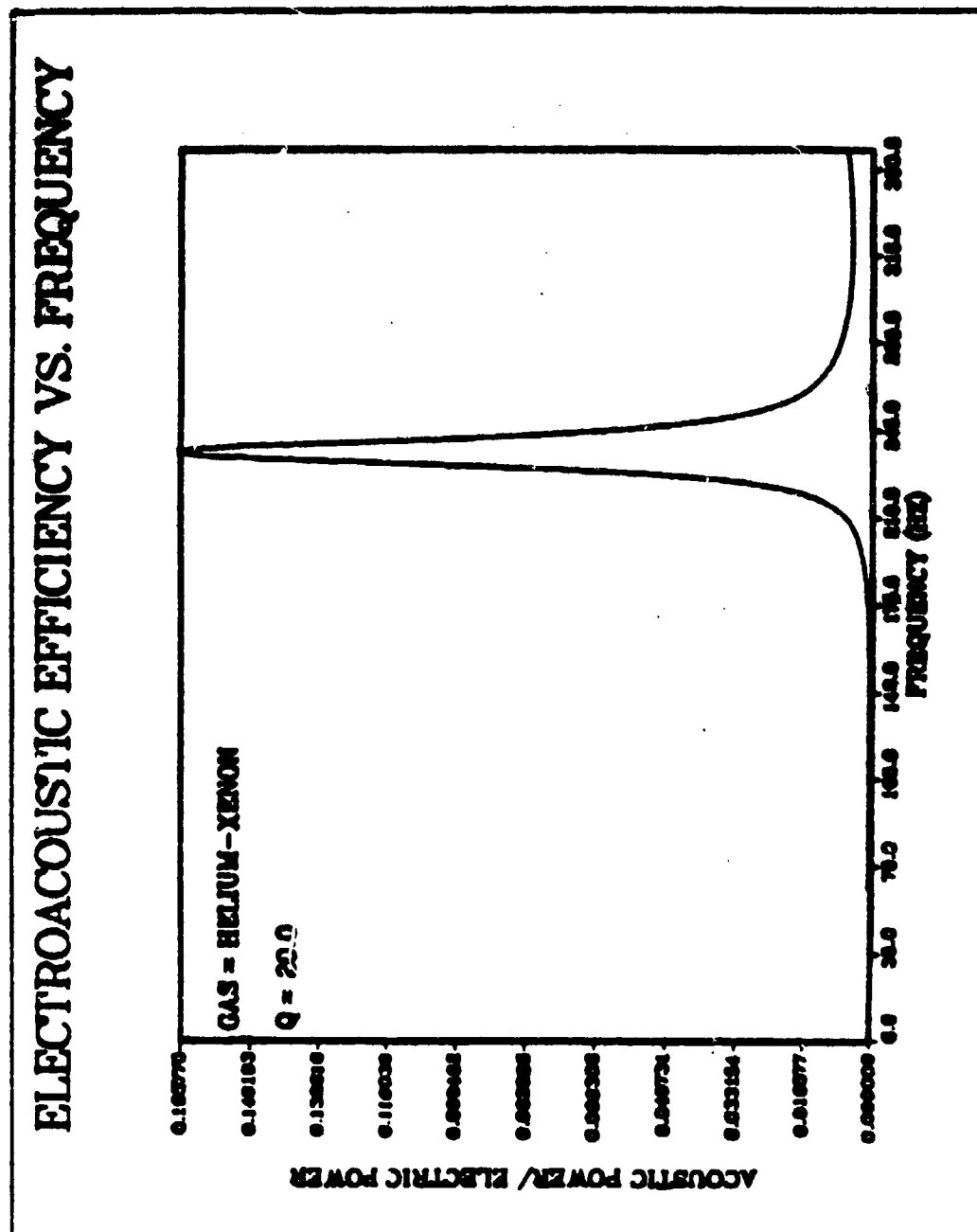
Figure IV-23. Computer Model Output for NIB with Helium-Xenon (Bl = 15, Q = 20)--Electroacoustic Efficiency vs. Frequency.

127

TABLE IV-5. COMPUTER MODEL RESULTS FOR NIB DRIVER--
PEAK ELECTROACOUSTIC EFFICIENCY (%)

Q	He (Bl=15)	He (Bl=19)	He-Xe (Bl=15)	He-Xe (Bl=19)
5			5.1	5.9
10	71.3	70.4	9.2	10.7
15	71.6	74.3	13.1	15.1
20	70.4	76.2	16.6	19.1
25			19.6	22.7
30			22.8	26.0

V. STAR DRIVER CONSTRUCTION

A. INTRODUCTION

This chapter describes the construction of the STAR driver. A large part of this thesis involved the design of the parts necessary to integrate the NIB driver with the resonator and GAS cannister, as illustrated in Figure I-4.

The major design work was for the driver housing. The requirements for the driver housing are:

1 - lightweight,

2 - strong (pressurized to 210 psi),

3 - interface to GAS canister lid (12 10-32 bolt holes centered at 9.5 inches diameter),

4 - interface with resonator (preferably interchangeable with earlier test resonators),

5 - helium leak-tight feed-through ports for electrical leads (driver electric power, accelerometer and microphone outputs), and

6 - hold NIB magnet structure securely.

Figure V-1 shows a cross-sectional drawing of the driver housing (not including any of the feed-through ports, which will be discussed later). Distinction between parts is shown by different hatching. Part A is the NIB magnet structure which was discussed in Chapter IV. Part B is the main body of the driver housing, machined out of 6061-T6 aluminum.

129
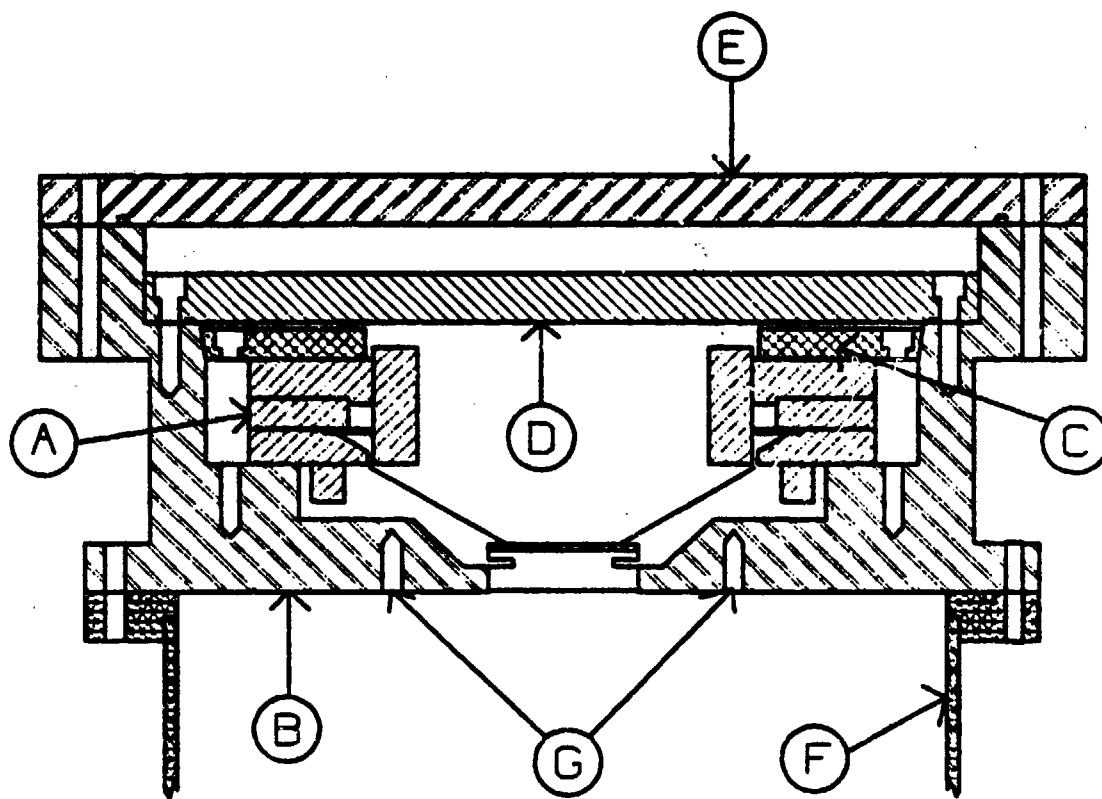
Figure V-1. Cross-sectional Schematic of the STAR Driver
Housing Showing (A) NIB Driver, (B) Driver
Housing Main Body, (C) Aluminum Pusher Plate,
(D) Pressure Lid, (E) Leak Test Lid,
(F) Resonator Vacuum Housing, and (G) Bolt
Holes for Interface with Resonator.

130

Part C is a 6061-T6 aluminum pusher plate used to hold the magnet structure securely in the body using six 10/32 bolts. Part D is the pressure lid, sealed a 1/16th inch diameter lead o-ring and held in place with six 10/32 bolts. Part E represents part of the leak test lid (see Figure C-1). When completed this will be replaced by the GAS can lid provided by NASA. The driver housing must match up with the GAS can lid's 9.5 inch diameter 10-32 bolt circle. Part F is the resonator section housing. The arrows labeled G point to the bolt holes which form the driver-resonator interface.

B. DESIGN CONSIDERATIONS

The driver-resonator system will be pressurized to ten atmospheres with a helium-xenon mixture (12.5% xenon). NASA's regulations say that it must be pressure tested to 1.5 times the operating pressure (NASA, 1986a), or 15 atmospheres ($=1.52X10^a$ Pa $=$ 220 psi). An added complication of working with helium (or helium mixtures) is that it diffuses through almost all materials except metals. As a result, we are not able to use rubber o-rings to seal metal parts together, but must use lead o-rings instead.

1. Electrical Feed-Throughs

NASA's regulations prohibit us from leaking gases into space, primarily to avoid contamination of other experiments and for the safety of the Shuttle and astronauts. This regulation is important not only for the major o-ring

seals, but also for the microphone and accelerometer outputs to the frequency control electronics (see Figure I-5), and connecting the audio amplifier to the driver. There are three individual wires and three co-axial connectors that must penetrate the driver housing without allowing leakage. The other housing penetrations are a DC pressure gage for the driver housing and a fill line from a helium-xenon bottle which will stabilize the pressure in the system against temperature changes in the environment and those generated by the refrigerator.

Based on prior experience in other applications, we decided that Emerson & Cuming's STYCAST‹TM› 2850FT epoxy (Canton, MA 02021) would be the best choice for providing the electrically insulating seal for the wires in the housing. STYCAST‹TM› 2850FT is a quartz-filled epoxy formulation with remarkably good over-all general properties. In addition to having excellent electrical grade insulation properties, good adhesion, and excellent resistance to chemicals and solvents, 2850FT has unusually high thermal conductivity and low thermal expansion. This combination of properties makes this epoxy valuable for applications where electrical insulation and mechanical protection must be maintained while coping with heat transfer considerations.

One definition for a sealed container is a helium leak rate of less than 10^{-4} standard cc's per second (NASA, 1986b). To test the epoxy we designed and built a test

fixture to be used with the Veeco MS-9 helium leak detector. A cross-sectional diagram of the test fixture is shown in Figure V-2. Part A is a copper tube with 1-1/8" outer diameter to interface with the leak detector. Soldered to the copper tube is a piece of solid brass stock about one inch thick (B) with a 0.052 inch diameter hole bored through the center. Epoxied into the hole is a 0.025 inch diameter bare copper wire (C). This design is motivated by the desire to provide as long a travel path and as small a cross-section as possible for the helium gas molecules. Part D is a hollow aluminum housing designed to hold pressurized helium. We decided that a rubber o-ring should hold the helium sufficiently well for a short term leak test. Part E is a 1/8" NPT (National Pipe Thread) hole for connecting to a helium fill line. A photograph of the test fixture with and without the housing is shown in Figure V-3.

The copper tube and brass stock were soldered together. We boiled the assembly to remove excess particulates and rinsed it with alcohol. We then etched the hole in the brass and the copper wire with nitric acid diluted with distilled water (about 20% acid) to provide a clean, rough surface for the epoxy. Before etching, cellophane tape was placed on the portion of the brass stock where the o-ring would be sealing (after making sure that the tape would not dissolve in the acid). We then rinsed the assembly with distilled water and dried it, mixed the epoxy, and inserted
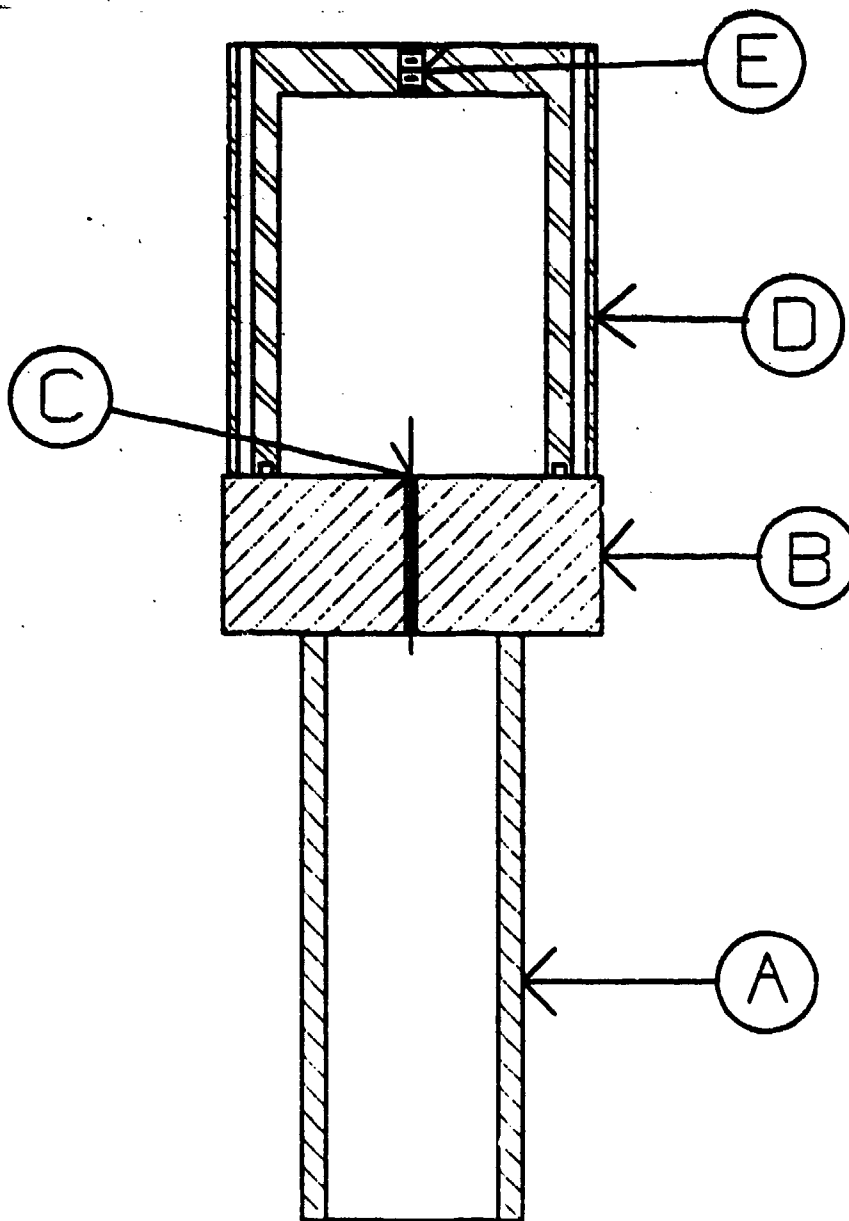
Figure V-2. Cross-sectional Schematic of the Helium
Leak Detector Test Fixture Showing
(A) Copper Tube for Leak Detector Interface,
(B) Solid Brass Stock, (C) Bare Copper Wire,
(D) Aluminum Housing, and (E) Connection for
Helium Fill Line.

Figure V-3. Photograph of the Helium Leak Detector Test Fixture.

the wire into the hole in the brass stock, making sure the epoxy filled the gap.

The following procedure was used to run the leak detector tests: first zero the meter, then do a test run on the sensitivity calibrator. The sensitivity calibrator used was a Veeco type SC-4 serial number 3179 with a leak rate of 6.5×10^{-8} std cc/sec (standard cubic centimeters per second). We would then remove the calibrator, recheck the meter for zero, attach the test fixture, read the meter, remove the fixture, and recheck for zero.

The test fixture was initially pressurized to 115 psi with helium. We tried to test it immediately but found that the detector would not draw enough of a vacuum to check for helium. We thought that there might be outgassing from flux or something in the tube. So we pulled a vacuum on the tube overnight and the next day it worked fine. We tested the fixture on the first, third, and sixth days after it had been pressurized. The numerical results are listed in Table V·1. Even after we had waited six days for the helium to diffuse through the epoxy, the fixture leakage rate was an order of magnitude less than the calibrator. The leakage rate was therefore four orders of magnitude less than that allowed by NASA to be considered leak-tight (1×10^{-4} std cc/sec). After the third leak test we checked the pressure in the aluminum chamber and found it to be within a few percent of the original pressure. We therefore concluded

that the bare wire-epoxy method with a length/diameter ratio of about 20 could be used for the driver housing penetrating electrical feed-throughs.

TABLE V-1. HELIUM LEAK DETECTOR TEST RESULTS
ON COPPER WIRE-EPOXY FIXTURE.

Number days after pressurization	null meter reading	calibrator reading	copper wire feed -through reading
1	0	1.1	0.02
3	0	1.2	0.08
6	0	1.1	0.10

Figure V-4 shows a close-up of the feed-through plug for the wire leads. It will house a total of five wires (with space available for a sixth if necessary). Two of the leads will be for the voltage supply to the voice coil. These leads will consist of bare copper wires epoxied into the small holes seen in the figure. Each wire will then be soldered to a 6/32 phillip-head screw with a 1-72 blind-tapped hole in it. The screw will be glued into an 8/32 hole, forming a mechanically stable, demountable, electrical terminal. The accelerometer and microphone leads will also have bare copper wire epoxied into the small hole, and will then be connected to Microdot(TM) coaxial fittings (Malco

137
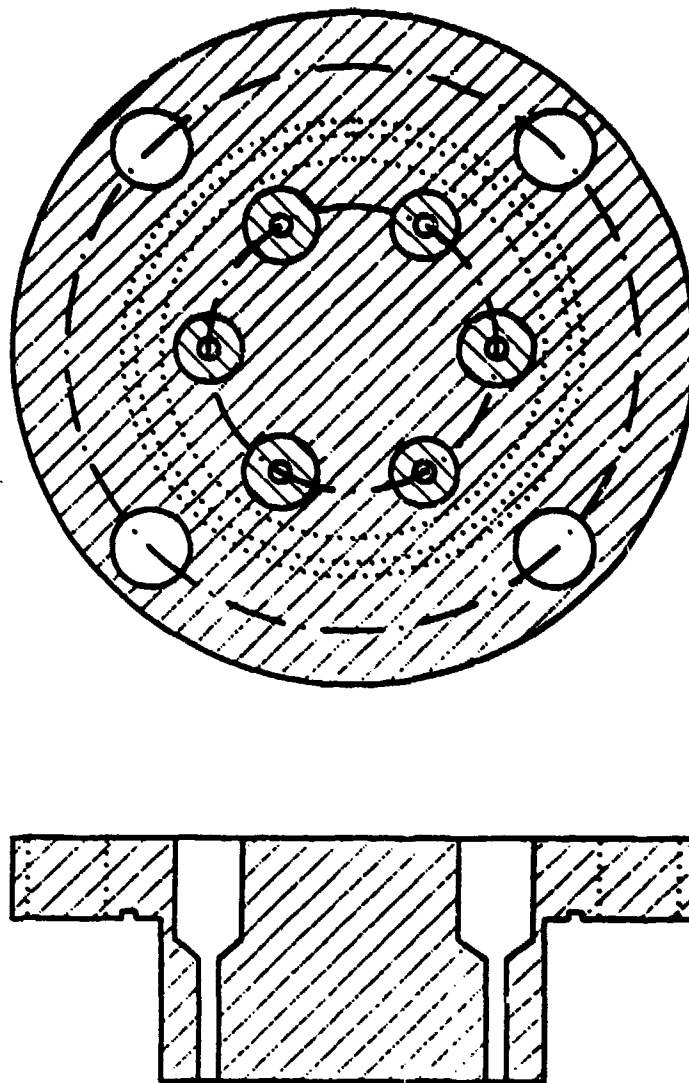
Figure V-4.   Driver Housing Feed-Through Plug
              for the Electrical Leads.

138

part number 031-0001-0001, South Passadena, CA 91030).
Figure V-5 shows an example of each of these leads.

2. **Measurement Devices**

The microphone and accelerometer used by STAR are similar to those used by Hofler (1986 and 1988). In fact, the resonator end of the driver housing was designed to accept Hofler's resonator, calibration volume, and instrumentation for testing. The microphone used to measure the acoustic pressure in the resonator is a small quartz-crystal (Valpey-Fisher, Hopkinton, MA 01748) or PZT dynamic pressure transducer (Piezoelectric Products lot number 4-9-84, FO13184, Metuchen, NJ). It is mounted in the driver housing where the housing connects to the resonator flange. The microphone will be calibrated by comparison to a standard transducer, which will have been previously calibrated via a reciprocity technique. The microphone will be connected to a miniature FET follower circuit. The FET buffer (Eletec model 304 impedance converter, Daytona Beach, FL 32020) converts the microphone's high impedance output signal to a low impedance to reduce sensitivity to electrical noise and maintain the output voltage and phase while driving the cables necessary to reach the signal processing electronics. The buffer's DC power supply and output cables are completely shielded through the driver housing to the buffer (see Figures C-3 and C-7 for location of microphone and FET in driver housing).
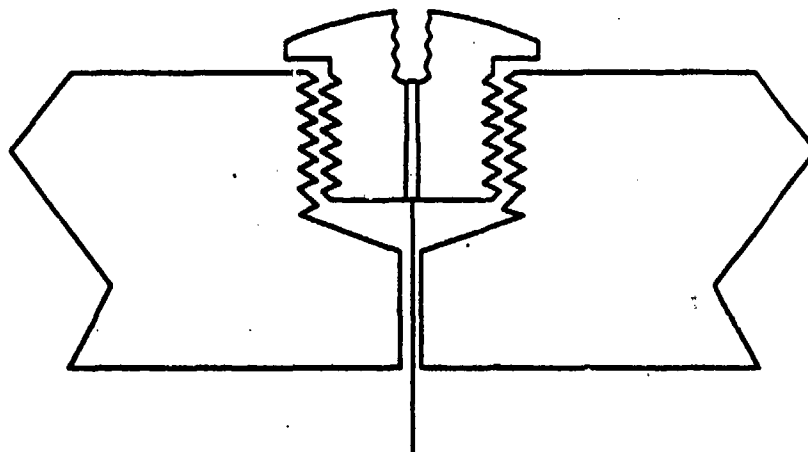
(a)
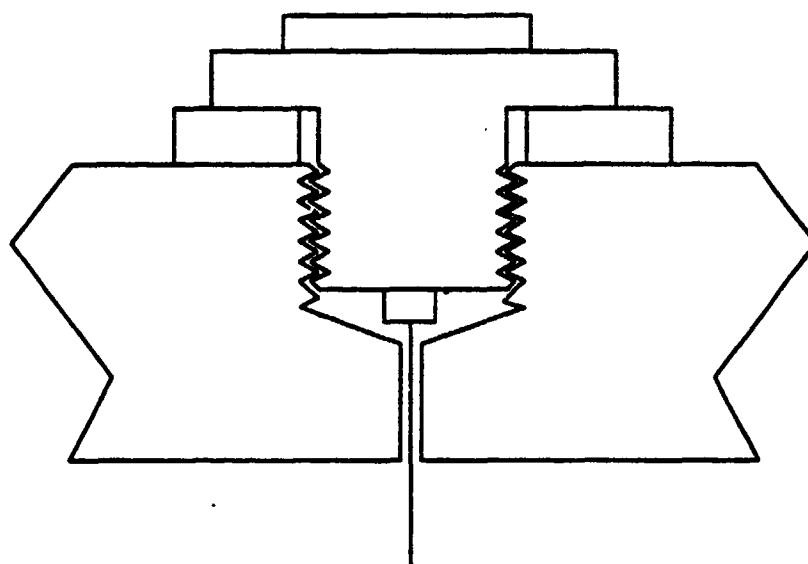
(b)

Figure V-5.   Example of Wire Lead Connectors
             for Feed-Through Plug: (a) Single
             Wire and (b) Co-axial Cable.

140

The Endevco model 22 Picomin^(TM) accelerometer is attached to the side of the bellows stiffener facing the driver. The integrated accelerometer signal will be used as a measure of the bellows velocity, which will be calibrated by driving a small cavity of calculable acoustic impedance. Thus the product of the outputs from the microphone and integrated accelerometer can be combined to yield the acoustic power and their relative phase can be used to keep the driver frequency at the tube resonance. The operation of the refrigerator at resonance is essential both to optimize the acoustic power delivered to the "stack" and to guarantee that the "stack" is always located at the proper position in the standing wave as discussed in Sub-section II.A.4.

The DC pressure transducer is an Omega^(TM) PX-80 designed for high pressure applications requiring long-term stability. Figure V-6 shows a drawing of the pressure transducer and its driver housing fitting.

The helium port in the housing is provided to empty and fill the driver and resonator and so that a stable pressure may be maintained in the driver and resonator through the ballast volume provided by the reservoir (see Figure I-4).

There is a 1/32 inch diameter hole filled with a ten thousandths inch inner diameter half inch long capillary in the driver housing where it connects to the resonator. The function of the capillary is to equilibriate the static

141
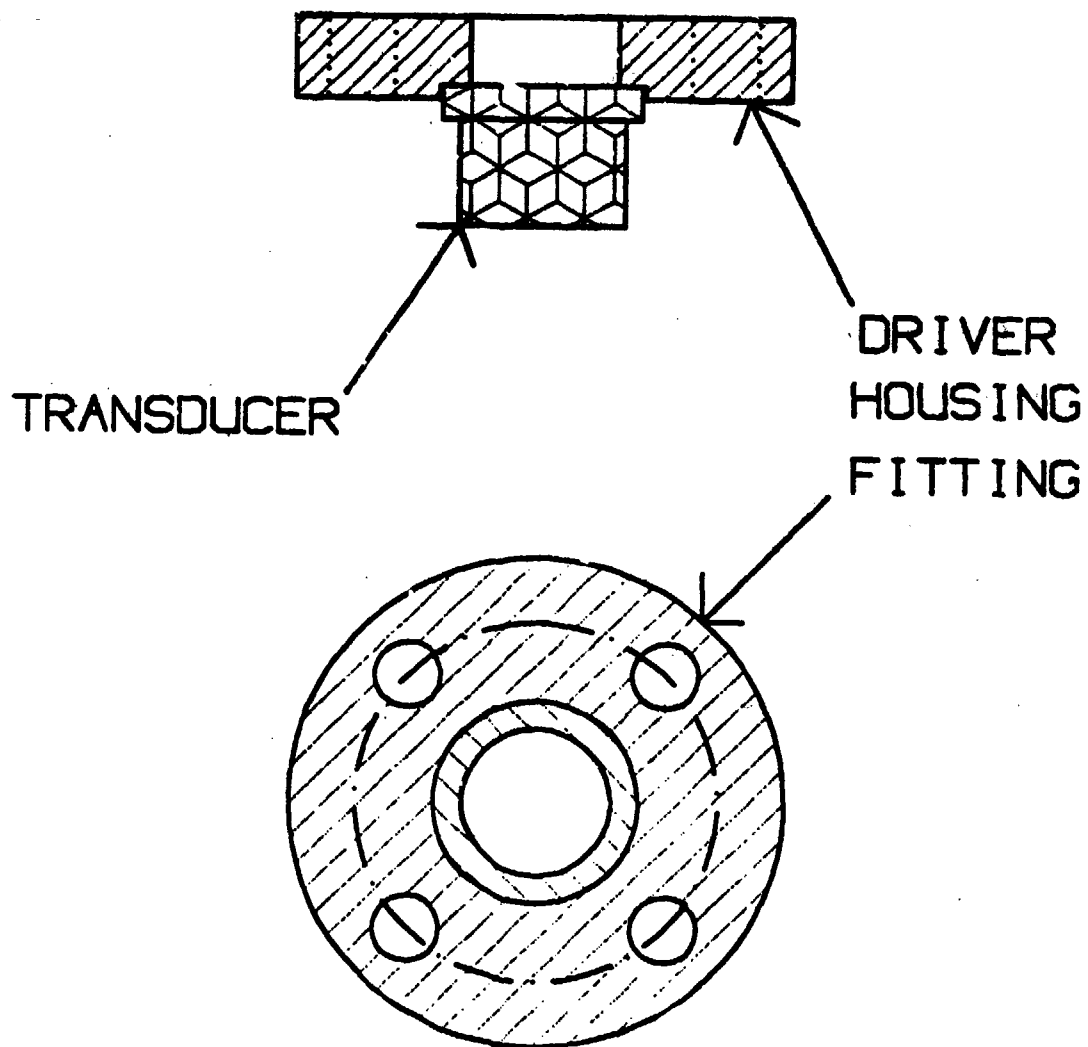
Figure V-6. DC Pressure Transducer and Driver
            Housing Plug Fitting.

pressure between the driver and resonator during filling and non-operating times while maintaining a pressure seal at acoustic operating frequencies.

A complete set of dimensioned drawings for the driver housing and its auxiliary equipment is given in Appendix C. A list of materials for the driver portion of the STAR is given in Appendix D.

VI.   CONCLUSION AND RECOMMENDATIONS

The objective of the STAR project is to test and space qualify a new continuous cycle cryogenic refrigeration system for cooling of sensors and electronics which is based upon the newly-discovered thermoacoustic heat pumping effect. The new refrigerator has no sliding seals, a cycle frequency of about 300 Hz, and uses acoustic resonance to enhance overall efficiency. This thesis is concerned specifically with the design and testing of the electrodynamic transducer which is responsible for the electro-acoustic power conversion. A computer model of the driver/resonator system was presented along with the techniques for measurement of the electrical and mechanical parameters used as input for the model.

A final driver design (including dimensional drawings) utilizing a modified JBL 2450J neodymium-iron-boron compression driver and associated leak-tight electrical feed-throughs, microphone, accelerometer, pressure gage, pressure housing, and resonator interface is provided.

Since we only received the NIB driver in late December 1987, there wasn't time to perform enough parameter measurements to obtain accurate values for the suspension stiffness (k) and transduction coefficient (Bl). The next

144

group of students should find these values for use in the model and efficiency calculations.

The resonator experiments (not reported here) indicate that Helium-Xenon may be the preferred gas mixture for the STAR. If this is the case, the NIB driver resonant frequency will have to be lowered for it to match the operating (resonant) frequency of the resonator. This could be accomplished by adding moving mass to the voice coil-reducer-bellows assembly, but that would decrease the velocity and lower the electroacoustic efficiency. The preferred option for driver resonance adjustment is to decrease the suspension stiffness by cutting away part of the surround (see Section III.H). Since the NIB voice coil has a titanium surround and diaphragm this operation will have to be performed carefully. The titanium diaphragm (dome) will also have to be removed. (The dome's function is performed by the reducer and bellows.)

The task for the next group of students is to assemble the NIB driver with its housing and accessories (feed-throughs, microphone, accelerometer, etc.) and perform efficiency measurements on the ground similar to those that will be performed in space. This series of measurements will closely resemble those performed on the Altec 290-16K driver as described in Chapter III.

APPENDIX A. COMPUTER MODEL CALCULATION PROGRAM

PROGRAM FRIDGE

```
C INTRODUCTION:
C
C      THE PURPOSE OF THIS PROGRAM WRITTEN BY LT.  MICHAEL P.
C SUSALLA  IS  TO  CALCULATE THE DATA POINTS  AND  PLOT  THE
C PERFORMANCE  CHARACTERISTICS  OF A CONCEPTUAL MODEL  OF  A
C THERMOACOUSTIC HEAT ENGINE. THE COMMENTS INCORPORATED INTO
C THIS PROGRAM AND THE COMMENTS INCORPORATED IN THE PLOTTING
C PROGRAM "GRAFRI FORTRAN A1",  WILL ALLOW THE USER TO  PRO-
C DUCE  FOUR GRAPHICAL PLOTS WHICH WILL CLOSELY  APPROXIMATE
C THE PERFORMANCE OF AN ACTUAL THERMOACOUSTIC HEAT ENGINE.
C      THE  GOAL  OF THE PROGRAM/SIMULATION IS TO  ALLOW  THE
C OPERATOR  TO VARY DIFFERENT PARAMETERS TO ACHIEVE WHAT  IS
C BELIEVED  TO  BE  AN OPTIMUM CONDITION WHERE  THE  ENGINES
C DRIVER RESONANCE IS MATCHED WITH THE TUBE RESONANCE.
C
C GENERAL INSTRUCTIONS:
C
C      THIS PROGRAM IS SET UP TO PROVIDE FOUR PLOTS:  VOLTAGE
C VERSUS FREQUENCY, PISTON VELOCITY VERSUS FREQUENCY,  ACOUS-
C TIC POWER VERSUS FREQUENCY, AND ELECTROACOUSTIC EFFICIENCY
C VERSUS  FREQUENCY.  IN GENERAL THE PROGRAM HAS HARD  INPUT
C DATA  SUCH  THAT ALL YOU MUST DO TO GET A SET OF PLOTS  IS
C COMPILE "GRAFRI FORTRAN A1" IN FORTVS AND THEN RUN "FRIDGE
C FORTRAN A1" IN WF77 FROM FLIST ON THE NPS MAINFRAME  USING
C A TEKTRONICS 618 TERMINAL. THIS ACTION WILL GIVE YOU A SET
C OF PLOTS FOR THE INPUT DATA. TO TRY OTHER DATA YOU MUST GO
C TO  XEDIT ON THE "FRIDGE FORTRAN A1" PROGRAM AND VARY  THE
C INPUT DATA.  AS LONG AS YOUR CHANGES ARE RESTRICTED TO THE
C "FRIDGE"  PROGRAM THE ONLY ACTION NECESSARY TO PRODUCE NEW
C PLOTS IS TO RUN THE PROGRAM IN WF77. IF YOU FIND IT NECES-
C SARY TO CHANGE THE PLOTTING PROGRAM,  "GRAFRI",  FOR WHAT-
C EVER REASON,  IT MUST BE RECOMPILED IN FORTVS PRIOR TO THE
C NEXT  ATTEMPT TO PLOT OR THE CHANGES WILL NOT BE  SEEN  BY
C THE MACHINE.
C
C INPUT SECTION:
C      A.   DEFINITION OF VARIABLES:
C           ALL OF THE VARIABLES HAVE BEEN ESTABLISHED AS REAL
C OR  COMPLEX  QUANTITIES BASED ON THE REQUIREMENTS  OF  THE
C ARITHMETIC  ALGORITHOM OF THE CONCEPTUAL MODEL..   EACH  OF
C THE VARIABLES WILL NOW BE DEFINED.
C      LCOIL=THE IMAGINARY PART OF THE IMPEDANCE OF THE VOICE
C COIL OF THE DRIVER, AND IS CALCULATED TO BE W*LE.
C      K=THE  PROPAGATION  CONSTANT OF THE WAVES IN THE  TUBE
C AND IS GIVEN BY W/C.
```

```
C        IMZM=THE IMAGINARY PART OF THE MECHANICAL IMPEDANCE OF
C THE TUBE/DRIVER COMBINATION.  IT IS GIVEN BY A RATHER LONG
C AND COMPLEX EQUATION IN THE CALCULATION SECTION OF THE
C PROGRAM.
C        MAGU=THE  MAGNITUDE OF THE COMPLEX  QUANTITY  "U",  IN
C METERS/SEC.
C        IMZT=THE  IMAGINARY PART OF THE TUBE MECHANICAL  IMPE-
C DANCE AND IS GIVEN BY SUBTRACTING THE DRIVER PORTIONS FROM
C IMZM.
C        M=THE MOVING MASS OF THE SYSTEM, AND IS THE SUM OF THE
C VOICE  COIL  AND THE DIAPHRAGM MASSES OF  THE  DRIVER,  IN
C KILOGRAMS.
C        L=THE LENGTH OF THE TUBE IN METERS.
C        LE=THE INDUCTANCE OF THE VOICE COIL, IN HENRYS.
C        I=THE INPUT CURRENT FROM THE SOURCE, IN AMPS.
C        MAGV=THE  MAGNITUDE  OF THE COMPLEX QUANTITY  "V",  IN
C VOLTS.
C        ZM=THE MECHANICAL IMPEDANCE OF THE TUBE/DRIVER SYSTEM,
C AND IT IS MADE UP OF THE REAL PART,  REZM,  AND THE IMAGI-
C NARY PART, IMZM.
C        ZE=THE  ELECTRICAL EQUIVALENT OF THE MECHANICAL  IMPE-
C DANCE OF THE TUBE/DRIVER SYSTEM.  IT IS GIVEN BY TRANSFOR-
C MING  ZM ACROSS A TRANSFORMER USING THE BL COEFFICIENT  OF
C THE DRIVER.
C        ZCOIL=THE  COMPLEX ELECTRICAL IMPEDANCE OF  THE  VOICE
C COIL.
C        ZTOT=THE  TOTAL  ELECTRICAL IMPEDANCE OF  THE  SYSTEM,
C COMPLEX.
C        V=THE  COMPLEX  VOLTAGE  OF THE SOURCE  NECESSSARY  TO
C PRODUCE THE SELECTED INPUT CURRENT.
C        U=THE  VELOCITY  OF  THE  PISTON,(DIAPHRAGM),  OF  THE
C DRIVER IN M/S.
C        ZTUBE=THE  COMPLEX  MECHANICAL IMPEDANCE OF  THE  TUBE
C ITSELF.
C        P=THE COMPLEX PRESSURE OF THE SYSTEM, IN NEWTONS/M**2.
C        PI=A  CONSTANT  FOR CONVERSIONS TO  AND  FROM  ANGULAR
C UNITS.
C        RM=THE MECHANICAL RESISTANCE OF THE MOVING MASS OF THE
C SYSTEM.
C        SSUP=THE MECHANICAL STIFFNESS OF THE SYSTEM DUE TO THE
C DRIVER SUSPENSION.
C        RHO=THE  DENSITY OF THE GAS IN THE TUBE AT A SPECIFIED
C MEAN TEMPERATURE.
C        C=THE  SPEED  OF  SOUND  FOR  THE  SPECIFIED  GAS  AND
C TEMPERATURE.
C        S=THE CROSS SECTIONAL AREA OF THE TUBE.
C        BL=A  COEFFICIENT OF THE DRIVER THAT IS BASED  ON  THE
C STEADY  AIR GAP FLUX DENSITY OF THE DRIVER AND THE  LENGTH
C OF ITS VOICE COIL.
C        G=THE QUALITY FACTOR OF THE TUBE.
C        FO=THE RESONANCE FREQUENCY OF THE TUBE.
C        A=THE  CROSS SECTIONAL AREA OF THE BACK VOLUME OF  THE
```

147

```
C DRIVER.
C      VOL=THE VOLUME OF THE BACK VOLUME OF THE DRIVER.
C      RG=THE INTERNAL ELECTRICAL RESISTANCE OF THE POWER
C SOURCE.
C      RE=THE ELECTRICAL RESISTANCE OF THE VOICE COIL.
C      SVOL=THE MECHANICAL STIFFNESS OF THE SYSTEM DUE THE
C BACK VOLUME OF THE DRIVER.
C      WO=THE RESONANCE FREQUENCY OF THE TUBE IN ANGULAR
C UNITS, RAD/SEC.
C      ALPHA=A CHARACTERISTIC QUANTITY OF THE TUBE THAT IS A
C FUNCTION OF THE RESONANT FREQUENCY, THE Q AND THE SPEED OF
C SOUND.
C      F=FREQUENCY, IN HERTZ.
C      W=THE FREQUENCY CONVERTED TO RAD/SEC.
C      FORCE=THE FORCE ON THE MOVING MASS DUE TO THE INTER-
C ACTION OF THE VOICE COIL MAGNETIC FIELD AND THE DRIVER
C MAGNET.
C      REZT=THE REAL PART OF THE COMPLEX MECHANICAL TUBE
C IMPEDANCE.
C      PU=THE PRESSURE TIMES THE VOLUME VELOCITY, ACOUSTIC
C POWER.
C      PWR=THE ELECTRICAL POWER NECESSARY TO DRIVE THE SYSTEM
C AT THE SPECIFIED INPUT CURRENT.
C      PUPWR=A POWER RATIO, ACOUSTIC TO ELECTRICAL. AN EFFI-
C CIENCY.
C
C      B.DATA DESCRIPTION.
C         FOR THE SELECTED INPUT DATA THAT IS HARD INPUT THE
C FOLLOWING VALUES WERE EMPIRICALLY DETERMINED: M, L, Q, FO,
C A, VOL, BL, S, SSUP, AND RE. RHO AND C WERE SELECTED FOR
C HELIUM GAS AT 10 ATMOSPHERES AND A MEAN TEMPERATURE OF 300
C DEGREES KELVIN. RM WAS CALCULATED FROM A THEORETICAL
C EQUATION USING RHO,C S AND THE DRIVER RESONANT FREQUENCY.
C RG WAS SET TO ZERO TO MODEL AN IDEAL POWER SOURCE. LE WAS
C SET TO ZERO FOR EASE OF CALCULATION, BUT WAS TESTED DURING
C RUNNING TO VERIFY THAT IT HAD LITTLE IF ANY EFFECT WHEN
C INCLUDED. A CURRENT, I, OF ONE AMPERE WAS SELECTED FOR
C EASE OF ANALYSIS.
C      SINCE YOU MAY WANT TO CHANGE MY INPUT DATA I WILL PUT
C A COPY IN THE COMMENTS SO THAT YOU CAN RETURN TO IT IF
C DESIRED. MY ANALYSIS HAS SHOWN THE BEST BACK VOLUME TO BE
C 9.50E-8, AND THE BEST RM TO BE 1.535 KG/S. THIS VALUE FOR
C RM WAS DETERMINED AFTER REVIEW OF PLOTS SHOWED HIGHER THAN
C EXPECTED VOLTAGES AND IT WAS DETERMINED BY MEASUREMENT IN
C THE LABORATORY.
C
C
C      DATA RM,M,SSUP,RHO,C/3.53E-3,0.0045,2.6E4,1.68,1000/
C      DATA S,BL,Q,FO,A/1.521E-3,8,15,800,7.13E-5/
C      DATA VOL,RG,LE,RE,I,L/2.715E-6,0,0,8,1,0.625/
```

```fortran
      REAL LCOIL,K,IMZM,MAGU,IMZT,M,L,LE,I,MAGV
      COMPLEX ZM,ZE,ZCOIL,ZTOT,V,U,ZTUBE,P
      PI=3.141592654
      DATA RM,M,SSUP,RHO,C/3.53E-3,0.0045,2.6E4,1.68,1 )0/
      DATA S,BL,Q,FO,A/1.521E-3,8,15,800,7.13E-5/
      DATA VOL,RG,LE,RE,I,L/2.715E-6,0,0,8,1,0.625/
      SVOL=(A*A*RHO*C*C)/VOL
      WO=2*PI*FO
      ALPHA=WO/(2*Q*C)


C CALCULATION SECTION:
C     THE  NEXT SIX LINES CREATE AN OUTPUT FILE FOR THE DATA
C THAT IS NECESSARY TO PRODUCE THE DESIRED PLOTS, AND PLACES
C HEADINGS ON THE DATA AS APPROPRIATE.


      OPEN(UNIT=69,FILE='FRIDGE OUTPUT A1',IOSTAT=IOS)
      WRITE(69,*)'     MASS          VOLUME'
      WRITE(69,1)M,VOL
      WRITE(69,*)'   FREQUENCY      PIST VEL  PRESS*PIST VEL  PWR RATIO
     *     VOLTAGE'
    1 FORMAT(E13.4,E13.4)


C     THE FOLLOWING DO LOOP PROVIDES FOR THE CALCULATION  OF
C THREE  HUNDRED DATA POINTS FOR EACH OF THE DESIRED  PLOTS,
C USING  A FREQUENCY RANGE OF ONE QUARTER TUBE RESONANCE  TO
C THREE HALVES TUBE RESONANCE.


      DO 10 J=1,300
      F=(FO/4)+((J-1)*(FO/240))


C     THE  NEXT  THREE LINES CALCULATE  VARIOUS  QUANTITIES,
C EXPLAINED ABOVE,  THAT ARE FUNCTIONS OF FREQUENCY, FOR USE
C IN FUTURE CALCULATIONS.


      W=2*PI*F
      K=W/C
      LCOIL=W*LE


C      THE  NEXT NINE LINES CALCULATE THE REAL AND  IMAGINARY
C PARTS  OF THE TUBE/DRIVER MECHANICAL IMPEDANCE AND COMBINE
C THEM INTO A COMPLEX QUANTITY, ZM.


      REZM=RM+(((RHO*C*S*ALPHA*COS(K*L)*SIN(K*L))+(K*RHO*C*S
     *   *SINH(ALPHA*L)*COSH(ALPHA*L)))/(K*(1+(ALPHA/K)**2)*((((
```

```
      *      SIN(K*L))**2)*((COSH(ALPHA*L))**2))+(((COS(K*L))**2)*((
      *      SINH(ALPHA*L))**2)))))
             IMZM=(W*M)-(SSUP/W)-(SVOL/W)+(((RHO*C*S*ALPHA*SINH(ALPHA*L)
      *      *COSH(ALPHA*L))-(K*RHO*C*S*COS(K*L)*SIN(K*L)))/(K*(1+(ALPHA
      *      /K)**2)*((((SIN(K*L))**2)*((COSH(ALPHA*L))**2))+(((COS(K*L))-
      *      **2)*((SINH(ALPHA*L))**2)))))
             ZM=CMPLX(REZM,IMZM)


C      THE   NEXT   THREE   LINES CONVERT ZM   TO   AN   ELECTRICAL
C QUANTITY AND THEN COMBINE ALL OF THE ELECTRICAL IMPEDANCES
C TO GET A TOTAL IMPEDANCE.


             ZE=(BL**2)/ZM
             ZCOIL=CMPLX(RE,LCOIL)
             ZTOT=RG+ZCOIL+ZE


C      THE   NEXT   SIXTEEN   LINES CALCULATE THE VALUES   TO   BE
C PLOTTED,  AND PUT THEM IN THE OUTPUT FILE,  AND THEN CLOSE
C THE FILE.


             V=I*ZTOT
             FORCE=BL*I
             U=FORCE/ZM
             MAGU=CABS(U)
             REZT=REZM-RM
             IMZT=IMZM-(W*M)+(SSUP/W)+(SVOL/W)
             ZTUBE=CMPLX(REZT,IMZT)
             P=(ZTUBE*U)/S
             PU=0.5*(REAL(P*CONJG(U))*S)
             PWR=0.5*(REAL(I*CONJG(V)))
             PUPWR=PU/PWR
             MAGV=CABS(V)
             WRITE(69,100)F,MAGU,PU,PUPWR,MAGV
100          FORMAT(E13.5,E13.5,E13.5,E13.5,E13.5)
  10 CONTINUE
    CLOSE(69)


C PLOTTING SECTION:
C      THE NEXT TWO LINES INTERFACE WITH MY PLOTTING PROGRAM,
C "GRAFRI FROTRAN A1",  AND THE DISSPLA ROUTINE TO PLOT  THE
C DATA.


    PAUSE 'PRESS ENTER TO START PLOTTING ROUTINE'
     CALL EXCMS('EXEC DISSPLA GRAFRI')
     STOP
     END
```

150

APPENDIX B.   COMPUTER MODEL GRAPH PROGRAM

```
    PROGRAM GRAFRI

C       THIS IS LT.  MICHAEL P. SUSALLA'S PLOTTING PROGRAM FOR
C USE  IN CONJUNCTION WITH "FRIDGE FORTRAN A1" IN "THE THER-
C MOACOUSTIC HEAT ENGINE SIMULALTION".  THIS PROGRAM MUST BE
C COMPILED IN FORTVS PRIOR TO RUNNING "FRIDGE FORTRAN A1" IN
C WF77.THIS PROGRAM IS FOR USE IN DISSPLA AND CALLS  VARIOUS
C DISSPLA  SUBROUTINES.   THESE VARIOUS SUBROUTINES ARE USED
C MORE  THAN ONCE IN THE PROGRAM BUT WILL ONLY BE  DESCRIBED
C ONCE EACH.   IN ORDER TO USE DISSPLA YOU MUST HAVE  ARRAYS
C OF  DATA POINTS TO BE PLOTTED.   MY ARRAYS ARE ALL  DIMEN-
C SIONED  TO 300 POINTS SINCE THAT IS THE NUMBER  CALCULATED
C BY  "FRIDGE FORTRAN A1".   YOU SHOULD BE AWARE THAT IF YOU
C CHANGE  THE  NUMBER OF POINTS TO BE  CALCULATED,  AND  THE
C NUMBER  IS  GREATER THAN 300,  YOU  MUST  REDIMENSION  THE
C ARRAYS.   TWO CHARACTER STRINGS ARE USED IN THIS  PROGRAM.
C NEW1$  IS  USED IN RENAMING FILES TO THE FORMAT  NECESSARY
C FOR DISSPLA,  AND DUMMY$ IS USED TO READ THE HEADINGS  OUT
C OF THE DATA FILE.  ALL OF THE DATA TO BE PLOTTED IS IN THE
C FORM  OF  REAL NUMBERS,  SO ALL OF THE VARIABLES ARE  MADE
C REAL.  D IS USED FOR THE FREQUENCY DATA, G IS USED FOR THE
C PISTON  VELOCITY DATA,  H IS USED FOR THE  ACOUSTIC  POWER
C DATA,  O  IS USED FOR THE ELECTROACOUSTIC EFFICIENCY  DATA
C AND,  T  IS USED FOR THE VOLTAGE DATA.   THE XMAX AND YMAX
C VARIABLES  ARE INITIALIZED TO ZERO AND ARE USED TO  CALCU-
C LATE  THE MAX VALUE OF EACH OF THE PARAMETERS AS THEY  ARE
C READ INTO THE ARRAYS.  THIS COMPLETES THE INTRODUCTION AND
C EXPLAINS THE FIRST FIVE LINES OF THE PROGRAM.



        DIMENSION D(300),G(300),H(300),O(300),T(300)
        CHARACTER*80 NEW1$,DUMMY$
        REAL D,G,H,O,T,M
        DATA XMAX,YMAX1,YMAX2,YMAX3,YMAX4/0.,0.,0.,0.,0./


C       THE  NEXT  SEVEN LINES OF THE PROGRAM RENAME  MY  DATA
C FILE TO THE FORMAT NECESSARY FOR USE IN DISSPLA,  OPEN THE
C FILE,  READ THE MASS AND VOLUME OUT OF THE FILE AND,  READ
C THE HEADINGS OUT OF THE FILE.


        NEW1$='RENAME '//' FRIDGE OUTPUT A1'//' FILE XYZ1 A1'
        CALL EXCMS(NEW1$)
        OPEN (69,FILE='XYZ1')
        READ (69,'(A80)') DUMMY$
```

```
      READ (69,1)M,VOL
      READ (69,'(A80)') DUMMY$
    1 FORMAT (E13.4,E13.4)


C        THE FOLLOWING DO LOOP READS THE PLOTTING DATA INTO THE
C ABOVE SPECIFIED ARRAYS FOR USE IN THE DISSPLA SUBROUTINES,
C AND   ALSO   CALCULATES   THE MAXIMUM VALUE OF   EACH   OF   THE
C ARRAYS FOR SETTING UP THE SCALES OF THE PLOT  AXES.     THEN
C THE  DATA FILE IS CLOSED.   THESE VALUES ARE LEFT AS   REAL
C NUMBERS  VICE  INTEGERS BECAUSE THE DATA FROM THE  PROGRAM
C CAN VARY SIGNIFICANTLY WITH DIFFERENT INPUT VALUES, AND IF
C THE MAX VALUE IS LESS THAN 10 AN INTEGER REQUIREMENT GIVES
C A PLOTTING ERROR.


      DO 20 J=1,300
         READ (69,15,END=21)D(J),G(J),H(J),O(J),T(J)
   15    FORMAT(E13.5,E13.5,E13.5,E13.5,E13.5)
      IF(D(J).GT.XMAX)THEN
      XMAX=D(J)
      ENDIF
      IF(G(J).GT.YMAX1)THEN
      YMAX1=G(J)
      ENDIF
      IF(H(J).GT.YMAX2)THEN
      YMAX2=H(J)
      ENDIF
      IF(O(J).GT.YMAX3)THEN
      YMAX3=O(J)
      ENDIF
      IF(T(J).GT.YMAX4)THEN
      YMAX4=T(J)
      ENDIF
   20 CONTINUE
   21 CLOSE(69)


C        THE   NEXT THREE LINES TAKE CARE OF ANOTHER   ODDITY   OF
C THE DATA,   IN THE CASE OF THE VOLTAGE PLOT.    DEPENDING ON
C THE  INPUT  DATA THE VOLTAGE WILL LOCK IN AT 8  VOLTS,   AS
C EXPECTED,  BUT  THIS IS ALSO THE MAX VALUE,  SO YOU GET  A
C STRAIGHT  LINE AT THE TOP OF THE PLOT  MARGIN.    THE  NEXT
C THREE LINES INCREASE THE MAX VALUE TO 9 VOLTS TO MAKE THIS
C PLOTTING CASE MORE CLEAR.


      IF(YMAX4.LE.9.0)THEN
      YMAX4=9.0
      ENDIF
```

```
C      THE   NEXT EIGHT LINES CALCULATE THE INCREMENTAL  STEPS
C FOR   EACH   AXIS OF THE VARIOUS PLOTS.    THE X AXIS IS  THE
C SAME FOR ALL,   AND IS LEFT IN INTEGER FORMAT FOR  CLARITY.
C EACH AXIS IS SET UP FOR TEN INCREMENTS.    THE DATA FILE IS
C THEN RENAMED TO THE DESIRED FORMAT FOR MY STORAGE.


       INC=INT(XMAX/10.)
       YINC1=YMAX1/10.
       YINC2=YMAX2/10.
       YINC3=YMAX3/10.
       YINC4=YMAX4/10.
       MAX=INT(XMAX)
       NEW1$='RENAME '//' FILE XYZ1 A1'//' FRIDGE OUTPUT A1'
       CALL EXCMS(NEW1$)


C      THIS  IS, THE   FIRST PLOTTING SECTION.    IT  DOES  THE
C INITIAL SET UP OF ALL OF THE CALLS THAT CAN BE COMMON  AND
C PLOTS THE VOLTAGE VERSUS FREQUENCY PLOT.   CALL TEK618 SETS
C UP   THE REQUIRED MACHINE FOR THE PLOTTING AND LINKS YOU TO
C THE PLOTTER.    CALL BLOWUP IS USED TO MAGNIFY THE PLOT FOR
C A   BETTER   PICTURE.   CALL YAXANG PUTS   THE   AXIS   NUMBERS
C PERPINDICULAR   TO   THE PLOT AXIS TO PREVENT  RUNNING  INTO
C EACH   OTHER.   CALL PAGE SETS UP THE PAGE SIZE IN  INCHES.
C CALL   AREA2D   SETS UP A TWO DIMENSIONAL PLOT AREA  OF  THE
C SPECIFIED  SIZE   IN INCHES.  CALL SCMPLX SELECTS THE  LET-
C TERING TYPE FOR THE HEADING.   CALL MESSAG AND CALL REALNO
C ALLOW ME TO PLACE A MESSAGE IN THE PLOT AREA AT A SPECIFIC
C POINT  SPECIFIED IN INCHES IN THE CALL.   CALL  XNAME  AND
C YNAME   ALLOW ME TO LABEL THE AXES.   CALL HEADIN ALLOWS ME
C TO PLACE A TITLE ON THE PLOT.  CALL THKFRM AND FRAME ALLOW
C ME   TO PUT FRAMES AROUND THE PLOT AREA AND THE WHOLE  PLOT
C OF A SET THICKNESS. CALL GRAF SETS UP THE PHYSICAL ORIGINS
C AND  MAX VALUES AND THE INCREMENTS FOR  EACH  AXIS.   CALL
C CURVE TELLS THE MACHINE TO PLOT THE DESIRED ARRAYS OF DATA
C POINTS.    CALL   ENDPL ENDS THAT SPECIFIC PLOT AND GIVES  A
C NEW PAGE FOR THE NEXT PLOT.


       CALL TEK618
       CALL BLOWUP(1.5)
       CALL YAXANG(0)
       CALL PAGE(11,8.5)
       CALL AREA2D(8.,6.)
       CALL SCMPLX
       CALL MESSAG('MASS=$',100,0.1,5.5)
       CALL REALNO(M,-2,'ABUT','ABUT')
       CALL MESSAG('KG$',100,'ABUT','ABUT')
       CALL MESSAG('VOLUME=$',100,0.1,5.)
       CALL REALNO(VOL,-2,'ABUT','ABUT')
       CALL MESSAG('M**3$',100,'ABUT','ABUT')
```

153

```
      CALL XNAME('FREQUENCY(IN HERTZ)$',100)
      CALL YNAME('VOLTAGE (IN VOLTS)$',100)
      CALL HEADIN('VOLTAGE VS. FREQUENCY$',100,2.,1)
      CALL THKFRM(.02)
      CALL FRAME
      CALL GRAF(0.0,INC,MAX,7.5,YINC4,YMAX4)
      CALL CURVE(D,T,300,0)
      CALL ENDPL(0)


C     THIS SECTION PLOTS PISTON VELOCITY VERSUS FREQUENCY.


      CALL AREA2D(8.,6.)
      CALL MESSAG('MASS=$',100,0.1,5.5)
      CALL REALNO(M,-2,'ABUT','ABUT')
      CALL MESSAG('KG$',100,'ABUT','ABUT')
      CALL MESSAG('VOLUME=$',100,0.1,5.)
      CALL REALNO(VOL,-2,'ABUT','ABUT')
      CALL MESSAG('M**3$',100,'ABUT','ABUT')
      CALL XNAME('FREQUENCY(IN HERTZ)$',100)
      CALL YNAME('PISTON VELOCITY(IN METERS/SEC)$',100)
      CALL HEADIN('PISTON VELOCITY VS. FREQUENCY$',100,2.,1)
      CALL THKFRM(.02)
      CALL FRAME
      CALL GRAF(0.0,INC,MAX,0.0,YINC1,YMAX1)
      CALL CURVE(D,G,300,0)
      CALL ENDPL(0)


C     THIS SECTION PLOTS ACOUSTIC POWER VERSUS FREQUENCY.


      CALL AREA2D(8.,6.)
      CALL MESSAG('MASS=$',100,0.1,5.5)
      CALL REALNO(M,-2,'ABUT','ABUT')
      CALL MESSAG('KG$',100,'ABUT','ABUT')
      CALL MESSAG('VOLUME=$',100,0.1,5.)
      CALL REALNO(VOL,-2,'ABUT','ABUT')
      CALL MESSAG('M**3$',100,'ABUT','ABUT')
      CALL XNAME('FREQUENCY(IN HERTZ)$',100)
      CALL YNAME('ACOUSTIC POWER (IN N-M/S)$',100)
      CALL HEADIN('ACOUSTIC POWER VS. FREQUENCY$',100,2.,1)
      CALL THKFRM(.02)
      CALL FRAME
      CALL GRAF(0.0,INC,MAX,0.0,YINC2,YMAX2)
      CALL CURVE(D,H,300,0)
      CALL ENDPL(0)


C     THIS SECTION PLOTS POWER RATIO VERSUS FREQUENCY.
```

154

```
        CALL AREA2D(8.,6.)
        CALL MESSAG('MASS=$',100,0.1,5.5)
        CALL REALNO(M,-2,'ABUT','ABUT')
        CALL MESSAG('KG$',100,'ABUT','ABUT')
        CALL MESSAG('VOLUME=$',100,0.1,5.)
        CALL REALNO(VOL,-2,'ABUT','ABUT')
        CALL MESSAG('M**3$',100,'ABUT','ABUT')
        CALL XNAME('FREQUENCY(IN HERTZ)$',100)
        CALL YNAME('ACOUSTIC PWR/ ELECTRIC PWR$',100)
        CALL HEADIN('POWER RATIO VS. FREQUENCY$',100,2.,1)
        CALL THKFRM(.02)
        CALL FRAME
        CALL GRAF(0.0,INC,MAX,0.0,YINC3,YMAX3)
        CALL CURVE(D,O,300,0)
        CALL ENDPL(0)


C       CALL  DONEPL ENDS THE PLOTTING SEQUENCE AND SENDS  YOU
C BACK TO CMS.


        CALL DONEPL
        STOP
        END
```
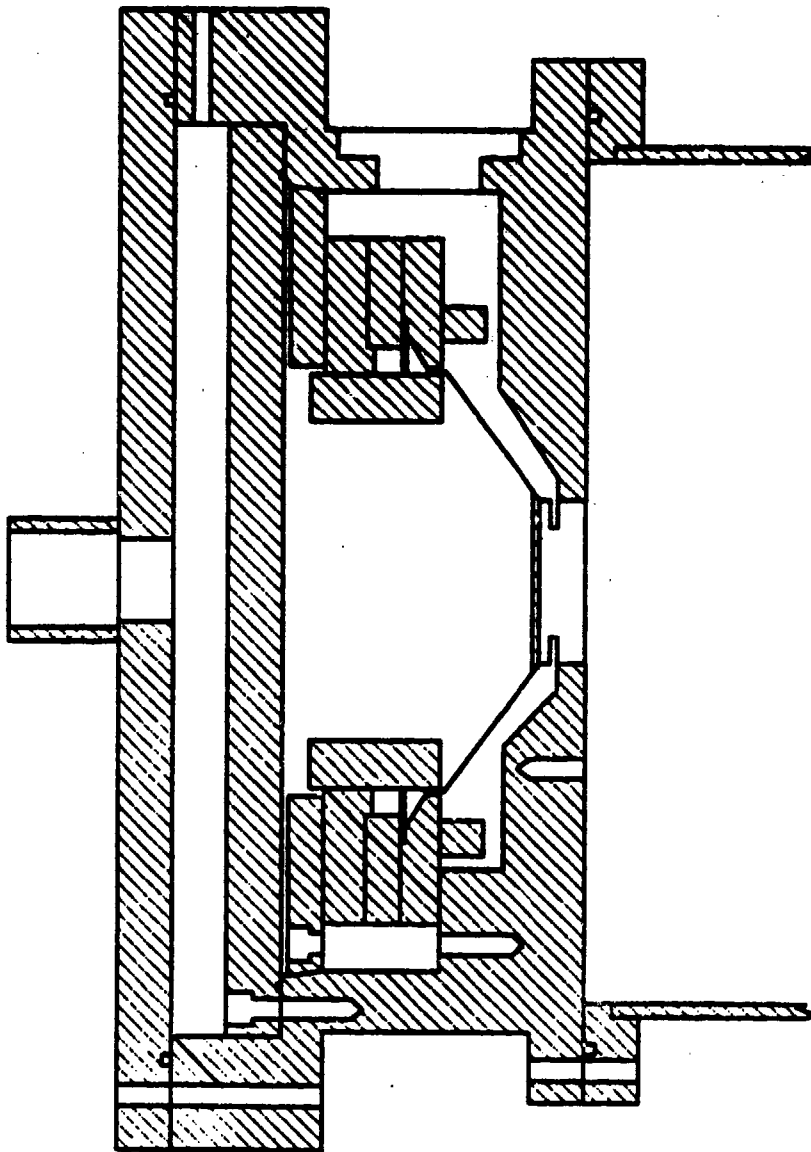
Figure C-1.   Assembly Drawing of NIB Driver with
all Housing Parts and Test Lid.

156
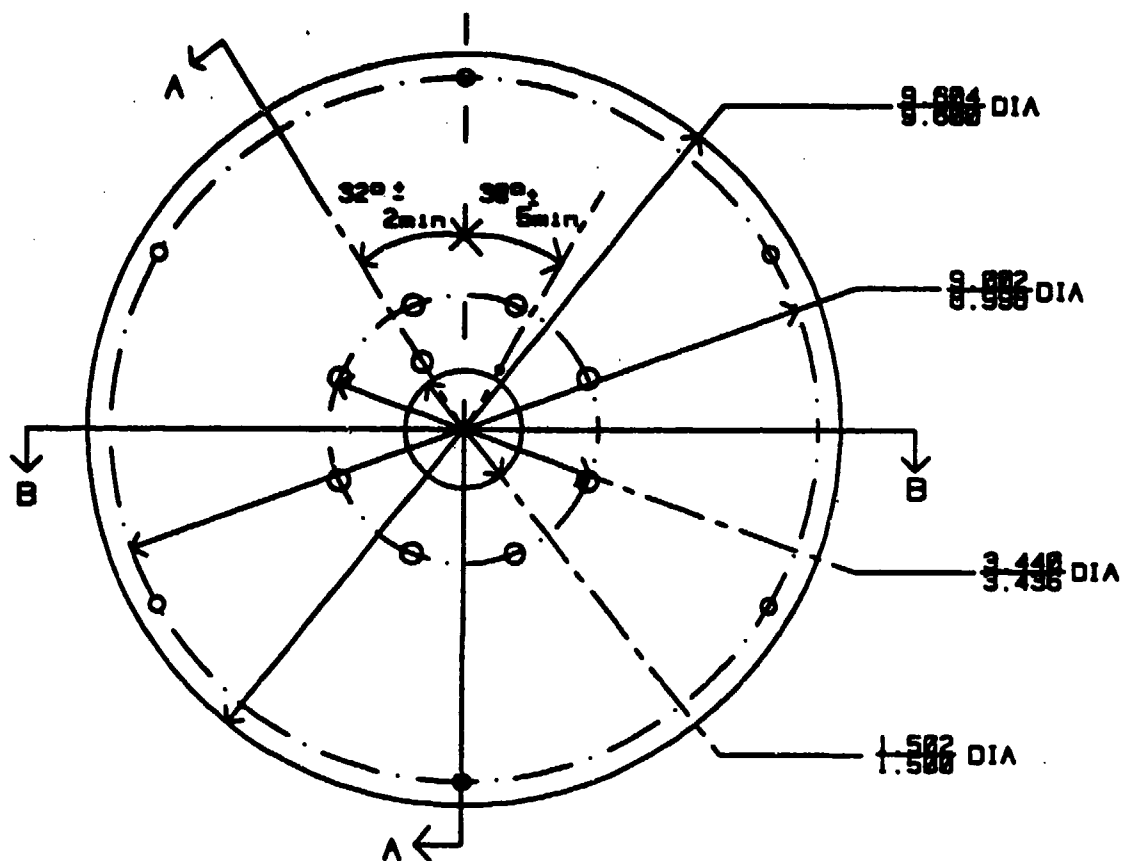
DRIVER HOUSING - RESONATOR VIEW

(Dimensions in inches)

Figure C-2.   Driver Housing--Resonator View.
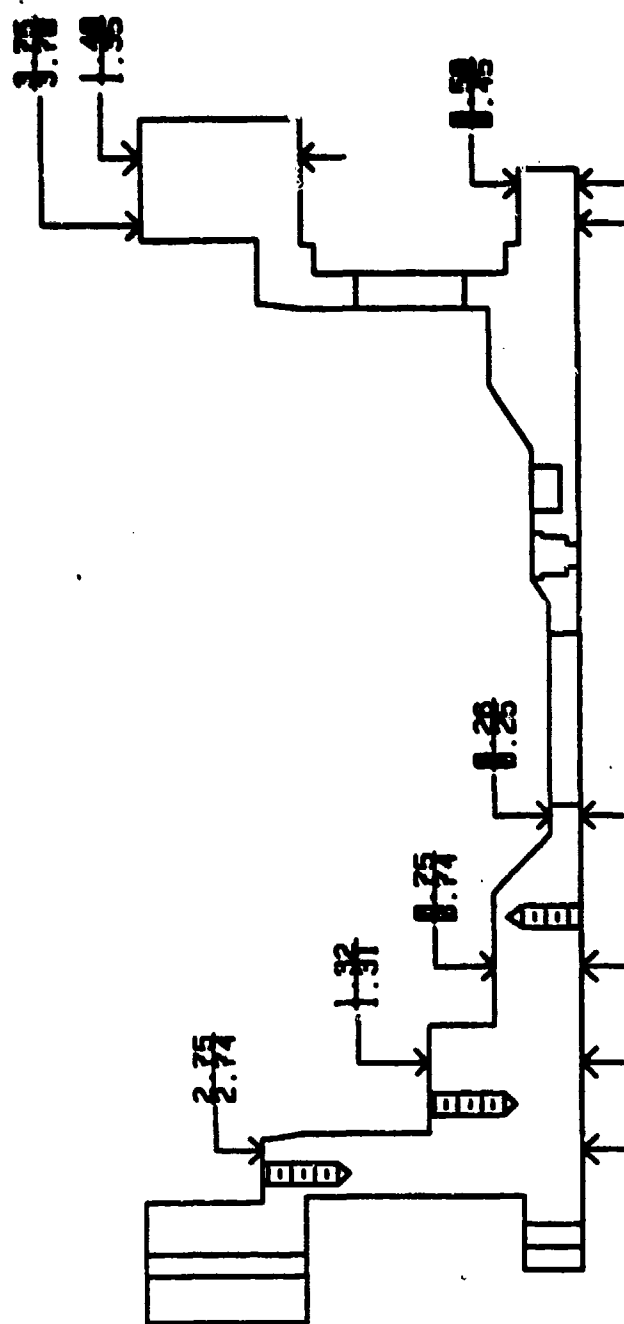
Figure C-3. Driver Housing—Side View Section AA
Showing Electrical Leads, Bolt Holes,
Microphone Penetration, and FET
Follower Housing.

158

VIEW AA
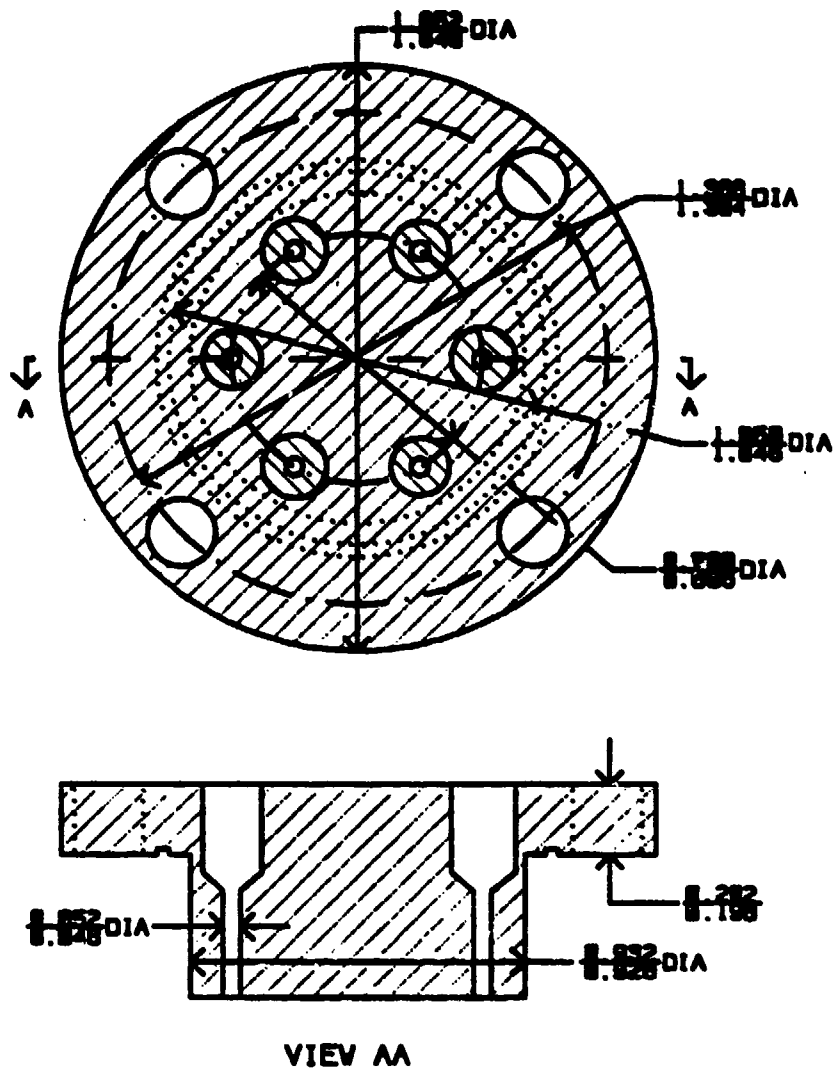
ELECTRONICS PLUG

(Dimensions in inches)

Figure C-4.   Feed-Through for Electrical Leads
Shown in Figure V-5.
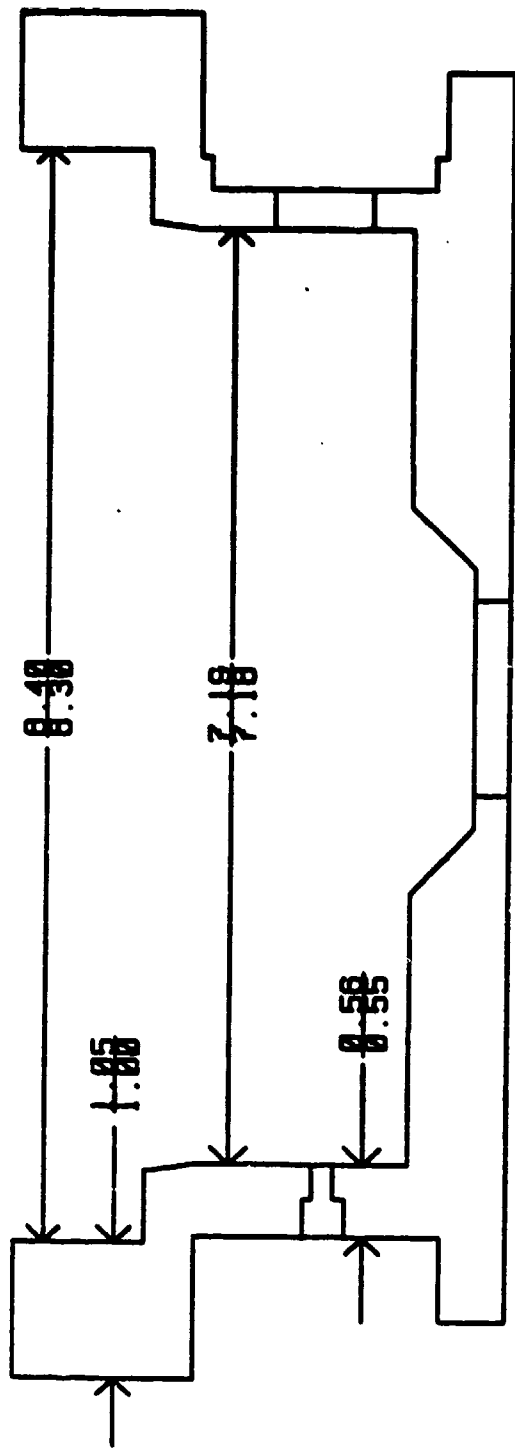
Figure C-5. Driver Housing--Side View Section BB
Showing Pressure Gage and Helium
Fill Ports.

VIEW AA
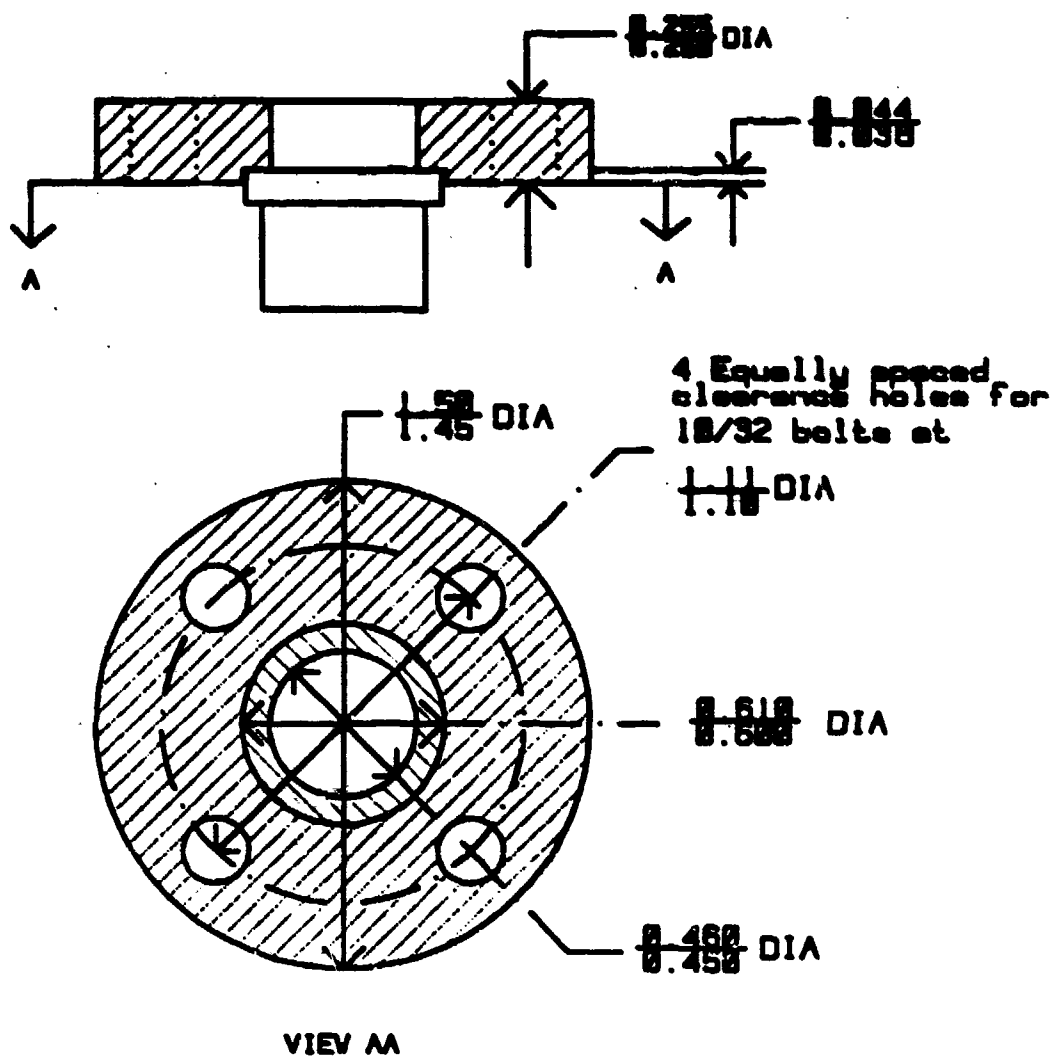
DC PRESSURE TRANSDUCER

(Dimensions in inches)

Figure C-6.   DC Pressure Gage Feed-
Through Plug Details.

161
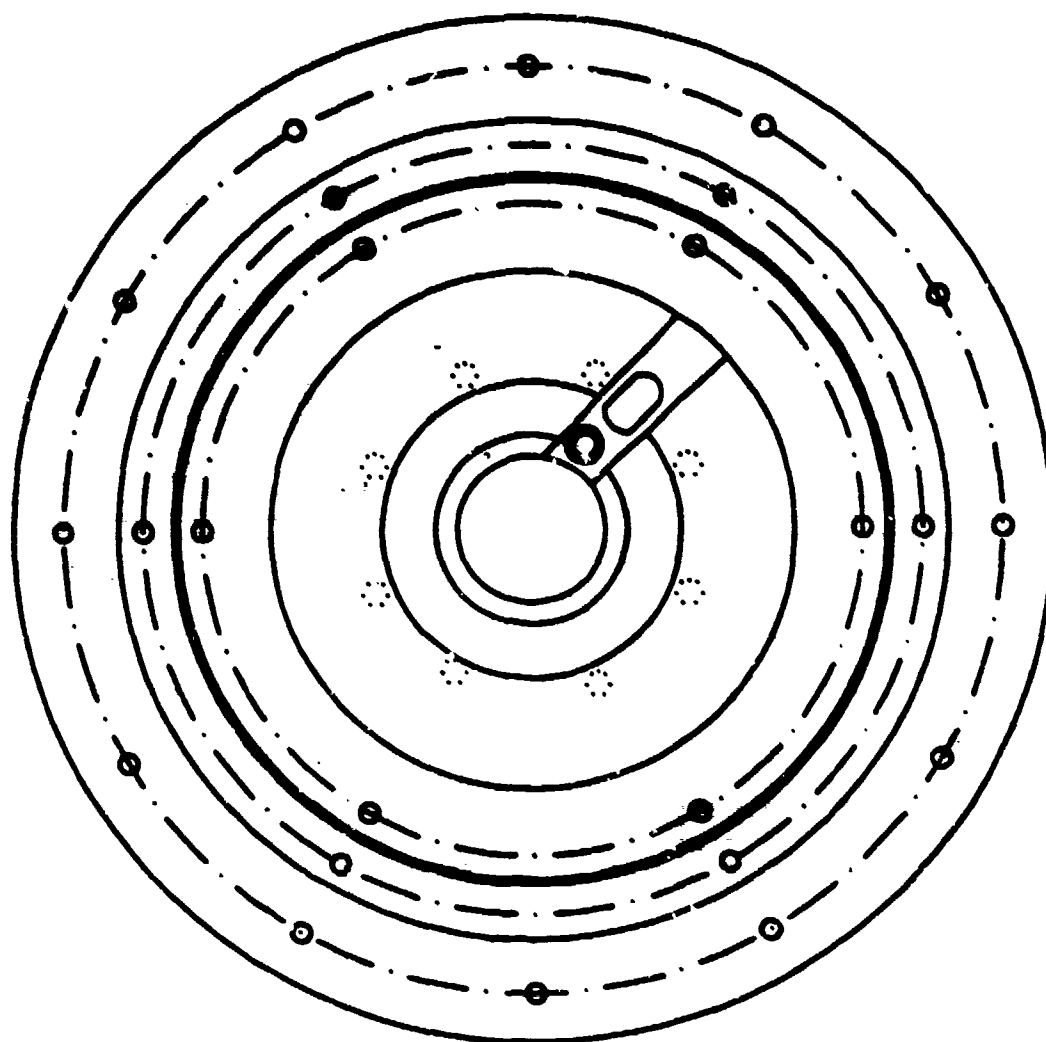
DRIVER HOUSING - LID VIEW

Figure C-7.   Driver Housing--Lid View Showing
             Capillary, Microphone, and Follower,
             and Bolt Circles for Resonator
             Attachment, Pusher Plate, Pressure
             Lid and GAS Can Lid.

7.295
7.285 DIA

6.700
6.690 DIA

3.98
3.97 DIA
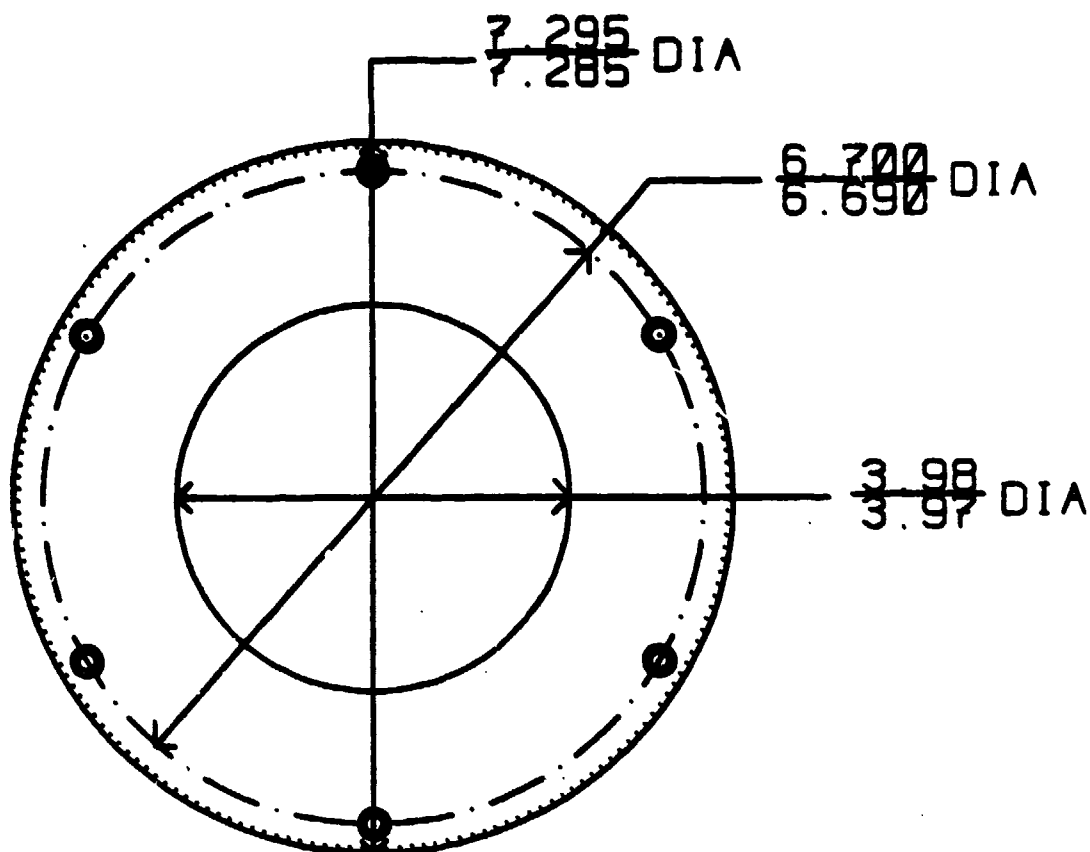
(Note: Plate is 3/10" wide and
        and slopes 10° at outer
        edge.)

PUSHER PLATE (LID VIEW)

(Dimensions in inches)

Figure C-8.   Aluminum Pusher Plate.

8.405 / 8.995 DIA

Groove for
1/16" lead
O-ring at

7.41 / 7.40 DIA

7.95 / 7.85 DIA
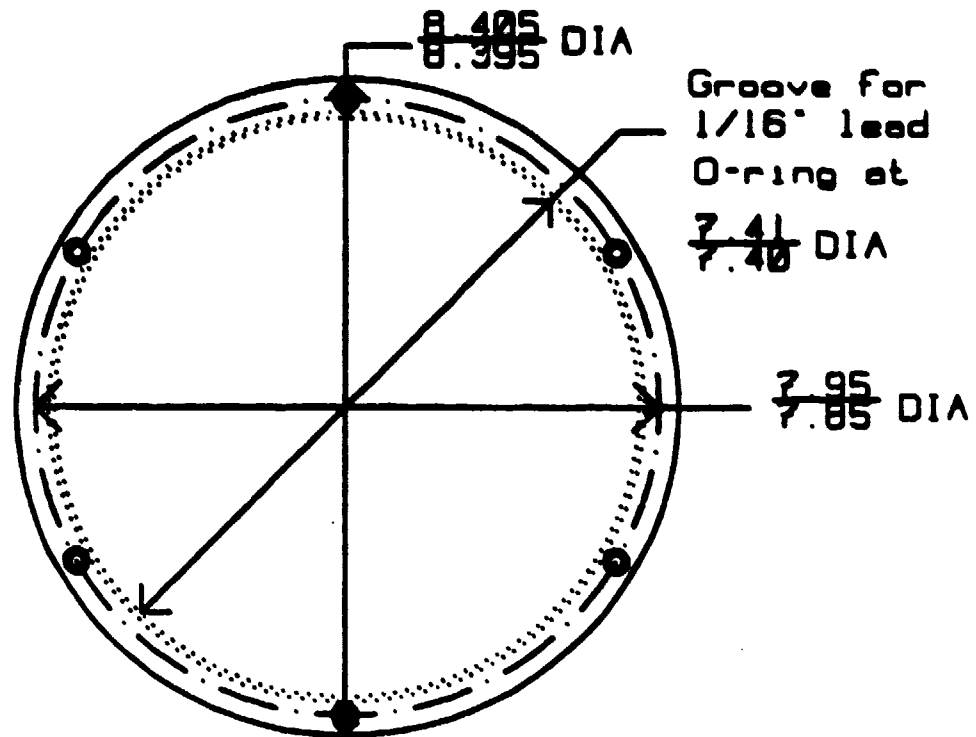
(Note: O-ring groove 0.018" wide
and .036" deep:

lid is 1/2" wide)

PRESSURE LID (LID VIEW)

(Dimensions in inches)

Figure C-9.   Pressure Lid with Lead
O-ring Groove.

O-RING GROOVE FOR
PARKER 2-174 O-RING
0.174 DEPTH 0.123 WIDTH
AT 8.737 I.D.
8.732

12 CLEARANCE HOLES
FOR18/32 BOLTS
AT 9.502 DIA
9.498

8.750 DIA
8.745

0.500
0.495

10.250 DIA
10.245

1 1/8 O.D.
ALUMINA TUBING
3 INCHES LONG
1/8 INCH THICK
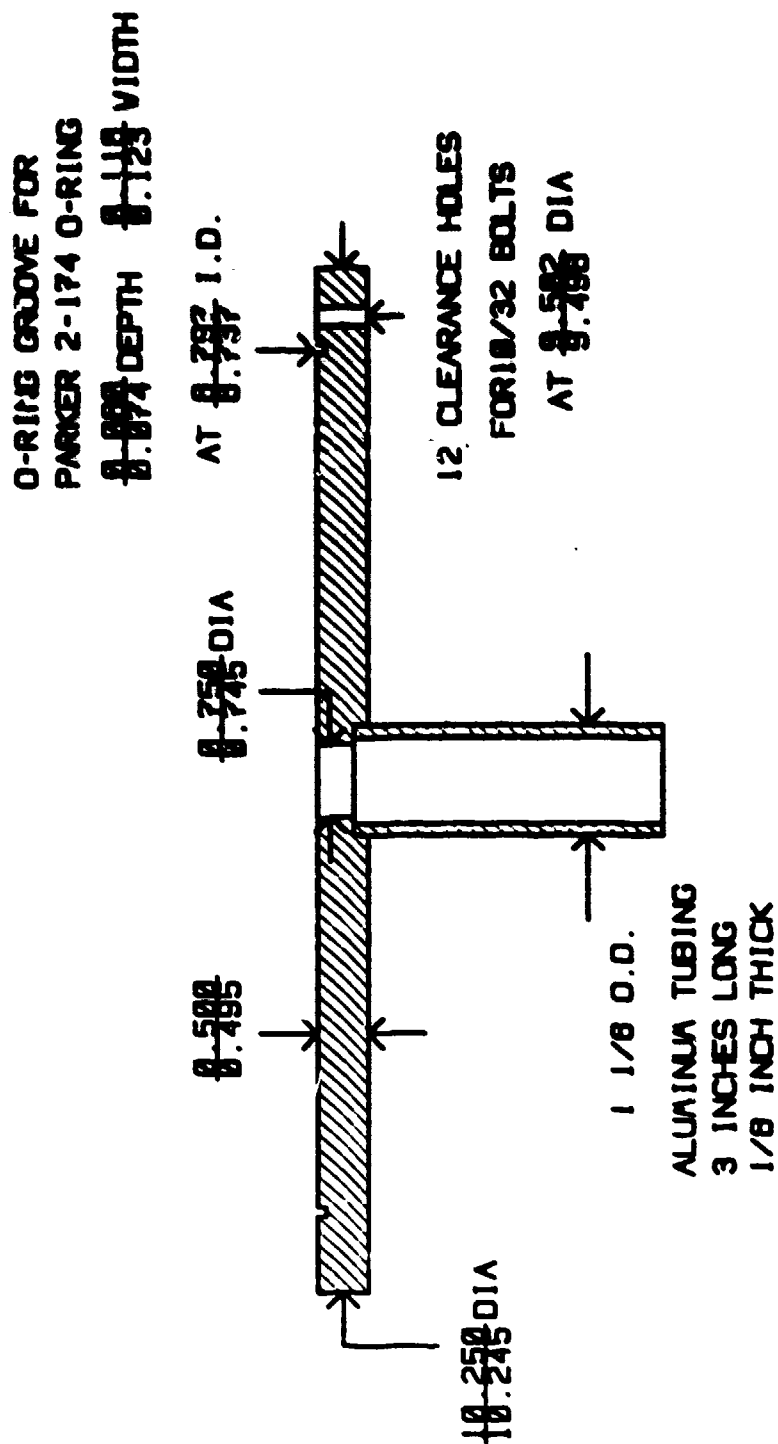
DRIVER TEST LID

(Dimensions in inches)

Figure C-10. Pressure and Helium Leak Test Lid.
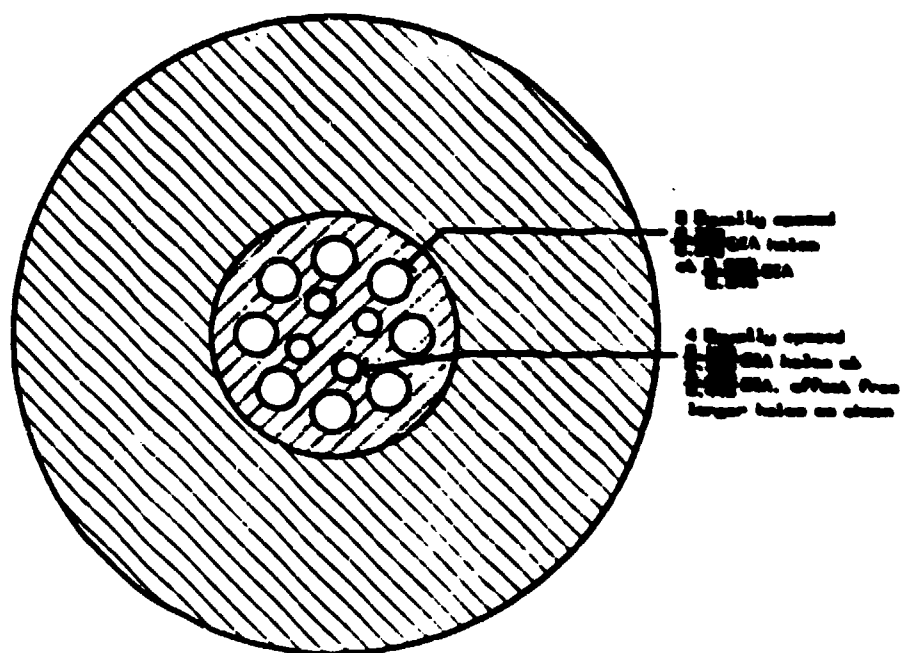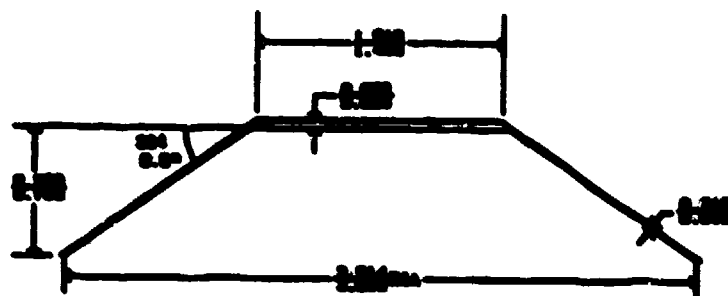
REDUCER CONE

(Dimensions in inches)

Figure C-11.   Reducer Cone.

APPENDIX D.   STAR DRIVER LIST OF MATERIALS

The driver consists of a modified JBL model 2450J neo-dymium-iron-boron magnet with iron pole pieces on either side. The diaphragm is titanium and the voice coil is aluminum.

The housing, pusher plate, pressure lid, and reducer cone will all be machined from 6061-T6 aluminum. All openings in the driver housing will be sealed with 1/16" or 1/32" diameter lead o-rings. The electrical feed-throughs will be sealed with Emerson & Cuming's STYCAST(TM) 2850FT epoxy. All wire leads are copper. The steel bolts connecting the resonator to the driver are size 1/4-20. All other steel bolts are size 10-32.

REFERENCES

Boyd, A. W., Kosinski, B. P., and Weston, R. L., "Autonomous Measurement of Space Shuttle Payload Bay Acoustics During Launch," Naval Research Reviews, vol. 39 (1), p. 9, 1987.

Burmaster, C. L., Reciprocity Calibration in a Plane Wave Resonator, Ph.D. Dissertation, Naval Postgraduate School, Monterey, CA, p. 73, December 1985.

Ceperley, P. H., "A Pistonless Stirling Engine - The Traveling Wave Heat Engine," Journal of the Acoustical Society of America, vol. 66, p. 1508, 1979.

Get Away Special Team, Get Away Special (GAS) Small Self-contained Payloads--Experimenter Book, National Aeronautics and Space Administration, Goddard Space Flight Center, Special Payloads Division, Greenbelt, MD, July 1984.

Gifford, W. E. and Longsworth, R. C., "Surface Heat Pumping," International Advances in Cryogenic Engineering, vol. 11, p. 171, Plenum, NY, 1966.

Gray, D. E., American Institute of Physics Handbook, Third Edition, p. 5-165, MacGraw-Hill, 1972.

Faraday, M., Quarterly Journal of Science, vol. 5, p. 274, 1818.

Hofler, T. J., Thermoacoustic Refrigeration Design and Performance, Ph.D. Dissertation, University of California, San Diego, CA, 1986.

Hofler, T. J., "Accurate Acoustic Power Measurements with a High-intensity Driver," Journal of the Acoustical Society of America, vol. 83 (2), p. 777, 1988.

Kempton, A. J., "Heat Diffusion as a Source of Aerodynamic Sound," Journal of Fluid Mechanics, vol. 78, p. 1, 1976.

Kinsler, L. E., Frey, A. R., Coppens, A. B., and Sanders, J. V., Fundamentals of Acoustics, Third Edition, John Wiley & Sons, Inc., New York, NY, 1982.

Merkli, P. and Thomann, H., "Thermoacoustic Effects in a Resonant Tube," Journal of Fluid Mechanics, vol. 70, p. 161, 1975.

NASA George C. Marshall Space Flight Center, Materials Selection List for Space Hardware Systems, Report No. MSFC-HDBK-527 Rev E, p. 12, NASA MSFC, AL, November, 1986a.

NASA Goddard Space Flight Center, *Get Away Special Payloads Safety Manual*, p. 151, Greenbelt, MD, May 1986b.

Rayleigh, Lord, *Proceedings of the Royal Society*, vol. VIII, p. 536; *Nature*, vol. XVIII, p. 319, 1878.

Rayleigh, Lord, *Theory of Sound*, Second Edition, Volume II, Section 322i, Dover, New York, 1945.

Rijke, P. L., *Annals of Physics* (Leipzig), vol. 107, p. 339, 1859.

Rott, N., "Damped and Thermally Driven Acoustic Oscillations in Wide and Narrow Tubes," *Journal of Applied Mathematics and Physics (ZAMP)*, vol. 20, 1969.

Rott, N., "The Heating Effect Connected with Non-linear Oscillations in a Resonant Tube," *Journal of Applied Mathematics and Physics (ZAMP)*, vol. 25, 1974.

Rott, N., "Thermally Driven Acoustic Oscillations, Part III: Second-Order Heat Flux," *Journal of Applied Mathematics and Physics (ZAMP)*, vol. 26, 1975.

Rott, N., "Thermoacoustics," *Advances in Applied Mechanics*, vol. 20, 1980.

Sears, F. W. and Salinger, G. L., *Thermodynamics, Kinetic Theory, and Statistical Thermodynamics*, Third Edition, pp. 113-115, Addison-Wesley, 1975.

Smith, J. L. Jr., Robinson, G. Y. Jr., and Iwasa, Y., *Survey of the State-of-the-Art of Miniature Cryocoolers for Superconductive Devices*, Naval Research Laboratory, Washington, D. C., 1984.

Sondhauss, C., *Annals of Physics and Chemistry*, Volume 79, (1), 1850.

Swift, G. W., untitled article to be published in the *Journal of the Acoustical Society of America*, circa 1989.

Swift, G. W., Migliori, A., Garrett, S. L., and Wheatley, J. C., "Two Methods for Absolute Calibration of Dynamic Pressure Transducers," *Review of Scientific Instruments*, vol. 53 (1), p. 1906, 1982.

Taconis, K. W., Beenakker, J. J. M., Nier, A. O. C., and Aldrich, L. T., "Measurements Concerning the Vapour-Liquid Equilibrium of Solutions of He^3 in He^4 Below 2.19°K," *Physica*, vol. 15, p. 733, 1949.

Walker, G., "Cryocoolers, Parts 1 and 2," International Cryogenics Monograph Series, Plenum Press, NY, 1983.

Wheatley, J. C. and Cox, A., "Natural Engines," Physics Today, August, 1985.

Wheatley, J. C., Hofler, T. J., Swift, G. W., and Migliori, A., "Experiments with an Intrinsically Irreversible Acoustic Heat Engine," Physical Review Letters, vol. 50 (7), p. 499, February 1983a.

Wheatley, J. C., Hofler, T. J., Swift, G. W., and Migliori, A., "An Intrinsically Irreversible Thermoacoustic Heat Engine," Journal of the Acoustical Society of America, vol. 74 (1), p. 153, July 1983b.

Wheatley, J. C., Hofler, T. J., Swift, G. W., and Migliori, A., "Understanding Some Simple Phenomena in Thermoacoustics with Applications to Acoustical Heat Engines," American Journal of Physics, vol. 53 (2), p. 147, February 1985.

Wheatley, J. C., Swift, G. W., and Migliori, A., "The Natural Heat Engine," Los Alamos Science, Number 14, Fall 1986.

Wilson, O. B., An Introduction to the Theory and Design of Sonar Transducers, Naval Postgraduate School, Monterey, CA, 1985.

Yazaki, T., Tominaga, A., and Narahara, Y., Journal of Low Temperature Physics, vol. 41, p. 45, 1980.

INITIAL DISTRIBUTION LIST

		No. Copies
1.	Defense Technical Information Center Cameron Station Alexandria, VA 22304-6145	2
2.	Library, Code 0142 Naval Postgraduate School Monterey, CA 93943-5002	2
3.	COMMANDANT (G-PTE-1) U. S. Coast Guard Headquarters 2100 Second Street, S. W. Washington, D. C. 20593	2
4.	Professor Richard Crissman Physics Department U. S. Coast Guard Academy New London, CT 06320	2
5.	Professor S. L. Garrett, Code 61GX Naval Postgraduate School Monterey, CA 93943-5000	6
6.	Dr. T. Hofler, Code 61HF Naval Postgraduate School Monterey, CA 93943-5000	3
7.	Professor A. Atchley, Code 61AY Naval Postgraduate School Monterey, CA 93943-5000	1
8.	Dr. L. E. Hargrove Office of Naval Research Physics Division - Code 1112 800 N. Quincy Street Arlington, VA 22217	1
9.	Professor I. Rubnick UCLA--Physics Dept. 405 Hilgard Ave. Los Angeles, CA 90024	1
10.	Commanding Officer Office of Naval Technology ATTN: Dr. Philip Selwyn (Code 20) CAPT R. S. Fitch (Code 23D) 800 N. Quincy Street Arlington, VA 22217	1 1

11. Commanding Officer
    Naval Air Development Center
    ATTN: Dr. T. Gabrielson   1
    Warminster, PA   18974

12. Commanding Officer
    Naval Research Laboratory
    ATTN: T. G. Giallorenzi   1
           F.   Hellrich   1
    4555 Overlook Avenue
    Washington, D. C.   20375-5000

13. Professor A. H. Fuhs, Code 67Fu   1
    Naval Postgraduate School
    Monterey, CA   93943-5000

14. Professor R. Panholtzer, Code 62Pz   2
    Naval Postgraduate School
    Monterey, CA   93943-5000

15. D. Rigmaiden, Code 72   1
    Naval Postgraduate School
    Monterey, CA   93943-5000

16. LT Scott Palmer   1
    Space and Naval Warfare Systems Command
    PDW 106/72A
    Washington, D. C.   20363-5100

17. Ms. Carol Tanner   1
    Mail Station N4/910
    Aerospace Corporation
    P. O. Box 92957
    Los Angeles, CA   90009

18. Commodore Truly   1
    Commander Naval Space Command
    Dahlgren, VA   22448-5170

19. Mr. Frank Deithrick   1
    Space and Naval Warfare Systems Command
    Washington, D. C.   20363-5100

20. The University of Texas at Austin
    ATTN: Prof. I. Busch-Vishniac (Mech. Eng.)   1
          Prof. W. D. McCormick (Physics)   1
    Austin, TX   78713-8029

21. Los Alamos National Laboratories
    Condensed Matter and Thermal Physics (Group P-10)
    ATTN: Dr. G. W. Swift   1
            Dr. A Migliori   1
    P. O. Box 1663/MS 764
    Los Alamos, NM 87545

22. Commanding Officer
    Naval Weapons Center
    Office of Counsel - Code 023
    ATTN: W. Thomas Skeer   1
    China Lake, CA 93555

22. LCDR Allen Hansen   1
    Navy Space System Activity
    P. O. Box 92960 WWP
    Los Angeles, CA 90009

24. LT Mary Cox   1
    Dept. of the Air Force
    Space Test Program Office (SD/CLTPC)
    HQ Space Division
    P. O. Box 92960
    Los Angeles, CA 90009-2960

25. Mr. Fancher Murray   3
    JBL Incorporated
    800 Balboa Boulevard
    Northridge, CA 91329

26. Dr. S. F. Watanabe   1
    Director, Technology Assessment
    McDonnell Douglas Corporation
    1550 Wilson Blvd., Suite 550
    Arlington, VA 22209

27. The Aerospace Corporation
    ATTN: Dr. Bruce C. Edgar (M1/120)   1
            Julie D. White (M1/122)   1
    P. O. Box 92957
    Los Angeles, CA 90009-2957

28. Cox Hobbies Inc
    ATTN: W. H. Selzer, President   1
    1525 East Warner Ave.
    Santa Ana, CA 92705

29. Endevco
    ATTN: W. H. Cooley   1
    1500 16th St., Suite 200
    San Francisco, CA 94103

30. LT Michele Fitzpatrick   6
    1634 W. Norwegian St.
    Pottsville, PA 17901

31. LT Michael Susalla   .1
    Code 33, WN63
    Naval Postgraduate School
    Monterey, CA 93943

32. LT R. Volkhert   1
    Code 33, UX
    Naval Postgraduate School
    Monterey, CA 93943

33. CPT D. Harris   1
    Code 33, UX
    Naval Postgraduate School
    Monterey, CA 93943

34. National Center for Physical Acoustics
    ATTN: Librarian   1
    P. O. Box 847
    Fraternity Row
    University, MS 38677